UNIVERSITAT POLITÈCNICA DE VALÈNCIA

Ultra Dense Networks Deployment for beyond 2020 Technologies

Departamento de Comunicaciones
Universitat Politècnica de València

A thesis submitted for the degree of
Doctor por la Universitat Politècnica de València
Valencia, July 2017

Author:
Sonia Giménez Colás

Supervisors:
Dr. Daniel Calabuig Soler
Dr. José F. Monserrat del Río
Dr. Narcís Cardona Marcet

A mis padres.

Abstract

A new communication paradigm is foreseen for beyond 2020 society, due to the emergence of new broadband services and the Internet of Things era. The set of requirements imposed by these new applications is large and diverse, aiming to provide a ubiquitous broadband connectivity. Research community has been working in the last decade towards the definition of the Fifth Generation (5G) mobile wireless networks that will provide the proper mechanisms to reach these challenging requirements. In this framework, three key research directions have been identified for the improvement of network capacity in 5G, which are the increase of the spectral efficiency by means of, for example, the use of massive Multiple Input Multiple Output (MIMO) technology, the use of larger amounts of spectrum by utilizing additional frequency bands such as the millimeter wave band, and the network densification by deploying more base stations per unit area.

This dissertation addresses densification as the main enabler for the broadband and massive connectivity required in future 5G networks. To this aim, this Thesis focuses on the study of the Ultra Dense Networks (UDNs). In particular, a set of technology enablers that can lead UDNs to achieve their maximum efficiency and performance are investigated, namely, the use of higher frequency bands for the benefit of larger bandwidths, the use of massive MIMO with distributed antenna systems, and the use of distributed radio resource management techniques for the inter-cell interference coordination.

Firstly, this Thesis analyzes whether there exists a fundamental performance limit related with densification in cellular networks or, contrarily, densification is associated with limitless performance gains. To this end, the UDNs performance is evaluated by means of an analytical model consisting of a 1-dimensional network deployment with equally spaced Base Stations (BSs). The inter-BS distance is decreased until reaching the limit of densification when this distance approaches 0. The achievable rates in networks with different inter-BS distances are analyzed for several levels of transmission power availability, and for various types of cooperation among cells.

Moreover, UDNs performance is studied in conjunction with the use of a massive number of antennas and larger amounts of spectrum. In particular, the performance of hybrid beamforming and precoding MIMO schemes are assessed in both indoor and outdoor scenarios with multiple cells and users, working in the millimeter wave (mmW) frequency band. On the one hand, beamforming schemes using the full-connected hybrid architecture are analyzed in BSs with limited number of Radio Frequency (RF) chains, identifying the strengths and weaknesses of these schemes in a dense-urban scenario. On the other hand, the performance of different indoor deployment strategies using Hybrid Precoding (HP) in the mmW band is evaluated, focusing on the use of Distributed Antenna Systems (DAS). More specifically, a Distributed Hybrid Precoding (DHP) suitable for DAS is proposed, comparing its performance with that of HP in other indoor deployment strategies. Lastly, the presence of practical limitations and hardware impairments in the use of hybrid architectures is also investigated for both indoor and outdoor scenarios.

Finally, the investigation of UDNs is completed with the study of their main limitation, which is the increasing inter-cell interference in the network. In order to tackle this problem, an enhanced Inter-Cell Interference Coordination (eICIC) scheduling algorithm based on resource partitioning techniques is proposed, which uses a time and frequency reuse pattern for the scheduling coordination of all the cells forming a cluster. Its performance is evaluated and compared to other scheduling algorithms under several degrees of network densification.

After the completion of this study, the potential of UDNs to reach the challenging capacity requirements of 5G networks is confirmed. Nevertheless, without the use of larger portions of spectrum, a proper interference management and the use of a massive number of antennas, densification could turn into a serious problem for mobile operators. Performance evaluation results obtained in this Thesis show large system capacity gains with the use of massive MIMO techniques in UDNs, and even greater when the antennas are distributed. Furthermore, regarding the application of interference management techniques, results reveal that, besides the increase in system capacity, the application of eICIC brings significant energy savings to the UDNs.

Resumen

A partir del año 2020 se prevé que un nuevo paradigma de comunicación surja en la sociedad, debido a la aparición de nuevos servicios de banda ancha y la nueva era del Internet de las cosas. El conjunto de requisitos impuesto por estas nuevas aplicaciones es muy amplio y diverso, y tiene como principal objetivo proporcionar conectividad de banda ancha y universal. En las últimas décadas, la comunidad científica ha estado trabajando en la definición de la Quinta Generación de redes móviles o 5G, que brindará los mecanismos necesarios para garantizar estos exigentes requisitos. En este marco, se han identificado tres mecanismos clave en las redes 5G para conseguir el necesario incremento de capacidad: el aumento de la eficiencia espectral a través de, por ejemplo, el uso de tecnologías MIMO masivas, la utilización de mayores porciones del espectro en frecuencia y la densificación de la red mediante el despliegue de más estaciones base por área.

Esta Tesis doctoral aborda la densificación como el principal mecanismo que permitirá la futura conectividad de banda ancha y universal requerida en la 5G. Con este objetivo, esta Tesis se centra en el estudio de las Redes Ultra Densas o UDNs. En concreto, se analiza el conjunto de tecnologías habilitantes que pueden llevar a las UDNs a obtener su máxima eficiencia así como sus máximas prestaciones, incluyendo el uso de altas frecuencias para el aprovechamiento de mayores anchos de banda, la utilización de MIMO masivo con sistemas de antenas distribuidas y el uso de técnicas de reparto de recursos distribuidas para la coordinación de la interferencia entre celdas.

En primer lugar, esta Tesis analiza si existe un límite fundamental en la mejora de las prestaciones en relación a la densificación en las redes celulares, o si por el contrario, la densificación brinda ganancias en las prestaciones de la red de manera indefinida. Con este fin, las prestaciones de las UDNs se evalúan utilizando un modelo analítico que consiste en un despliegue de red unidimensional con estaciones base equiespaciadas, en el que la distancia entre estaciones base se disminuye hasta alcanzar el limite de densificación cuando ésta se aproxima a 0. Las tasas alcanzables en redes con distintas distancias

entre estaciones base son analizadas, considerando distintos niveles de potencia disponible en la red y varios grados de cooperación entre celdas.

Además, el comportamiento de las UDNs se estudia junto al uso masivo de antenas y la utilización de anchos de banda mayores. Más concretamente, las prestaciones de ciertas técnicas híbridas MIMO de precodificación y conformación de haces se examinan tanto en escenarios de exteriores como de interiores, considerando múltiples celdas y usuarios y trabajando en la banda de frecuencias milimétricas. Por una parte, los esquemas de conformación de haces aplicados en estaciones base con arquitectura híbrida se analizan en función de la disponibilidad limitada de cadenas de radiofrecuencia, identificando los puntos fuertes y débiles de estos esquemas en un escenario urbano denso. Por otra parte, se evalúan las prestaciones de ciertos esquemas de precodificación híbrida en escenarios de interiores, utilizando distintas estrategias de despliegue de red y centrando la atención en los sistemas de antenas distribuidos o DAS. Además, se propone un algoritmo de precodificación híbrida distribuido para su aplicación en DAS, y se evalúan y comparan sus prestaciones con las de los algoritmos de precodificación híbrida utilizados en los otros despliegues. Por último, se investiga el impacto de algunas limitaciones prácticas y ciertas deficiencias introducidas por el uso de dispositivos no ideales en las prestaciones de todos los esquemas anteriores, tanto para escenarios de exteriores como de interiores.

Finalmente, el estudio de las UDNs se completa con el análisis de su principal limitación, que es el nivel creciente de la interferencia entre las celdas de la red. Para tratar este problema, se propone un algoritmo de control de interferencias basado en la partición de recursos, el cual utiliza un patrón de reuso en tiempo y frecuencia que coordina las decisiones de asignación de recursos en grupos de celdas. Las prestaciones del algoritmo propuesto son evaluadas y comparadas con las de otras técnicas de asignación de recursos.

Completado el estudio presentado en esta Tesis, se puede afirmar que las UDNs tienen un gran potencial para la consecución de los ambiciosos requisitos planteados para la futura 5G. Sin embargo, sin el uso conjunto de mayores porciones del espectro, adecuadas técnicas de control de la interferencia y el uso masivo de antenas, las UDNs pueden convertirse en serios obstáculos para los operadores móviles. Los resultados derivados de la evaluación de prestaciones de estas tecnologías confirman el gran aumento de la capacidad de las redes obtenido mediante el uso masivo de antenas y la introducción de mecanismos de coordinación de interferencias que, además, proporcionan un ahorro de energía en las UDNs.

Resum

A partir de l'any 2020 es preveu un nou paradigma de comunicació en la societat, degut a l'aparició de nous serveis de banda ampla i la nova era de la Internet de les coses. El conjunt de requeriments imposat per aquestes noves aplicacions és molt ampli i divers, i té com a principal objectiu proporcionar conectivitat universal i de banda ampla. En les últimes dècades, la comunitat científica ha estat treballant en la definició de la Cinquena Generació (5G) de xarxes mòbils, que proveirà els mecanismes necessaris per a garantir aquests exigents requeriments. En aquest marc, s'han identificat tres mecanismes claus en les xarxes 5G per a aconseguir l'increment necessari en la capacitat: l'augment de l'eficiència espectral a través de, per exemple, l'ús de tecnologies MIMO massives, la utilització de majors porcions de l'espectre i la densificació mitjançant el desplegament de més estacions base per àrea.

Aquesta Tesi doctoral aborda la densificació com a principal mecanisme que permetrà la conectivitat de banda ampla i universal requerida en la futura 5G. Amb aquest objectiu, aquesta Tesi es centra en l'estudi de les xarxes ultra denses (UDNs). Concretament, el conjunt de tecnologies habilitants que poden dur a les UDNs a la seua màxima eficiència així com a les seues màximes prestacions és analitzat, incloent l'ús d'altes freqüències per a l'aprofitament de majors amplàries de banda, la utilització de MIMO massiu amb sistemes d'antenes distribuïdes i l'ús de tècniques distribuïdes de repartiment de recursos per a la coordinació de la interferència entre cel·les.

En primer lloc, aquesta Tesi analitza si existeix un límit fonamental en les prestacions en relació a la densificació en les xarxes mòbils, o si al contrari, la densificació proporciona ganàncies en les prestacions de les xarxes de manera indefinida. Amb aquesta finalitat, les prestacions de les UDNs s'avaluen utilitzant un model analític que consisteix en un desplegament unidimensional amb estacions base equidistants, en les quals la distància entre estacions base es redueix fins assolir el límit de densificació quan aquesta distància s'aproxima a 0. Les taxes assolibles en xarxes amb diferents distàncies entre estacions base

s'analitzen considerant diferents nivells de potència disponible i varis graus de cooperació entre cel·les.

A més, el comportament de les UDNs s'estudia conjuntament amb l'ús massiu d'antenes i la utilització de majors amplàries de banda. Més concretament, les prestacions de certes tècniques híbrides MIMO de precodificació i conformació de feixos s'examinen tant en escenaris d'exteriors com d'interiors, considerant múltiples cel·les i usuaris i treballant en la banda de freqüències mil·limètriques. D'una banda, els esquemes de conformació de feixos aplicats a estacions base amb arquitectures híbrides és analitzat amb disponibilitat limitada de cadenes de radiofreqüència, amb l'objectiu d'identificar els punts forts i dèbils d'aquests esquemes a un escenari urbà dens. D'altra banda, s'avaluen les prestacions de certs esquemes de precodificació híbrida en escenaris d'interior, utilitzant diferents estratègies de desplegament i centrant l'atenció en els sistemes d'antenes distribuïdes (DAS). A més a més, es proposa un algoritme de precodificació híbrida distribuïda per a la seua aplicació en DAS, i s'avaluen i comparen les seues prestacions amb les dels algoritmes de precodificació híbrida utilitzats en els altres desplegaments. Per últim, s'investiga l'impacte de les limitacions pràctiques i altres deficiències introduïdes per l'ús de dispositius no ideals en les prestacions de tots els esquemes anteriors, tant per a escenaris d'exteriors com d'interiors.

Finalment, l'estudi de les UDNs es completa amb l'anàlisi de la seua principal limitació, que és el nivell creixent d'interferència entre les cel·les de la xarxa. Per tractar aquest problema, es proposa un algoritme de control d'interferències basat en la partició de recursos, el qual utilitza un patró de reutilització en temps i freqüència que coordina les decisions d'assignació de recursos entre grups de cel·les. Les prestacions de l'algoritme proposat s'avaluen i comparen amb les d'altres tècniques d'assignació de recursos.

Una vegada completat l'estudi presentat en aquesta Tesi, es pot afirmar que les UDNs tenen un gran potencial per l'aconseguiment dels ambiciosos requeriments plantejats per a la futura 5G. Tanmateix, sense l'ús conjunt de majors amplàries de banda, apropiades tècniques de control de la interferència i l'ús massiu d'antenes, les UDNs poden convertir-se en seriosos obstacles per als operadors mòbils. Els resultats derivats de l'avaluació de prestacions d'aquestes tecnologies confirmen el gran augment de la capacitat de les xarxes obtingut mitjançant l'ús massiu d'antenes i la introducció de mecanismes de coordinació d'interferències que, a més, proporcionen un estalvi d'energia en les UDNs.

Acknowledgements

I would like to express my gratitude to all those who helped me to accomplish this Thesis. First and foremost, I would like to thank my supervisors. Thanks to Professors Jose F. Monserrat and Narcís Cardona for giving me the opportunity to conduct my research within the Mobile Communications Group, surrounded by a great team of scientists. Thanks to Dr. Daniel Calabuig for his valuable help in many scientific issues and for many fruitful technical discussions. I would like to thank specially Professor Jose F. Monserrat for his guidance and support along all these years. I really appreciate the excellent opportunities he offered me to grow personally and professionally.

It is also a pleasure to thank three excellent researchers that invited me to visit their research institutions. Thanks to Dr. Lars Thiele for accepting me as a member of his group during my stay in the Fraunhofer Heinrich Hertz Institute in Berlin. It was a great experience where I got to know a very nice group of people, specially Kai, Martin and Miguel. I am also grateful to Dr. Hans-Peter Mayer for giving me the opportunity to complete an internship in Bell Labs Stuttgart. During this time, I was able to work together with brilliant professionals from which I learned a lot, such as Volker and Hardy, and specially Paolo, who was a major support during my stay in Bell Labs. I should not forget to thank the nice international team led by Genevieve, which made my stay there even nicer. Last but not least, I would like to thank Professor Stephan ten Brink for inviting me to visit the Institut für Nachrichtenübertragung at the University of Stuttgart, and for his trust and confidence from the very beginning of my stay. I enjoyed my time at the institute, surrounded by great people like Katie, Xiaojie, Christian and many others.

I would also like to thank my colleagues at iTEAM, Sandra and David MS, for their continuous support and good teamwork. And all my colleagues at the institute for making all this way much more pleasant: Salva, Miguel, Pablo, Jordi, Juanan, Jorge, Charlie, Irene, Tere, Alicia, David G, Conchi, Jordi Joan,

Dani, Toni, Nora and many others. It has been a pleasure to share so many working days with all of them.

I thank Dr. Matías Toril, Dr. David López-Pérez, and Dr. David Gutiérrez for their work as reviewers of the Thesis. Special thanks also to Dr. David Gutiérrez, Dr. Carmen Botella, and Dr. Gema Piñero for acting as members of the committee.

Por último, me gustaría agradecer a mi familia y amigos todo el apoyo mostrado durante estos años y sus ánimos en los momentos más duros. Gracias a mis padres, Pilar y Pedro, por su apoyo incondicional en todo momento, por creer siempre en mis posibilidades y ayudarme a creer en ellas a mi también, pero sobre todo por haberme enseñado cuales son las cosas verdaderamente importantes en la vida. Thanks to Marc for his support and patience during these years, for his understanding in the periods of more stress, and for giving me an extra motivation to complete this Thesis.

Sonia
Valencia, July 2017

Contents

List of acronyms

3D	3-Dimensional
3GPP	Third Generation Partnership Project
4G	Fourth Generation
5G	Fifth Generation
5GPPP	Fifth Generation Public Private Partnership
ABF	Analog Beamforming
ABS	Almost Blank Subframes
BB	Baseband
BS	Base Station
CDF	Cumulative Distribution Function
CRE	Cell Range Extension
CSI	Channel State Information
DAB	Distributed Analog Beamforming
DAS	Distributed Antenna Systems
DFT	Discrete Fourier Transform
DHP	Distributed Hybrid Precoding
DP	Digital Precoding
DTFR	Dynamic Time and Frequency Reuse

EGT	Equal Gain Transmission
eICIC	enhanced Inter-Cell Interference Coordination
FB	Frequency Block
FDD	Frequency Division Duplexing
FFR	Fractional Frequency Reuse
FS	Frequency Selective
HBF	Hybrid Beamforming
HetNet	Heterogeneous Network
HP	Hybrid Precoding
ICI	Inter-Cell Interference
ICIC	Inter-Cell Interference Coordination
InH	Indoor Hotspot
INR	Interference to Noise Ratio
IoT	Internet of Things
ITU	International Telecommunication Union
ITU-R	International Telecommunication Union Radiocommunication
LoS	Line of Sight
MC	Macrocell
METIS	Mobile and wireless communications Enablers for Twenty-twenty (2020) Information Society
MIMO	Multiple Input Multiple Output
MMSE	Minimum Mean Square Error
mmW	millimeter wave
MRT	Maximum Ratio Transmission
MU	Multi-User

NFS	Non Frequency Selective
NLoS	Non Line of Sight
NPSb	Non-Preferential Sub-band
OFDM	Orthogonal Frequency Division Multiplexing
OSb	Ordinary Sub-band
PAPC	Per-Antenna Power Constraints
PF	Proportional Fair
PFR	Partial Frequency Reuse
PPP	Poisson Point Process
PSb	Preferential Sub-band
RAU	Remote Antenna Unit
RB	Resource Block
RF	Radio Frequency
RPS	Reduced Power Subframes
RR	Round Robin
RSS	Received Signal Strength
RZF	Regularized Zero Forcing
SC	Small Cell
SFR	Soft Frequency Reuse
SINR	Signal to Interference plus Noise Ratio
SIR	Signal to Interference Ratio
SISO	Single Input Single Output
SNR	Signal to Noise Ratio
SON	Self-Optimized Network
SU	Single-User

TDD	Time Division Duplexing
UDN	Ultra Dense Network
UE	User Equipment
ULA	Uniform Linear Array
WRR	Weighted Round Robin
ZF	Zero Forcing

Chapter 1

Introduction

1.1 Background

In the last years, the evolution of wireless systems and, more specifically, of the end-user devices, are enabling the emergence of a rich variety of new mobile applications in diverse fields such as agriculture, locomotion, health care and manufacturing, among others. As a consequence, a huge increase of mobile networks capacity will be essential for beyond 2020 societies, not only to satisfy the exponential rise of user traffic derived from these new mobile broadband services but also to allow for the massive connectivity of devices required for their application. Motivated by the inability of current technologies to satisfy such requirements, research community has been actively working during the last decade towards the establishment of the new Fifth Generation (5G) of mobile wireless networks. Three main paradigms are being considered as possible enablers to boost network capacity in 5G: the increase of the cell spectral efficiency, the use of larger amounts of spectrum, and the ultra-densification of cells [1, 2].

1.1.1 Next generation wireless systems

The increase in the number of connected devices and the wide diversity of their service requirements impose an additional burden to the already loaded Fourth Generation (4G) wireless networks. Due to this, new enhanced capabilities must be added up in the next generation wireless systems to those already available in 4G networks. With this aim, industrial partners and academia are working together in the definition of the 5G system concept and the radio access technologies that will provide the future communication needs.

In this line, the first efforts were dedicated to identify the main use cases and scenarios of the 5G. In the Fifth Generation Public Private Partnership (5GPPP) projects, 6 families of use cases that represent the future of mobile networks have been identified [3]:

- Urban dense: this family of use cases encompasses both indoor and outdoor urban environments, considering dynamic hotspots, cloud services, smart homes, etc.
- Broadband everywhere: the focus of these use cases is to provide services with more than 50 Mbps in suburban, rural and high speed trains.
- Connected vehicles: in this family are grouped the vehicular communications use cases, such as road safety, traffic jam, automatic driving and mobile broadband in vehicles.
- Future smart offices: this set of use cases addresses the indoor communications requiring high capacity and low latency, as it is the case of the virtual reality or smart offices.
- Low bandwidth Internet of Things (IoT): in this group are collected the use cases that require a very large number of connected objects, like networks with massive deployment of sensors, smart cities, etc.
- Tactile internet or automation: this family includes use cases in which the reliability of the communication is extremely important, as in remote control or remote surgery applications.

As pointed out by the families of use cases identified for the future communications, the requirements of 5G networks are diverse. Indeed, while the most important service requirements for road safety applications are the reliability and low latency, for smart cities the massive connectivity of devices is much more important, highlighting the variability of the use cases demands. In order to synthesize the needs of all the aforementioned use cases, the large variety of requirements to be supported by 5G networks has been outlined in the following points [4]:

- 1 to 10 Gbps data rates in real networks, what implies a 10 times increase from the theoretical peak data rate in LTE networks.
- 1 ms end to end latency.
- Higher bandwidth per area.
- Enormous number of connected devices to support the emerging IoT.

- Perceived availability of 99.999% of the time.
- Almost 100% coverage for anywhere connectivity.
- Reduction in energy usage by almost 90% to support the progressive introduction of green communications.
- High battery life for the devices, by reducing their power consumption.

The research community is exploring new mechanisms to reach these challenging capacity requirements. Among them, disruptive changes including renovated system designs with device-centric architectures, or the use of smarter devices with local caching and interference rejection capabilities are pointed out as interesting research lines [5]. Even so, the three fundamental research directions identified for the improvement of network capacity in 5G are the increase of the spectral efficiency by means of massive Multiple Input Multiple Output (MIMO) technology [6], the use of larger amounts of spectrum by utilizing additional frequency bands such as the millimeter wave band [7], and the network densification by deploying more base stations per area [8], as exemplified in Figure 1.1.

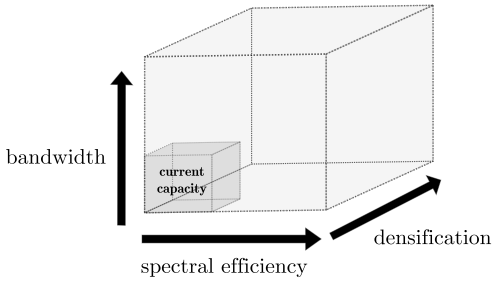

Figure 1.1: The three main directions to improve network capacity in 5G wireless systems.

Massive MIMO technology is characterized by the use of antenna arrays with many more elements per site than in current systems. This feature allows Base Stations (BSs) to achieve larger beamforming gains, increasing their cell spectral efficiencies. Besides, narrower beams can be conformed for the transmission to a higher amount of users in parallel, what makes this technology especially useful to support the increasing number of connections expected by the new device-to-device and machine-type communications services [1]. On the other hand, the use of the available spectrum in the millimeter wave (mmW)

band enables the allocation of much larger bandwidths, resulting in a great increase of the data rates [7]. Furthermore, at these higher frequencies antennas can be miniaturized, which makes the application of massive MIMO in mmW even more appealing. Although the combination of larger bandwidths and higher spectral efficiencies provides a significant growth in system capacity, it has been proved in contemporary cellular networks that, in order to satisfy growing user demands, they should be accompanied by further cell densification [8], understood as the deployment of more base stations per unit area. Indeed, densification is considered as the key enabler for the demanding requirements of future networks, without which it will clearly not be sufficient to provide the ubiquitous immerse connectivity requirements of the 2020-and-beyond mobile society.

1.1.2 Ultra Dense Networks deployment

Ultra Dense Networks (UDNs) are one of the main scenarios used to illustrate the 5G network challenges, which addresses the high traffic demands via infrastructure densification [9]. Several definitions for UDN can be found in the literature, being the most widely accepted the ones considering [10]: a) networks in which the number of deployed base stations is greater than the number of active users; b) networks in which the density of BSs is higher than 10^3 cells/km^2. In both cases, UDNs imply the denser deployment of access points in comparison to current conventional deployments.

From an architectural point of view, spatial densification can be implemented either by adding more BSs per area or increasing and distributing the number of deployed antennas by using Distributed Antenna Systems (DAS) [8]. As a result, all kind of cells may coexist in ultra dense deployments, such as macrocells, picocells or relays, what leads to consider the UDNs as a further evolution of Heterogeneous Networks (HetNets) [11]. Nevertheless, the deployment of additional macro base stations with the corresponding elaborated site planning would involve significant costs. This is the reason why, in UDNs, Small Cells (SCs) are preferred to conventional macrocells, since they are a simpler cost-effective alternative for spatial densification. Indeed, densification is expected to be dominated by SCs, thanks to their ability of being deployed opportunistically in a very irregular fashion [11].

The main benefits of UDNs can be summarized as follows:

- The deployment of more BSs or antennas per unit area increases the spatial reuse of the resources. As a result, more resources can be allocated to each user, improving the final data rates delivered to them.

- The higher density of BSs or antennas results in shorter distances between the users and their closest access point, improving the average radio link quality and increasing the probability of Line of Sight (LoS) transmission.

The latter feature turns UDN into a very suitable scenario for the use of mmW, where large amounts of bandwidth enable very high throughput under LoS conditions. Indeed, the synergy between UDNs and the logical combination of massive MIMO and mmW technologies brings important rewards that motivate the joint analysis of these three mechanisms.

On the other hand, densification also presents big challenges to the network design. The most important one is how to face the growing level of interference provoked by the increased number of deployed base stations. The closer proximity of users and access points reduces not only the path loss between a user and its serving BS, but also the distance to the non-serving base stations in the network that will act as strong interfering sources. This side effect makes the application of enhanced interference coordination schemes mandatory in UDNs. Besides, mobility has also been pointed out as an important issue in dense deployments, where an excessive number of handovers among cells may deteriorate the user experience. Backhaul dimensioning as well as energy efficiency are other important challenges in UDNs [12]. This Thesis focuses on the management of interferences, leaving for further research the other aspects.

1.2 State of the art analysis

This section presents an analysis of the state of the art in the field of study of this Thesis based on a deep literature review. This analysis is divided into four parts. The first is devoted to review the most important works related to the study of the theoretical limits of densification. The second part presents an overview of the Distributed Antenna Systems (DAS) topic in the literature. The third part deals with massive MIMO in millimeter wave frequencies. Finally, the last part conducts a revision of prior art regarding Inter-Cell Interference Coordination (ICIC) in cellular networks.

1.2.1 Limits of densification

Densification is the most promising solution to provide ubiquitous broadband connectivity. Thanks to the higher density of nodes deployed, the spatial resource reuse is increased, and the distance between users and access points reduced, what improves the average radio link quality. However, the close proximity of non-serving base stations increases also the interference in such a way that the application of ICIC techniques becomes unavoidable [11, 13].

These techniques reduce the spatial resource reuse, and hence, they counteract, to certain extent, one of the main benefits of UDNs. All this raises the question of whether a fundamental limit of densification exists [10].

In a first attempt to analyze the limits of densification from a theoretical point of view, the work in [14] derived analytically the Signal to Interference Ratio (SIR) distribution in a cellular network modeled by a homogeneous Poisson Point Process (PPP). The main conclusion drawn by [14] states that, as long as noise power can be considered negligible in comparison to the interference, Signal to Interference plus Noise Ratio (SINR) remains constant when BSs density increases. In other words, SINR is independent of the BSs density and thus, system throughput increases linearly with the number of deployed BSs. Same conclusion was obtained for a more generalized scenario in [15] consisting of a multi-tier heterogeneous cellular network.

Further studies presented in [16] and [17] introduced the consideration of more sophisticated path loss models. In particular, these works analyze the SINR distribution in cellular networks when considering a dual-slope path loss model with a different path loss exponent for the near-field and far-field regions. This allows for the inclusion of the subduction effect that occurs in the near-field region, which consists in the reduction of the path loss exponent when the distance between transmitter and receiver decreases due to densification. Analytical results show that under the dual-path loss model consideration and for interference-limited scenarios, SINR decreases monotonically as the BSs density increases, which contrasts with the behavior observed with standard path loss models in [14] and [15]. With regards to system throughput, [16] and [17] concluded that its behavior with densification is determined by the specific value of the near-field path loss exponent. More specifically, it can be described by dividing the near-field path loss exponent in three regions: values larger than 2 provide a linear scale of the system throughput with densification, values between 1 and 2 provide a sublinear scale of the throughput with base station density, and values below 1 lead to zero throughput in the limit of densification.

The system models used in [14–17], however, present several limitations. The most relevant are the following:

- Fixed power per BS is considered in all of them, resulting in a growing amount of power per area as the density of BSs increases. This consideration prevents an isolated analysis of the effects of network densification, and the impact of having increasing power per area.

- The models do not limit the minimum distance between users and BSs, i.e. they can be at distance zero. This fact together with the used path loss model implies that the received signal power can be greater than that

of the transmitted signal, and even infinite when the distance is zero. This behavior is highly unrealistic and may lead to wrong conclusions.

- Each BS is assumed to always have an active user, and hence, BS density is lower or equal to user density. This contrasts with one of the widely accepted definitions of UDN in which the density of access points is considered ultra-dense if it is greater or equal to the density of users. This fact can be used to question whether these works actually consider UDNs.

- BSs do not apply any type of interference coordination technique among them, essential in UDNs where the high reuse of resources generate high level of interference. Note that the application of any kind of resource management would modify the expression of SIR derived in these works, according to the particular criterion maximized by the resource allocation algorithm applied. A common approach in cellular networks is to choose a proportionally fair resource allocation algorithm [18].

A different system model, which typically consists on a one-dimensional deployment with infinite base stations, was proposed by Wyner [19] to analyze the effect of interference. Even though this model has been of great interest thanks to its capability to yield new insights about cellular networks by means of an analytical simple approach [20], it presents some major limitations [21]:

- Wyner model assumes that interference takes place only between adjacent base stations, which leads to very inaccurate conclusions in the case of UDNs, since a large amount of interference is neglected.

- The contribution of the adjacent cells to interference is simplified to a deterministic value, which implies that user locations are predefined and fixed.

1.2.2 Distributed Antenna Systems

In order to address the huge data rate demands and high connectivity and mobility required by next generation mobile networks, a deep change in the cellular architecture design is needed. Specially for indoor users, which represent approximately the 80% of the total traffic conveyed by a network, the definition of new deployment strategies is essential [22]. Together with the use of small cells, DAS was proposed as a promising deployment strategy to improve coverage and capacity in large indoor zones [23].

DAS are network architectures in which the antenna elements of a BS are geographically distributed throughout the coverage area. The main advantage of this approach is that the average distance from any point of the scenario

to the nearest antenna is reduced [24]. Due to this fact, the link budget, coverage and outage probability can be in most cases improved. Although the deployment of SCs can be more flexible and scalable, the use of DAS as a means for densification allows a simpler coordination among the different antennas distributed over the space, thanks to the high-bandwidth and low latency dedicated connection between them and BSs, such as wires, fiber optic or Radio Frequency (RF) links [25].

DAS can be deployed using either passive or active architectures. On the one hand, passive DAS is the most used approach for indoor [26], where only passive components are used to distribute the signals over the space, being a cost-effective solution for medium-sized distances. On the other hand, active DAS are the best solution for large areas, since they can provide better radio link performances and higher data rates but at the expense of a more elevated costs of deployment and maintenance [26]. Several works studied active DAS from an energy efficiency perspective [27–29], proposing power allocation schemes that distribute the transmission power among Remote Antenna Units (RAUs) in order to maximize the energy efficiency in single-cell scenarios with multiple users. The work in [30] conducted a performance comparison between active and passive DAS in an indoor scenario.

Either with active or passive architectures, DAS can be viewed as a multi-antenna system where the antennas are not co-located with the BS [25]. In order to make the most of the MIMO channel richness, advanced Single-User (SU) MIMO and Multi-User (MU) MIMO techniques can be applied to DAS. The simplest DAS transmission schemes select the RAU with lowest path loss to the user, what reduces the total network transmission power and increases the battery life. As a result of the lower transmission power, the interference level in the network is reduced, and hence, the system capacity is increased [31]. However, these schemes cannot benefit from the natural RAUs cooperation ability of DAS. At the other end, the transmission from every RAU to serve a user can be inefficient, due to the significant path loss differences between the distributed antennas in DAS, so techniques selecting only a subset of the antennas for transmission can bring large benefits to the system [32]. The performance of SU and MU MIMO techniques in DAS with different degrees of cooperation among RAUs was analyzed in [24] and [33]. Both works concluded that large performance gains are achieved when enhanced antenna selection schemes are applied.

In the last years, the joint utilization of DAS and mmW band for indoor scenarios has been pointed out by the research community as the mechanisms to improve indoor network capacity [22]. The large penetration losses at mmW caused by the external surfaces of the buildings make indoor scenarios to be well

isolated from outdoor interference while, at the same time, indoor materials are shown to introduce relatively low losses [7].

1.2.3 Massive MIMO in millimeter waves

A promising technology to meet the challenging 5G data rate requirements is the use of massive MIMO systems [6]. Defined as multi-antenna configurations in which the number of antennas is much higher than the number of users to be served, massive MIMO implies the use of, at least, an order of magnitude more antenna elements than in current systems [34]. The application of MIMO techniques has been used either to compensate the propagation losses of backhaul and access links through beamforming, or to boost capacity with multi-stream transmission. With the use of large antenna arrays, current trends point towards the joint application of MIMO spatial multiplexing techniques and beamforming to better exploit the richness of the channel [35].

Increasing the number of antennas brings also important challenges in the system design. From a signal processing perspective, transmission with massive arrays increases the processing complexity derived from the computation of the required precoders when precoding schemes are applied to hundreds of antennas. Due to this, low complexity linear Digital Precoding (DP) techniques are preferred in massive MIMO systems over non-linear precoding techniques able to achieve the capacity of the channel [36]. In particular, linear precoding techniques such as Maximum Ratio Transmission (MRT) or Zero Forcing (ZF) are shown to provide near-optimal performance with an increasing number of antennas [37]. Another drawback of massive MIMO technology is the large physical size of the antenna arrays at currently used cellular frequencies, what prevents for its successful incorporation into cellular networks. As a solution, massive MIMO is being considered in conjunction with mmW frequencies [34, 38], where antenna arrays of reasonable physical sizes are feasible [39].

With the use of mmW technology, the application of the aforementioned DP techniques using a fully digital architecture at the transmitter is not suitable. The reason is that multi-antenna DP is carried out at baseband and, thus, an architecture with as many RF chains as antenna ports to perform the digital to analog data conversion and subsequent upmixing to RF is required for the application of DP techniques. However, the use of digital architectures with one RF chain per antenna is not only a very costly option for massive MIMO systems at mmW, but it also leads to a extremely high power consumption [34, 40]. Motivated by this, the research community has focused its interest in alternative transmission schemes based on Analog Beamforming (ABF) and Hybrid Beamforming (HBF) architectures, where all or part of the processing is based on RF beamforming [41].

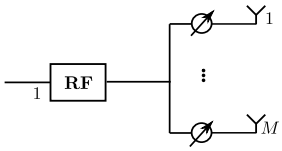

Figure 1.2: Analog beamforming architecture.

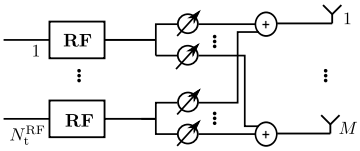

Figure 1.3: Full-connected hybrid architecture.

On the one hand, ABF architecture is the most simple approach for massive MIMO in mmW and consists of a single RF chain connected to the antennas via phase shifters [34] (see Figure 1.2). The main limitation of this architecture is that it is not possible to realize spatial multiplexing for multi-stream or multi-user transmission. As an alternative, HBF architectures provide a good compromise between ABF and DP with respect to both flexibility and complexity. Several variants of HBF architectures were proposed in the recent years [42–44].

For a transmitter considering M antennas, the full-connected architecture [42] is shown in Figure 1.3. It consists of a limited number of RF chains $N_t^{RF} < M$ and a set of M phase shifters applied to each RF chain. The outputs of the i-th phase shifters of every RF chain are combined to feed the i-th antenna element in the array. Using this architecture, N_t^{RF} data streams can be simultaneously transmitted with full array gain.

Another interesting architecture with reduced complexity is the sub-array configuration shown in Figure 1.4, where the elements of the antenna array are divided in as many sub-arrays as available RF chains [43]. Thanks to this, the number of necessary phase shifters is reduced to M, compared to the $N_t^{RF} \times M$ necessary at the full-connected architecture. However, the N_t^{RF} transmitted data streams come with a lower array gain due to the smaller number of elements per sub-array. Based on this architecture, a novel technique was presented in [44], where the specific antenna elements to be grouped at each sub-array can be dynamically selected to optimize the system performance according to the long-term channel characteristics.

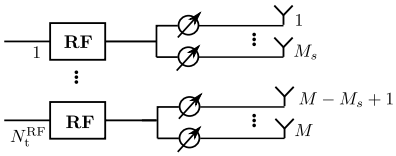

Figure 1.4: Subarray hybrid architecture.

Several precoding approaches for HBF architectures were proposed in the last years, all of them using a substantially reduced number of RF chains with respect to the number of antennas. In particular, hybrid precoding for single-user scenarios was addressed in [45–48] for both transmitter and receiver implementing hybrid architectures. The work in [45] proposed a precoding solution for large antenna arrays systems based on the sparse nature of the channel. By considering a single-path channel model, [46] presented a multi-resolution codebook with the ability to adjust the beamwidth for the transmissions according to performed estimations of the channel between the base station and the user. Assuming perfect channel state information at the transmitter, [47] proposed four hybrid precoding strategies providing different trade-offs between computational complexity and performance. Finally, [48] analyzed the minimum number of RF chains required to achieve the same performance as fully digital precoding schemes given a certain number of transmitted data streams. Besides, this works provided an heuristic algorithm to design the hybrid precoding when the number of RF chains is below that minimum.

Further studies analyzed the performance of massive MIMO at mmW by including more realistic scenarios and non-ideal assumptions. [49] assessed the performance of several multi-user techniques with large scale antenna arrays with calibration errors. The work in [50] presented a hybrid precoding algorithm for multi-user scenarios and analyzed the rate loss when only limited feedback is available and channel information is quantized. Furthermore, a preliminary performance study of hybrid precoding considering a realistic channel model was carried out for a single-link scenario in [43]. Moreover, some works are found in the literature regarding the presence of non-ideal devices in real implementations, which may bring in several error sources affecting the performance of the algorithms under study. In particular, real phase shifter implementations introduce phase errors whose magnitude was studied in [51, 52], and non-ideal combiners introduce power losses that were characterized, for instance, in [53]. The effect of hardware-constrained base stations in massive MIMO systems was extensively analyzed in [54], where a scaling law of the increase of some particular imperfections with the number of antennas was provided. In addition, hardware constraints impose practical limitations that

should be desirably considered in the algorithms design. This was highlighted in [55] and [56], which propose constant envelope precoders suitable for the use of power-efficient RF power amplifiers as a constraint to avoid the problems of such non-ideal amplifiers with their inherent non-linear behaviour.

1.2.4 ICIC in cellular networks

The first ICIC schemes were designed to be applied on Macrocell (MC) deployments, where cell edge users suffer from high levels of interference from neighbor cells. These schemes are based on different power and resource allocation mechanisms, being one of the most important ones those based on time and frequency resource partitioning. This is the case of the Fractional Frequency Reuse (FFR) based techniques, which consist in the application of a frequency reuse factor of one in areas close to the BS, and a higher factor of reuse in areas close to the cell border with the aim to reduce the interference among cells [57]. Several variants of FFR are found in the literature, depending on how the power and bandwidth are distributed between the center and the edge of cells. In Partial Frequency Reuse (PFR) schemes, sub-bands assigned to cell-edge users and cell-center users are disjoint [58–60]. Contrarily, Soft Frequency Reuse (SFR) schemes allow for the use of the whole bandwidth at the center of the cell, by reducing the transmitted power on those sub-bands that are also used at the cell-edge [61]. SFR is more bandwidth efficient than PFR, but it results in more interference to both cell-center and cell-edge users. Resource partitioning has also been proposed simultaneously in both time and frequency domains in [62].

One of the challenges of FFR schemes is how to define the criterion to consider that a user is located at the center or at the border of the cell. Another important challenge is the selection of the optimal number of sub-bands in which the total bandwidth has to be partitioned to be assigned to inner and border areas. In line with this, the optimal frequency reuse factor at the cell-edge as well as the bandwidths to assign to the center and the edge of the cell are determined for a regular deployment in [63], by solving an optimization problem. However, [64] showed that in real networks with irregular cell patterns, the number of interfering cells and the amount of interference varies highly from cell to cell, so optimum parameters obtained in [63] may not be suitable. Indeed, it is remarked that a reasonable definition of border areas should be based on SINR instead of distances. Besides, the scheduling fraction of sub-channels may vary with the network topology, so static designs might not improve the global throughput of the network.

The references aforementioned apply a static configuration of the resource partitioning, so they are not able to adapt to dynamic cell load variations.

More sophisticated schemes including dynamical capabilities for MC deployments were proposed in [65–69]. [65] proposed a dynamic FFR scheme with the ability to redistribute the radio resources among cells in order to adapt to their load conditions. This adaptation is accomplished via a graph approach in which the resource and power allocation problems are translated to a graph coloring problem. A channel and power allocation sub-optimal algorithm was proposed in [66] to maximize cell-edge users throughput in a decentralized fashion. Although in this scheme the definition of cell-center and cell-edge is fixed, resource allocation is performed in a dynamical way and with minimum coordination between base stations. Another dynamic FFR approach was designed in [67], where classification of users as cell-edge or cell-center is performed according to their experienced SINR. A variable threshold of SINR is used to balance user classification and the bandwidth used for each group is optimized to adapt to the network dynamics. The cell-edge sub-bands assigned to each cell can be dynamically changed by using an X2 interface. Also based in the exchange of messages, the work in [68] proposed a dynamic FFR scheme where frequency resources are divided in different categories depending on their priority for transmission. Cell-edge users allocated to those resources with maximum priority are able to sense their strongest interfering BSs and to request them to reduce transmit power over them. Lastly, [69] presented a game-theory based algorithm for self-organizing networks, where a centralized network manager configures the frequency reuse and power allocation patterns according to the information feedback sent by the users. Moreover, users select the cell they connect to based on the configuration decisions of the central manager, and are able to stay silent if they do not achieve a minimum target SINR.

With the recent inclusion of SCs as a mechanism to further improve network capacity through densification, the variety of scenarios to be addressed by the ICIC algorithms has been enlarged, including indoor and outdoor deployments, with and without MC coverage [70]. HetNets arise as scenarios in which nodes with different level of power are deployed in the same coverage area, usually sharing the same frequency band, to maximize area spectral efficiency by taking advantageous of improved spatial reuse [71]. On the one hand, picocells are deployed by operators for offloading the traffic from the overlaid MC, especially in areas of heavy traffic, and for removing coverage holes typically present in MC networks. On the other hand, femtocells are mainly deployed indoors, where conventional macro-cellular networks may most likely fail to deliver broadband experience to users because the transmitted signal faces high attenuation when passing through walls [71].

The large difference of transmission power between SCs and MCs in HetNets causes that the area served by an SC may comprise only a few users located in its close proximity, which receive the strongest downlink Received Signal

Strength (RSS) from the SC [72]. In order to extend the coverage area of the SCs, the Third Generation Partnership Project (3GPP) introduced the use of Cell Range Extension (CRE), based on adding a positive bias to the SCs RSS in the cell selection procedure. Nevertheless, CRE results in an increase of the interference created by the MC to the SC users located at the extended coverage area. In fact, it has been shown that the use of CRE in outdoor HetNets without the application of any ICIC mechanism results in a degradation of the overall network performance due to the inter-tier interference [12].

Considerable efforts have been devoted to design ICIC schemes that solve the inter-tier interference in co-channel SC and MC deployments. With this aim, Almost Blank Subframes (ABS) was introduced by 3GPP in Rel-10 [73] as a time-domain enhanced Inter-Cell Interference Coordination (eICIC) mechanism. In ABS, a set of protected subframes are used at the MC to transmit only reference signals. As a result, SC users allocated to those protected subframes experience a reduction in the amount of interference suffered from the overlaid MC, leading to an improved SINR and consequently, higher throughput. SC users situated in the expanded coverage region must be allocated to the protected subframes in order to avoid the strong interference that they receive from the MC, while the rest of users can be scheduled to any other subframe. An alternative to ABS is Reduced Power Subframes (RPS), where the MC reduces the transmission power for the data symbols at the protected subframes, instead of totally eliminating it. In both ABS and RPS, MC inform the underlaid SCs about the intended configuration of protected subframes by sending messages to them.

Several works related to ABS can be found in the literature, such as [74–78]. The work in [74] presented an ABS algorithm with fast adaptation of the ABS patterns to the network load conditions, which improves the fairness among users by means of dynamic muting decisions. A cell selection scheme for HetNets was proposed in [75] based on the expected user rate, which is estimated as a function of the proportion of configured protected subframes at the MC. Dynamic assignation of protected subframes at both MCs and SCs was presented in [76] and [77] to prevent not only inter-tier but also intra-tier interference. Protected subframes are configured in these works according to the user distribution and/or their cell association, in order to optimize the fairness among users. Finally, a performance comparison between ABS and RPS schemes for different traffic conditions and several bias values for cell selection with CRE was performed in [78].

In addition to ABS, other schemes have been proposed for ICIC in HetNets. An approach based on interference estimation in two-tier deployments was presented in [79], where an algorithm for optimizing power and bit allocation over a joint time-frequency domain is designed. The interference is sensed and

estimated over successive slots using a Markov model. The algorithm follows two different strategies: to maximize expected rate under a transmit power constraint and to minimize transmit power under the expected rate constraint. Comparison between reinforcement learning and game theory techniques for the optimization of the resource allocation in self-organized HetNets was done in [80]. A reinforcement-learning technique was presented in [81] for HetNets with closed-access femtocells. In this approach, femtocells are non-cooperative, so they need to self-organize by gradually learning from their environment, and adapting their strategy until reaching convergence. On the other hand, a case of game theory can be found in [82], where the authors proposed a scheme based on non-cooperative games, in which each femtocell user attempts to select the most appropriate subset of resource blocks in a decentralized manner in order to manage the inter and intra-tier interference in the network.

HetNets where SCs and MCs operate in different frequency bands were studied in [83][84]. In this case, inter-tier interference does not exist and thus, ICIC schemes focus on the control of the interference generated among the SCs. In [83], the authors proposed a time-domain ICIC algorithm based also on ABS. Different ABS ratios and patterns are selected at each SC to adapt to user distribution and traffic load, but only moderate gains are shown for finite buffer traffic. Additionally, a cognitive ICIC algorithm was presented in [84] for HetNets using an architecture that separates control and data planes. An analytical characterization of the received aggregated interference at a user is provided in order to decide whether it will be scheduled at a certain subframe, with the final aim of improving the user throughput.

Another scenario where only intra-tier interference prevails is indoor SC deployments, where due to the penetration losses introduced by the walls of the buildings, SCs are usually considered to be isolated from MC interference. Contrary to MC networks, in which BSs are finely deployed through cell-planning, indoor SC deployments are composed by a variable amount of nodes that are randomly deployed by customers. For that reason, Inter-Cell Interference (ICI) management in this kind of networks is even more challenging than in MC scenarios, and applied mechanisms must have the ability to adapt to changing scenarios in a dynamical and distributed manner. The application of ICIC algorithms in such isolated indoor deployments has received less attention by the research community, and some works point towards a limited benefit of using resource partitioning schemes in SC deployments [85–87]. For instance, an adaptive FFR scheme for femtocell deployments was presented in [85], showing a large improvement of the cell-edge user throughput but at the expense of a degradation of cell-center user throughput. Moreover, a self-organized FFR-based allocation algorithm for femtocell deployments was proposed in [86], but the impact of the resource partitioning on the system throughput was not ana-

lyzed. [87] emphasized the decrease of the obtained benefit of ICIC application when advanced receivers are implemented, since they are able to suppress inter-cell interference at reception. However, moderate gains were achieved for the case of femtocells networks configured as closed access, since femtocells having users in their coverage area that do not belong to their control access list generate more aggressive interference on them. This is the case of the fuzzy logic ICIC scheme proposed in [88], which shows an improvement of the system performance and the fairness among users.

UDNs can be seen as the natural evolution of HetNets, where the number of deployed SCs per area is increased significantly [11]. Although several eICIC techniques have been designed for HetNets, most of them are not suitable for their application in UDNs, since the expected increasing number of nodes in this kind of networks prevents those solutions requiring a centralized unit or high amount of coordination among nodes to be applicable. Indeed, future networks may include the ability of their nodes to self-configure and self-organize, as introduced by 3GPP with the definition of Self-Optimized Networks (SONs) capabilities as a way to reduce operational effort and increase network reaction to environment changes [89]. In this line, [90] proposed a dynamic resource scheduling procedure designed for self-organizing femtocell networks, based on a mechanism of user contention. Also, two self-organized approaches for frequency assignment in femtocell networks were presented in [91]. On the other hand, ICIC techniques based on the clustering of cells can be found in [92][93]. [92] proposed a scheme in which femtocells are grouped in virtual clusters that maximize distance among its members. Each cluster is managed independently and schedules all the sub-bands among the femtocells belonging to that cluster. Another clustering-based algorithm was applied to femtocell deployments in [93], where each femtocell creates a cluster with its interfering neighbors and coordinates with them to allocate orthogonal sets of resources to the cell-edge users of the cluster. A semi-static resource allocation scheme based on FFR and optimized using graph coloring techniques to create cluster of cells was proposed in [94] for buildings with dense femtocell deployments.

1.3 Open problems identified from the literature review

Densification has been pointed out as a straightforward mechanism to boost network capacity, thanks to the approximation of users to BSs, and the employment of a higher spatial reuse of the resources. Nevertheless, these two advantages are in turn a limiting factor for the dense networks, since they lead to higher levels of interference that might constrain the system performance.

The addition of resource partitioning techniques can alleviate the inter-cell interference in the network but at the expense of a reduction of the spatial reuse of resources. This arises the question of whether it is worth to indefinitely increase the density of nodes in cellular networks, motivating the analysis of the fundamental limits of densification. Although some works in the literature have already addressed this issue, their analysis are based on system models with several limitations that may lead to wrong conclusions, as described in Section 1.2.1. Further work is required to analyze the limits of densification by using new models that overcome these limitations [95].

In parallel to the study of the limits of densification, the integration of mmW communications with the use of UDNs has received a lot of interest in the last years. The reason is that the shorter distances between transmitter and receiver in this type of networks increase the probability of the users to be in LoS propagation conditions, making the most of the large bandwidth available for transmission in the mmW band. However, the use of mmW is accompanied by hardware limitations inherent to this technology, mainly caused by the high cost and power consumption of the radio components working at these extremely high frequencies. In this regard, an exhaustive analysis of UDNs working in the millimeter frequency band is required to identify the best architecture for these systems, including accurate channel models and more realistic scenarios with multiple cells and users. Besides, the quantification of the effect of hardware impairments and other practical limitations on real implementations is of paramount importance to better understand the mmW system performance bounds.

Another promising technology to boost network capacity, especially in indoor scenarios, is the use of DAS. In this kind of deployments, the distribution of the antennas over the coverage area of the cell also increases the probability of the users of being in LoS propagation conditions. Thanks to this, DAS appears as a natural enabler for the use of mmW in indoor deployments, and large benefits of synergy are expected from the joint utilization of both technologies. However, the use of hybrid architectures in distributed scenarios is still an unexplored topic in the literature, what brings the need for researching on hybrid precoding solutions suitable for DAS and their performance under non-ideal assumptions.

Finally, independently on the technology used, the application of mechanisms for ICIC has been identified as fundamental for a correct system performance in UDNs. ICIC solutions must provide a good compromise between spatial reuse of the resources and interference management, i.e., resource orthogonalization must be performed in such a way that the reuse of resources is maximized while guaranteeing acceptable levels of interference. Furthermore, the particularities of UDNs call for new ICIC solutions that need to be not only

scalable and distributed to be suitable for the high density of nodes, but also need to function with a limited coordination signaling among nodes to avoid overloading the already loaded backhaul link.

1.4 Objectives and Thesis scope

This Thesis aims at investigating the nature of the UDNs deployment for beyond 2020 communications, analyzing their benefits and drawbacks, evaluating their performance with current and new technologies, and proposing suitable solutions for their optimal performance. This main goal can be divided into the following partial objectives listed below.

- To use new models for UDNs characterization in [95] to analyze the limits of densification, and in particular:
  - to determine under which conditions further densification is beneficial and improves the system capacity;
  - and to identify which degree of coordination among cells is more interesting in UDNs.
- To assess the performance of UDNs using mmW bands in both outdoor and indoor deployments, including:
  - the evaluation of hybrid beamforming and precoding solutions in multi-cell and multi-user scenarios working in the mmW band;
  - the study of the suitability of DAS for indoor deployments and the comparison of its performance with other indoor deployment strategies using the mmW band;
  - and the quantification of the impact of practical limitations and hardware impairments inherent to the mmW technology on system performance.
- To identify an ICIC solution suitable for its application in UDNs. In particular:
  - to design an enhanced ICIC algorithm with scalable and distributed capabilities, reduced power consumption and simple coordination among nodes;
  - and to evaluate the proposed solution in an indoor ultra dense deployment with several degrees of densification and under different load conditions.

1.5 Thesis outline and main contributions

This Thesis is organized into five chapters as follows:

- **Chapter 2** provides an analysis of the fundamental limits of densification in cellular networks, from a theoretical point of view.
- **Chapter 3** assesses the performance of hybrid beamforming schemes in a multi-cell and multi-user scenario working in the mmW frequency band. The focus is on the study of the impact of practical limitations and hardware impairments inherent to the mmW technology on the system performance.
- **Chapter 4** proposes a distributed hybrid precoding scheme for its application in DAS indoor deployments working in the mmW frequency band. The performance of this scheme is compared to that of two other typical indoor deployment strategies, considering again the practical limitations derived from the use of hybrid architectures for mmW communications.
- **Chapter 5** introduces an eICIC algorithm suitable for UDNs indoor deployments. Its performance is evaluated for several degrees of densification and under different load conditions.
- **Chapter 6** outlines the main conclusions of this Thesis and presents the future work of this research.

The main contributions of this Thesis are summarized in the following items:

I An analysis of the fundamental limits of densification is presented, taking into consideration different coordination schemes between BSs. Results provide a more comprehensive view of UDNs behavior as a function of BS and user densities, as well as of some particular scenario parameters such as power density availability or path loss exponent propagation.

II The understanding of beamforming performance using hybrid architectures in mmW frequencies have been extended, bringing new insights about the strengths and limitations of these schemes depending on the propagation conditions among users and BSs. In addition, existing studies about the impact of practical limitations and hardware impairments are complemented with further research, including the effects of non-ideal considerations such as outdated Channel State Information (CSI), phase shifter errors, Per-Antenna Power Constraints (PAPC) or power losses introduced by real combiners.

III The benefits and drawbacks of different dense indoor deployment strategies working in the mmW frequency band are established, including regular SC deployments and DAS. A new distributed hybrid precoding algorithm is proposed for its application in DAS implementing hybrid architectures, suitable for distributed antennas and with antenna selection capabilities. Furthermore, the most suitable deployment strategy considering different practical limitations is determined for each case.

IV A new eICIC algorithm for indoor UDNs is proposed, with scalable and distributed features. Its application increases both cell-edge and cell-center user throughputs at the same time as decreases the power consumption of the cell, being an excellent solution for UDNs.

1.6 List of publications

The work developed during this Thesis made possible the publication of the following journals, conference papers, reports with special relevance and book chapters.

International journals

[J1] D. Calabuig, S. Barmpounakis, **S. Giménez**, A. Kousaridas, T. R. Lakshmana, J. Lorca, P. Lundén, Z. Ren, P. Sroka, E. Ternon, V. Venkatasubramanian, and M. Maternia, "Resource and Mobility Management in the Network Layer of 5G Cellular Ultra-Dense Networks", in *IEEE Communications Magazine*, 162-169, June 2017.

[J2] **S. Giménez**, S. Roger, P. Baracca, D. Martín-Sacristán, J.F. Monserrat, V. Braun, H. Halbauer, "Performance Evaluation of Analog Beamforming with Hardware Impairments for mmW Massive MIMO Communication in an Urban Scenario", *Sensors*, 1555-1572, 2016.

[J3] **S. Giménez**, D. Calabuig, J.F. Monserrat, N. Cardona, "Dynamic and Load-Adapting Distributed Fractional Frequency Reuse Algorithm for Ultra-Dense Networks", *Waves*, 27-34, 2015.

[J4] **S. Giménez**, J.F. Monserrat, P. Gómez, Ó. Carrasco, N. Cardona, "Realistic Implementation of X2-based Interference Management for LTE Femtocells", *Waves*, 5-13, 2013.

Journal papers under review

[S1] **S. Giménez**, D. Calabuig, S. Roger, J.F. Monserrat, N. Cardona, "Distributed Hybrid Precoding for Indoor Deployments using Millimeter Wave Band", submitted 2017.

[S2] D. Calabuig, **S. Giménez**, J.F. Monserrat, "Asymptotic Analysis of Ultra-Dense Networks based on a Spatially Periodic System Model", submitted 2017.

International conferences

[C1] **S. Giménez**, D. Martín-Sacristán, D. Calabuig, J.F. Monserrat, "Self-Configurable Coordinated Scheduling for Ultra-Dense Small Cell Deployments", *International Wireless Communications and Mobile Computing Conference*, June 2017.

[C2] **S. Giménez**, S. Roger, D. Martín-Sacristán, J. F Monserrat, P. Baracca, V. Braun, H. Halbauer, "Performance of hybrid beamforming for mmW multi-antenna systems in dense urban scenarios", *IEEE 27th Annual International Symposium on Personal, Indoor, and Mobile Radio Communications (PIMRC)*, September 2016.

Book chapters

[B1] J. Cabrejas, D. García, I. Alepuz, C. Herranz, and **S. Giménez**, "Tecnologías SON", en *3GPP LTE-Advanced: Hacia la 5G móvil*, N. Cardona, M. García, J.F. Monserrat, J. Olmos, Marcombo S.A., 2017.

Reports with special relevance

[R1] M. Maternia, A. Kousaridas, O. Aydin, S. Valentin, Z. Ren, M. Botsov, T. R. Lakshmana, Y. Sui, W. Sun, T. Svensson, E. Ternon, G. Fodor, N. Brahmi, N. Lindqvist, R. L. G. Cavalcante, E. Pollakis, M. Racealа-Motoc, S. Stanczak, C. Zhou, Ö. Bulakci, J. Eichinger, P. Spapis, H. Nikopour, K. Au, M. Stamatelatos, S. Barmpounakis, P. Lundén, A. Prasad, R. Holakouei, V. Venkatasubramanian, F. Sanchez Moya, M. Rodziewicz, P. Sroka, J. Lorca, J.Lianghai, N. Kuruvatti, A. Klein, A. Rauch, D. Calabuig, **S. Giménez**, *D4.3 Final Report on Network-Level Solutions*, EU FP7 INFSO-ICT-317669 METIS, 2015

[R2] O. Aydin, S. Valentin, Z. Ren, T. Lakshmana, S. Yutao, T. Svensson, L. Hu, E. Ternon, P. Agyapong, G. Fodor, N. Brahmi, F. Penna, S. Stanczak, Ö. Bulakci, C. Zhou, J. Eichinger, P. Spapis, A. Kaloxylos, K. Chatzikokolakis, M. Stamatelatos, O. Yilmaz, M. Maternia, V. Venkatasubramanian, R. Holakouei, P. Marsch, M. Rodziewicz, P. Sroka, J.F. Monserrat, **S. Giménez**, L. Cucala, J. Lianghai, N. Kuruvatti, A. Klein, *D4.1 Summary on preliminary trade-off investigations and first set of potential network-level solutions*, EU FP7 INFSO-ICT-317669 METIS, 2013.

Chapter 2

Asymptotic analysis of Ultra Dense Networks

2.1 Introduction

Ultra Dense Networks (UDNs) have been identified as a promising deployment solution to guarantee the high data rates and massive connectivity required in future networks. As introduced in Section 1.1.2, UDNs are generally defined as those networks having higher densities of access points in comparison to current conventional deployments. The benefits of densification are twofold: on the one hand, the higher amount of Base Stations (BSs) per area increases the spatial resource reuse; on the other hand, average radio link quality is improved thanks to the closer proximity of users and BSs.

However, the main benefits of UDNs can in turn be limiting factors of these networks, since higher densities of BSs lead as well to higher levels of interference that might hamper the system performance. The application of resource partitioning techniques, which is studied in Chapter 5, can alleviate the inter-cell interference in the network, but at the expense of a reduction of the spatial resource reuse, counteracting one of the main UDN benefits. All these issues arise the question of whether it is worth to indefinitely increase the density of nodes in cellular networks, motivating an analysis of the fundamental limits of densification.

Several works in the literature have already partially addressed this issue [14–17, 20, 21], as described in Section 1.2.1. However, all these analysis are based on system models including specific simplifications that may limit the validity of these models, leading them to draw maybe wrong conclusions.

In this chapter, an asymptotic analysis of the UDNs performance is accomplished by using an enhanced Wyner-based system model proposed in [95], which includes the appropriate updates to overcome the problems present in the aforementioned works. The behavior of UDNs is assessed by means of this model, comparing the network performance under different assumptions.

In particular, UDNs performance with and without cooperation among BSs for the transmission to the users is investigated. In the case of cooperation, non-overlapped and overlapped clusters of cells are considered. The achievable rates in the network as a function of the position are evaluated for all the cooperation schemes with different cluster configurations. Furthermore, the expected rate density is also analyzed with respect to the BS density and for the same available power per meter. Hence, the effects of densification without the distortion caused by introducing more available power in denser networks are evaluated. Finally, the performance of UDNs in the limits of densification, i.e., when the inter-BS distance approaches 0, is also assessed in this study. The rest of this chapter is organized as follows:

- Section 2.2 summarizes the basic elements of the new model, including the clustering algorithms considered for the cooperation among BSs. In addition, it emphasizes those updates incorporated to the model that overcome the main limitations of the system models used in similar works in the literature.

- Section 2.3 analyzes the UDNs performance with finite densities of BSs, i.e., considering inter-BS distances greater than 0, showing results for different clustering configurations and available levels of power per meter.

- Section 2.4 presents the assessment of the UDNs performance in the limits of densification, i.e., when the inter-BS distance approaches 0.

- Section 2.5 outlines the most important conclusions of this study.

2.2 System model

In this section, the system model in [95] and the assumptions considered for subsequent analysis are described. A description of the considered deployment is provided, including the definition of the overlapped and non-overlapped clustering methods under study. Furthermore, the resource and power allocation models are exposed, as well as the expressions of the achievable rates when these allocation models are applied.

2.2.1 Deployment description

Let us consider a network composed of infinite User Equipment (UE) devices and BSs, which are uniformly distributed along two parallel lines separated h meters. Thus, h is the minimum distance between any UE-BS pair. The inter-UE and inter-BS distances are d_{U} and d_{B}, respectively. Besides, the BS 0 is located at the origin, and the location of UE 0 with respect to the origin is denoted by the parameter s. This scenario is depicted in Figure 2.1.

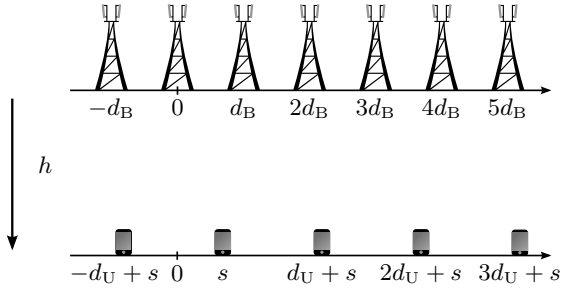

Figure 2.1: Network deployment.

Regarding BS cooperation, non-overlapped and overlapped BS clusters are considered. In the non-overlapped clustering, BSs are grouped into clusters of K elements, in which they cooperate for the transmission of information to the M UEs in their coverage area. An example of non-overlapped transmission is depicted in Figure 2.2, for $K = 3$ and $M = 2$. The numbers represent the BSs and UEs indexes, and the arrows indicate the UEs served by each BS. The clusters of cells serving consecutive UEs are here either coincident or have not any BS in common, what leads to the apparition of cluster edges. For instance, a cluster edge can be observed between BS 0 and BS 1 and between BS 3 and BS 4.

In the overlapped clustering, the K closest BSs to each UE cooperate in the transmission of information to the corresponding UE, as exemplified in Figure 2.3. For instance, the closest BSs to UE 0 are BS 0, 1 and 2, which cooperate for the transmission to this UE. Note that in this case the clusters of BSs serving any two consecutive UEs overlap but are not coincident. For example, clusters of BSs serving UEs 0 and 1 have only BS 2 in common.

For both non-overlapped and overlapped clusters, any two UEs with an index difference greater than or equal to M are served by clusters without any BS in common. For the sake of simplicity of the model, it is assumed that:

$$Md_{\mathrm{U}} = Kd_{\mathrm{B}},\ M \in \mathbb{N}^{+},\ K \in \mathbb{N}^{+}. \tag{2.1}$$

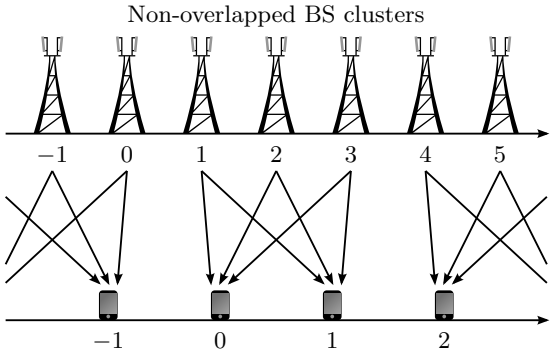

Figure 2.2: Non-overlapped BS clusters for $K = 3$ and $M = 2$.

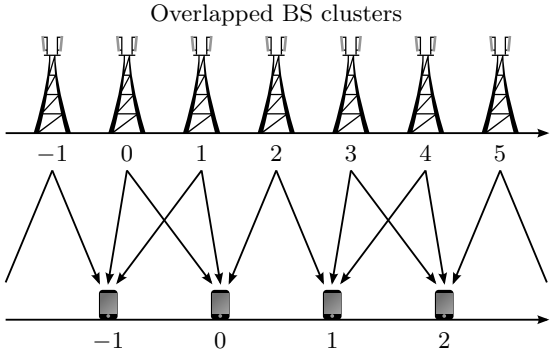

Figure 2.3: Overlapped BS clusters for $K = 3$ and $M = 2$. The arrows indicate the UEs served by each BS.

2.2.2 Resource and power allocation models

BSs transmit information using a set of W orthogonal resource elements. Coordinated BSs transmit to a particular UE using the same resources, and each BS uses orthogonal resources for different UEs. The resource allocation algorithm is the same in all BSs, which, along with the periodic structure of the system, implies that the resource allocation pattern is repeated every M UEs and K BSs. The amount of resources allocated to user m is Ww_m. This repetition is depicted with an example in Figure 2.4 for the cluster configurations of Figures 2.2 and 2.3, assuming $W = 1$ and $w_m = 1/M = 0.5$.

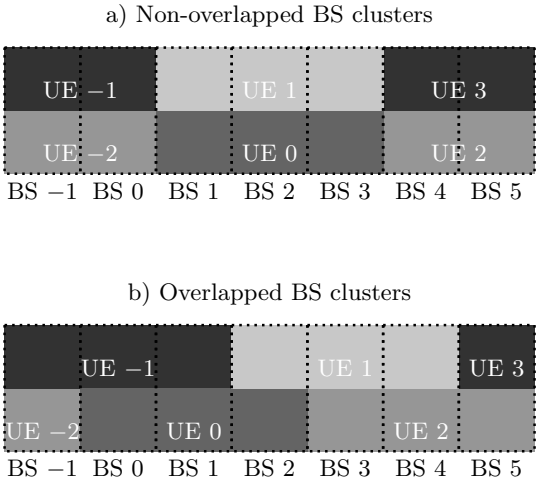

Figure 2.4: Resource allocation example for the system model of Figures 2.2 and 2.3. The dotted rectangles represent the resource pool in each BS.

Regarding the power allocation, it is assumed that the transmit power is limited in each resource element to the same maximum value P. Let $\rho_{k,m} \in [0, 1]$ be the portion of the maximum power that is used by BS k to transmit to UE m.

The resource and power allocations applied, i.e., $w_m, \forall m$ and $\rho_{k,m}, \forall k, m$, were optimized to render proportionally fair achievable rates to the UEs, following the fairness definition proposed in [18].

2.2.3 Achievable rates

In this model, path loss is computed considering 1-norm distances. Assuming that the location of the k-th BS is denoted as $l_{\mathrm{B}}(k)$ and the location of the m-th UE as $l_{\mathrm{U}}(m, s)$, the distance between the k-th BS and the m-th UE is $h + |l_{\mathrm{B}}(k) - l_{\mathrm{U}}(m, s)|$, and hence, the path loss from this BS to this UE is:

$$L_{km}(s) = \big(h + |l_{\mathrm{B}}(k) - l_{\mathrm{U}}(m, s)|\big)^{\gamma}, \tag{2.2}$$

where γ is the path loss exponent.

Let us denote as $\lambda_m(s)+1$ the first BS serving user m, which depends on the clustering transmission mode selected. Moreover, the indexes of BSs serving UE m when the cluster size is K are given by $\lambda_m(s)+k, k = 1, ...K$. Therefore,

the signal power received by UE m is:

$$p_m(s) = P \sum_{k=1}^{K} L^{-1}_{\lambda_m(s)+k,m}(s) \rho_{\lambda_m(s)+k,m}. \tag{2.3}$$

Similarly, the interference power received by UE m is:

$$z_m(s) = P \sum_{\substack{i=-\infty \\ i\neq 0}}^{\infty} \sum_{k=1}^{K} L^{-1}_{\lambda_m(s)+iK+k,m}(s) \rho_{\lambda_m(s)+iK+k,m}. \tag{2.4}$$

Note that the interference power received by each UE is composed of the sum of infinite terms. It can be shown that this sum converges if $\gamma > 1$, and its convergence point is given by the Hurwitz zeta function [96].

Using the previous signal and interference levels, the achievable rate of UE m in a particular resource element is:

$$r_m(s) = B \log\Big(1 + \frac{p_m(s)}{N + z_m(s)}\Big), \tag{2.5}$$

where B is a constant that accounts for the effects of bandwidth and multiple antennas, and N is the noise power corresponding with the used bandwidth. The total achievable rate of UE m considering all its assigned resource elements is given by:

$$R_m(s) = W w_m r_m(s). \tag{2.6}$$

2.2.4 Summary of the system model strengths

As introduced in Section 2.1, the system model used in this chapter incorporates several updates that overcome the main limitations presented by other models addressing the study of the densification limits, which were described in Section 1.2.1. These model updates can be summarized as follows [95]:

- The model defines a parameter characterizing the available power per meter in the scenario. Thanks to this, the same total available power can be considered independently of the density of BSs, allowing for a separate analysis of the impact on the network performance of densification and growing transmission power.

- A minimum distance between UEs and BSs is guaranteed by considering that BSs are deployed along a line located h meters above the line of users deployment. This assumption implies that the minimum distance

between any pair of user and base station is h, avoiding that received signal powers approach infinite when the distance between UEs and BSs is zero.

- The relation between UE and BS densities in the network can be varied in the model, allowing for the analysis of UDNs in which the density of BSs is much greater than that of the UEs.

- The model considers that BSs can cooperate inside both overlapped and non-overlapped clusters of BSs.

- Contrarily to other studies that take into consideration only the interference generated by the adjacent BSs to the serving BS of each user, this model computes the interference generated by the infinite BSs of the network. To this aim, the signals transmitted from different BSs are considered to be statistically independent in such a way that a user can coherently combine the received signal from a pool of base stations as in [97]. The Hurwitz zeta function is used to compute the sum of the infinite interfering sources in the network.

- The network performance can be characterized for different segments of the path loss exponent, in the same way as in the works in [16] and [17]. This is possible because the sum of the infinite contributions to the interference is governed by the Hurwitz zeta function, and one of the inputs to this function in the model is precisely the path loss exponent. Therefore, analyzing the regions in which the Hurwitz zeta function does or does not converge, it is possible to find regions of the path loss exponent value for which the network performance is drastically different.

2.3 Achievable rates with $d_{\mathbf{B}} > 0$

In this section, the behavior of the achievable rates is analyzed with respect to the inter-BS distance d_{B} and for the same available power per meter and resource element, η. Hence, the maximum power transmitted by a BS in each resource element is $P = \eta d_{\mathrm{B}}$. By comparing achievable rates with different d_{B} values and the same η, the effects of densification without the distortion caused by introducing more available power in denser networks will be evaluated. The rates were obtained assuming $h = B = W = N = 1$ and $\gamma = 3$.

2.3.1 Rates versus UE position

In this subsection, the achievable rates with respect to the UEs position are shown for four different inter-BS distances and three clustering techniques: overlapped, non-overlapped, and no clustering. Figures 2.5 to 2.8 show the achievable rates considering $d_{\mathrm{U}} = 0.1$, $\eta = 100$ and $M = 4$ for the four inter-BS distances $d_{\mathrm{B}} = 0.2, 0.1, 0.05$ and 0.025, and the corresponding values of K given by the relation in Eq. (2.1). The results without clustering were obtained with the same system model by making $K = 1$ and locating the UE in the interval $[-\frac{d_{\mathrm{B}}}{2}, \frac{d_{\mathrm{B}}}{2}]$. The rates at the rest of positions were obtained as periodic repetitions of the rates in the original interval.

Note that the maximum rates are achieved when the UEs are located exactly below a BS, and the minimum rates are obtained by those UEs located in the middle position between two BSs. Results also show that, in all studied cases, the achievable rates with the overlapped clusters are higher or equal than those with the non-overlapped clusters. Near the cluster center, both clustering techniques have a very similar behavior in which denser networks are able to provide more uniform achievable rates. However, around the cluster edges, non-overlapped clusters are significantly damaged, as shown in the figures by the drops in the rates values. Besides, this effect is aggravated in denser networks.

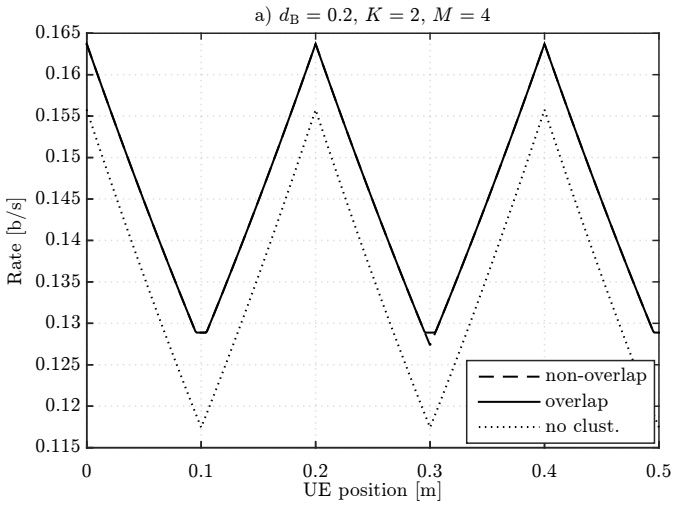

Figure 2.5: Achievable rates with respect to the UEs position for $d_{\mathrm{B}} = 0.2$, $K = 2$ and $M = 4$ and different clustering techniques.

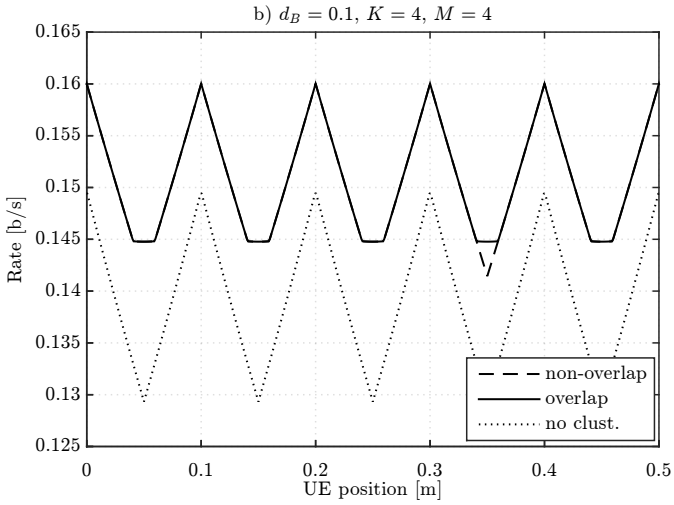

Figure 2.6: Achievable rates with respect to the UEs position for $d_{\mathrm{B}} = 0.1$, $K = 4$ and $M = 4$ and different clustering techniques.

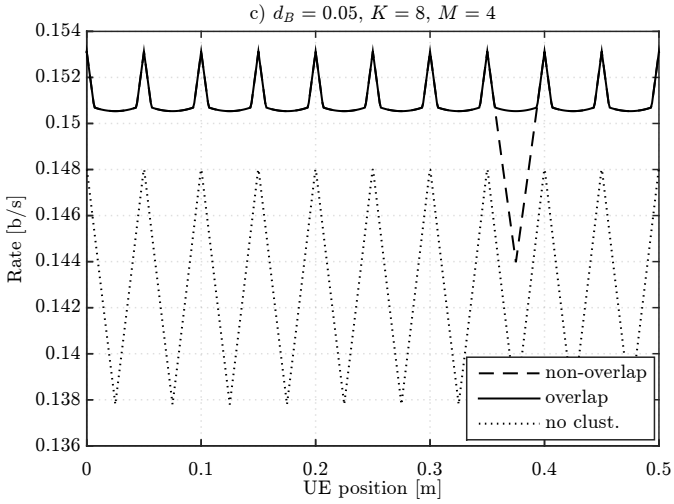

Figure 2.7: Achievable rates with respect to the UEs position for $d_{\mathrm{B}} = 0.05$, $K = 8$ and $M = 4$ and different clustering techniques.

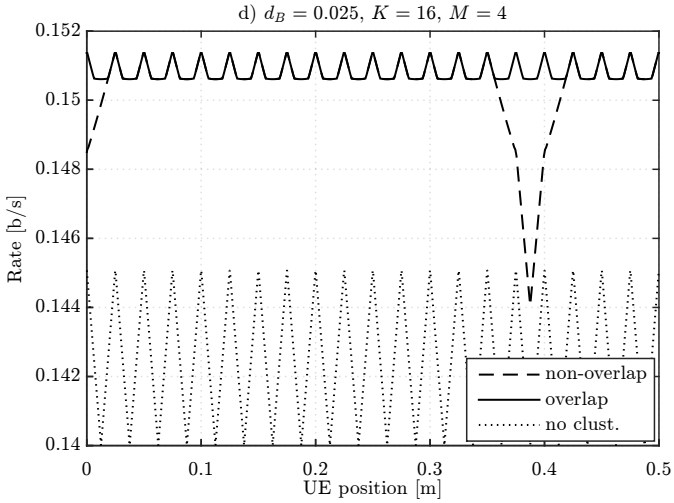

Figure 2.8: Achievable rates with respect to the UEs position for $d_{\mathrm{B}} = 0.025$, $K = 16$ and $M = 4$ and different clustering techniques.

Regarding the comparison with no clustering, the rates achieved without clustering are shown to be always lower than those with clustering, becoming the gap greater for denser networks.

The maximum and minimum rates achieved by all the clustering modes with different BS densities are shown in Figure 2.9. The main effect observed in this figure is the diminution of the gap between the maximum and minimum rates achieved by each cooperation scheme as long as the inter-BS distance decreases. This is caused by both the decrease of the maximum rates and the increase of the minimum rates with higher BS densities. The reason is that, with more BSs per meter, the distances from any user location to its closest BSs are decreased, thus improving the minimum rates relative to those users located between BSs. However, also the transmission power per BS is reduced due to the preservation of the available power per meter, deteriorating the maximum rates achieved by those users located below a BS, which are optimally served by its closest BS with a lower transmission power.

In the following subsection, results will be focused on the overlapped clustering technique due to its good performance.

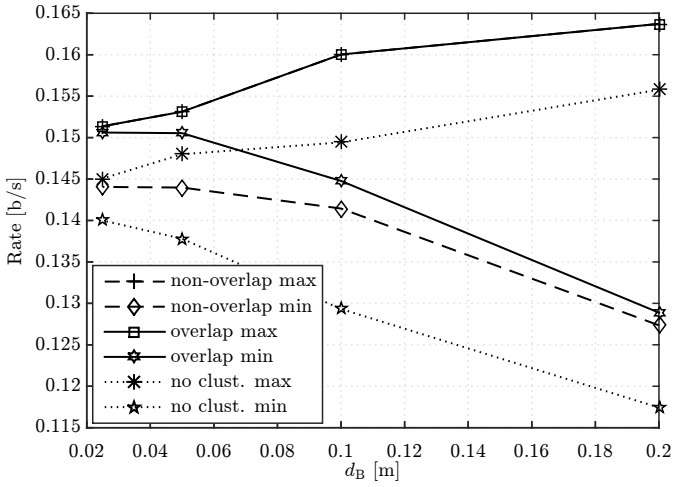

Figure 2.9: Maximum and minimum rates with respect to d_{B} for the different clustering techniques.

2.3.2 Rates versus inter-BS distance

In this subsection, figures representing the achievable rates versus the inter-BS distance are provided. To this aim, an averaged metric of the achievable rates was computed, in particular, the expected rate provided by the network per meter, where expectation is taken with respect to the UEs position.

In Figure 2.10, the impact of the available power per meter on the expected rate density is analyzed. UE density in this figure increases together with the BS density, i.e., $d_{\mathrm{U}} = d_{\mathrm{B}}$. Therefore, from Eq. (2.1), this implies that $K = M$. Two cluster sizes were analyzed, namely $K = 1$ and $K = 4$. Independently of the cluster size, it can be observed that the expected rate density increases with the available power. However, this increment has a limit, which is illustrated in Figure 2.10 with the curves for $\eta = \infty$. In other words, regardless of how much power is available in the BSs, the expected rate density cannot be higher than that shown in the curves for $\eta = \infty$. These curves can be obtained assuming a null noise power, i.e., $N = 0$, in which case the network is clearly interference limited.

Moreover, the best cluster size depends on the available power. Specifically, for $\eta = 1$ and $\eta = 10$, the expected rate density is higher with $M = 1$ than with $M = 4$, although for $\eta = 100$ and $\eta = \infty$ this order is reversed (except for

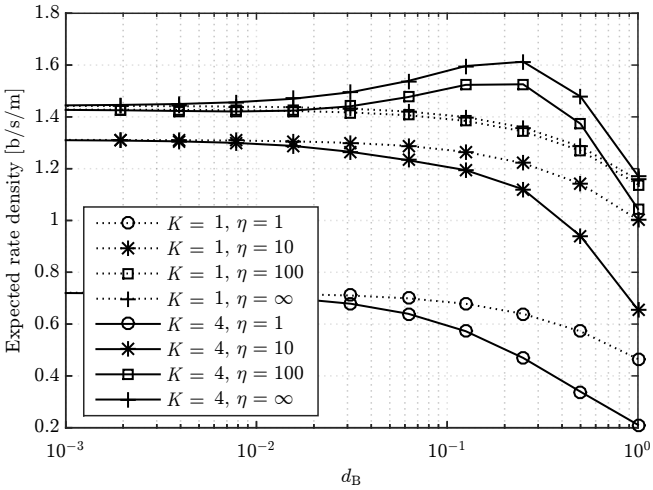

Figure 2.10: Expected rate density versus BS density for different values of available power per meter ($\eta = 1, 10, 100, \infty$).

$\eta = 100$ and $d_B = 1$). This result highlights the need of increasing the cluster size with the available power in order to mitigate the effect of interference.

Probably, the most unforeseeable result shown in Figure 2.10 is that the expected rate density converges for $d_B \to 0$ to the same value independently of the cluster size. The convergence point, however, increases with the available power. This result highlights that, in networks with very high density of BSs and UEs, it is beneficial to increase the available power, and the use of interference avoidance mechanisms is not critical.

Due to this surprising result, one may wonder if the same behavior is exhibited if only the BS density increases. This question is answered in Figure 2.11, where curves of the expected rate density with $\eta = \infty$ are shown for fixed UE densities. In particular, the figure shows results for all possible combinations of cluster sizes from $M = 1$ to $M = 3$ and inter-UE distances of $d_U = 0.125$, $d_U = 0.5$, and $d_U = 2$. In this case, all the curves converge when $d_B \to 0$ but to different values. The optimum cluster size depends on the inter-UE distance. Specifically, while for the lowest density ($d_U = 2$) the best cluster size is $M = 1$, for $d_U = 0.5$ is $M = 2$ for the denser networks, and for $d_U = 0.125$ increases to $M = 3$.

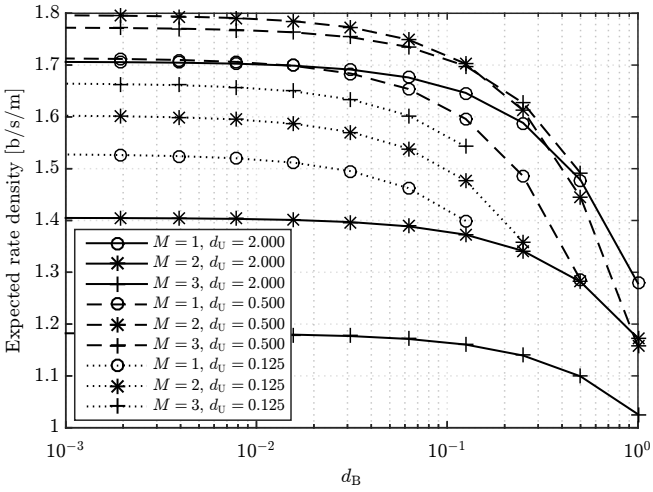

Figure 2.11: Expected rate density versus BS density for different values of UE density ($d_U = 0.125, 0.5, 2$).

2.4 Achievable rates in the limits of densification

In this section, the limit when $d_B \to 0$ is analyzed for a fixed available power per meter. Given M, it follows from (2.1) that the number of BSs that form one cluster is $K = \frac{M d_U}{d_B}$, which approaches ∞ when $d_B \to 0$. In this section, we show results for the case $d_B \to 0$. The rates were obtained assuming $h = B = W = N = 1$ and $\gamma = 3$.

Figure 2.12 shows the achievable rates for different UE locations when $M = 4$, $d_U = 0.1$ and $\eta = 100$. This figure corresponds to the limit when $d_B \to 0$ of Figures 2.5 to 2.8. In this case, the achievable rates are uniform along the UE positions for the overlapped clusters, as it is expected from the diminution between the maximum and minimum rates in denser networks shown in Figure 2.9. Moreover, it can be observed that the uniform rate achieved with overlapped clusters is the maximum rate achieved with non-overlapped clusters around the cluster centre. The performance of the non-overlapped clusters is damaged in the cluster edges even when $d_B \to 0$, although in the cluster center the difference between the two types of clustering is negligible.

The expected rate density at the limit of densification with overlapped clusters is presented in Figure 2.13, with respect to d_U and for different values

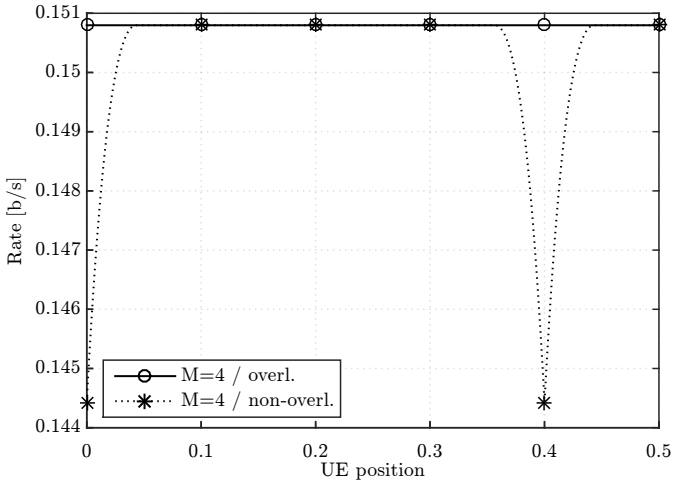

Figure 2.12: UEs achievable rate with respect to their location for $d_{\mathrm{B}} \to 0$ with both overlapped and non-overlapped clusters.

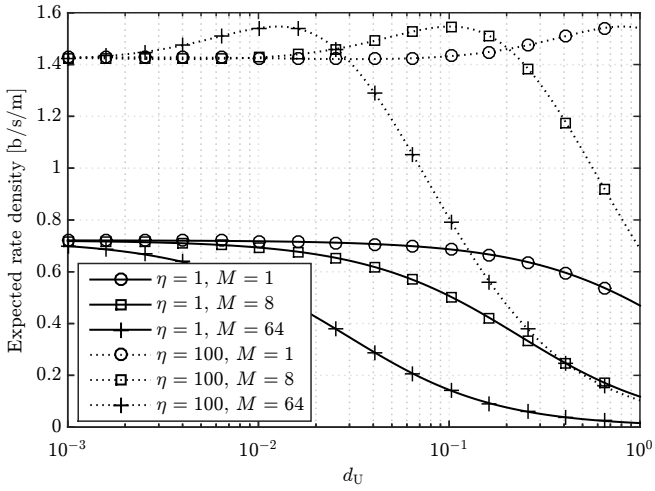

Figure 2.13: Expected rate density with respect to d_{U} with overlapped clusters.

of M and η. The figure shows that, for the lower level of available power per meter ($\eta = 1$) the best cluster size is $M = 1$. This leads to a interesting conclusion remarking that even though the BS density is ∞, the network behaves like being noise-limited so that interference management based on the partition of the resources should not be used. However, for the higher level of available power per meter ($\eta = 100$), the best cluster size depends on the inter-UE distance d_{U}. In particular, larger cluster sizes should be chosen for higher UE densities.

2.5 Conclusion

In this chapter, the fundamental limits of UDNs performance are analyzed by means of an enhanced Wyner-based 1D-deployment of infinite BSs and UEs, in which cooperation for the transmission to UEs is considered among BSs belonging to the same cluster. To this aim, the performance of the considered deployment has been firstly assessed by studying the achievable rates as a function of the UEs location in networks with finite density of BSs and different modes of cooperation among cells. These results show that, with high levels of power per meter, the introduction of cooperation among cells is always beneficial and brings a significant gain in the achievable rates. In addition, it has been shown that overlapped clusters provide a more homogeneous rate with respect to the UE location, avoiding the bad performance of non-overlapped clusters around the cluster edges. For both types of clustering, however, achievable rates are shown to become more homogeneous with respect to UE location as long as the BS density is increased.

Secondly, results regarding the expected average rate per meter in the network have been analyzed for the particular case of overlapped clusters of cells. From these results, it is concluded that further densification does not always provide an increase of the average rate per meter, existing certain BS density from which a further increase of the density of BSs does not result in an increase of the average achievable rate, which reaches a saturation point. Indeed, once reached that saturation point, the only way to increase the average achievable rates per meter is, in some cases, to increase the cluster size of the cooperative BSs. Furthermore, it has been shown that the optimum cluster size depends not only on the user and BSs densities, but also on the available level of power per BS. In general, for higher levels of available power per meter, bigger clusters of cells are preferred. However, for lower levels of available power per meter, increasing the BSs density leads to noise-limited networks, and better achievable rates per meter are obtained without cooperation among cells.

Finally, the performance of UDNs in the limits of densification has been evaluated. Results show that in this case the best cluster configuration is again dependent on the available power per meter, leading to similar conclusions to that of finite BS densities. Again, no cooperation is preferred in the case of lower levels of available per meter. Contrarily, for higher levels of available power per meter, higher densities of users are proved to perform better with bigger cluster sizes. Results prove that the optimum cluster size must be chosen for a particular density of users, since further increasing the cluster size above its optimum deteriorates the performance of the network.

Based on all these results, it is concluded that, even in the limit of densification, the application of cooperation schemes based on resource partitioning will provide performance gains only for those networks having high densities of available power. This conclusion motivates the performance study of Inter-Cell Interference Coordination (ICIC) techniques based on resource partitioning in practical UDN deployments, which will be addressed in Chapter 5.

Chapter 3

Hybrid precoding for urban-micro deployments using millimeter wave band

3.1 Introduction

The use of massive Multiple Input Multiple Output (MIMO) techniques for communication at millimeter wave (mmW) frequency bands has become a key enabler to meet the data rate demands of the upcoming Fifth Generation (5G) cellular systems. In particular, analog and hybrid beamforming solutions are receiving increasing attention as less expensive and more power efficient alternatives compared to fully digital precoding schemes, as described in Section 1.2.3. Despite the proven good performance of hybrid beamforming schemes in simple setups, their suitability for realistic cellular systems with many interfering base stations and users is still unclear. Furthermore, in real systems the performance of massive MIMO beamforming and precoding methods are also affected by practical limitations and hardware constraints that deteriorate the system performance, reason why an analysis of the extent of these aspects in the system is fundamental.

In this sense, this chapter provides a thorough assessment of some Hybrid Beamforming (HBF) schemes for Single-User (SU) and Multi-User (MU) single-stream transmission under realistic channel conditions in the lower edge of the mmW frequency band. To this end, exhaustive system level simulations using a carrier frequency of 28 GHz have been conducted, assuming a multi-cell deployment in which the channel is accurately emulated and there is a

coexistence of users with very different channel conditions. The main objective of the chapter is to complement existing theoretical studies by assessing under which conditions HBF schemes can approach the performance of fully-digital precoders.

Simulation results assuming ideal conditions will be contrasted with that including more realistic assumptions. More specifically, aspects such as the outdated availability of Channel State Information (CSI), the presence of non-ideal phase-shifters and combiners in the hybrid architecture and the existence of Per-Antenna Power Constraints (PAPC) in the digital schemes will be evaluated. The rest of the chapter is organized as follows:

- Section 3.2 provides a detailed description of the full-connected hybrid architecture for communication at mmW band.
- Section 3.3 presents an overview of the best-known analog and digital precoding techniques in the literature, including those utilized throughout the chapter.
- Section 3.4 describes the system model considered and presents the simulation setup. Moreover, this section describes the implementation particularities of the multi-antenna schemes assessed in this chapter, namely Digital Precoding (DP) and HBF schemes.
- Section 3.5 includes the performance evaluation with ideal assumptions for both SU and MU transmission schemes.
- Section 3.6 is devoted to the performance evaluation of MU schemes including practical limitations and hardware impairments.
- Finally, Section 3.7 draws the main findings of the chapter.

3.2 Hybrid Architecture for millimeter waves

Hybrid architectures emerged as a way of providing enhanced benefits to Radio Frequency (RF) beamforming at mmW frequencies, dividing the precoding process between analog and digital domains [34]. Several hybrid architectures have been defined in the literature, as described in Section 1.2.3, providing different performances. In this Thesis, the full-connected hybrid architecture is considered in both Chapters 3 and 4, due to its higher flexibility. Figure 3.1 depicts the transmission block diagram of a Base Station (BS) serving K User Equipment (UE) devices, both BS and UEs implementing a full-connected hybrid architecture.

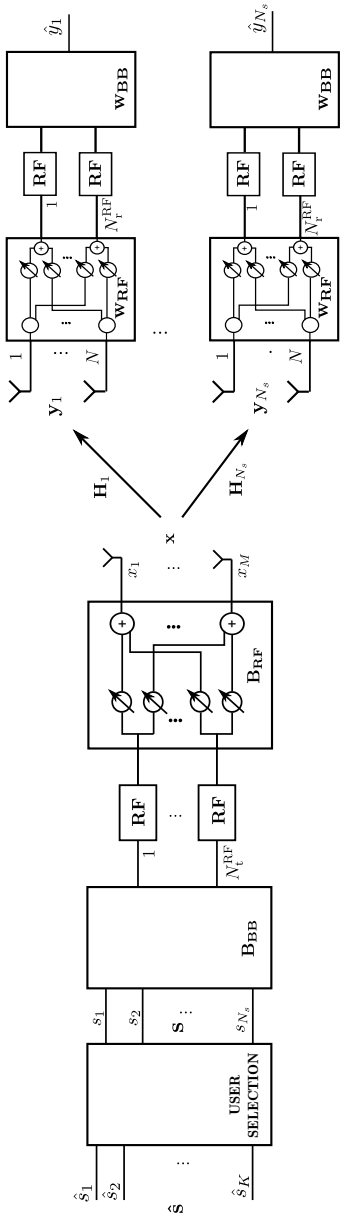

Figure 3.1: Hybrid precoding transmission model.

Let us consider a cellular network with N_{BS} BSs and N_{UE} UE devices, where $N_{\mathrm{UE}} = KN_{\mathrm{BS}}$. As depicted in the figure, each BS is equipped with $N_{\mathrm{t}}^{\mathrm{RF}}$ RF chains and M antennas, while at the UE the number of RF chains and antennas is given by $N_{\mathrm{r}}^{\mathrm{RF}}$ and N, respectively. The first stage of the preprocessing at the BS corresponds to the user selection process, where N_s out of the K users are selected to be served, $N_s \leq N_{\mathrm{t}}^{\mathrm{RF}}$. Assuming that only a single data stream is transmitted to each user, the vector of data symbols to be transmitted by one BS at each time instant, $\mathbf{s} \in \mathbb{C}^{N_s \times 1}$, can be expressed as:

$$\mathbf{s} = [s_1, ..., s_{N_s}]^{\intercal}, \tag{3.1}$$

where s_l, $l = 1, ..., N_s$, are the independent symbols with equal power to be transmitted to the selected users. Then, preprocessing at Baseband (BB) is applied by means of the matrix $\mathbf{B}_{\mathrm{BB}} \in \mathbb{C}^{N_{\mathrm{t}}^{\mathrm{RF}} \times N_s}$, using any kind of linear precoding technique satisfying $\mathrm{tr}\{\mathbf{B}_{\mathrm{BB}}(\mathbf{B}_{\mathrm{BB}})^{\dagger}\} = 1$. The last stage of the data preprocessing is performed at RF, i.e., after the upconversion of the signals, when beamforming is applied by means of phase shifters and combiners. A set of M phase shifters is applied to the output of each RF chain. Afterwards, the outputs of the i-th phase shifters of every RF chain are combined to feed the i-th antenna element in the array. As a result of this process, $N_{\mathrm{t}}^{\mathrm{RF}}$ different beams are conformed in order to transmit the RF signals. This process can be modeled by means of an $M \times N_{\mathrm{t}}^{\mathrm{RF}}$ complex matrix, $\mathbf{B}_{\mathrm{RF}}$. In particular, the data vector $\mathbf{x} \in \mathbb{C}^{M \times 1}$ transmitted by the BS can be expressed as:

$$\mathbf{x} = \mathbf{B}_{\mathrm{RF}}\mathbf{B}_{\mathrm{BB}}\mathbf{s}. \tag{3.2}$$

In order to limit the power transmitted by the antennas, power normalization is applied to $\mathbf{x}$ in such a way that $\mathrm{tr}\{\mathbb{E}[\mathbf{x}\mathbf{x}^{\dagger}]\} = P$, being P the total available power per BS.

Considering the multi-cell scenario, and using the superscript (l) to denote that a variable is related to BS l, the received signal at the u-th user served by BS i can be expressed as:

$$\mathbf{y}_{u,i} = \sum_{l=1}^{N_{\mathrm{BS}}} \mathbf{H}_{u,i}^{(l)}\mathbf{x}^{(l)} + \mathbf{n}, \tag{3.3}$$

where $\mathbf{H}_{u,i}^{(l)} \in \mathbb{C}^{N \times M}$ is the MIMO channel matrix between BS l and the u-th UE served by BS i, $\mathbf{x}^{(l)}$ is the data vector transmitted by BS l, and $\mathbf{n} \in \mathbb{C}^{N \times 1}$ is an Additive White Gaussian Noise (AWGN) with zero mean and covariance $\mathbb{E}[\mathbf{n}\mathbf{n}^{\dagger}] = \sigma_n^2\mathbf{I}_N$, where $\mathbf{I}_N$ is the $N \times N$ identity matrix.

Using Eq. (3.2) and (3.3), the Signal to Interference plus Noise Ratio (SINR) for the u-th UE served by BS i before the RF and BB processing at the receiver,

$\text{SINR}_{u,i}$, can be expressed as:

$$\text{SINR}_{u,i} = \frac{P|\mathbf{H}_{u,i}^{(i)}\mathbf{B}_{\text{RF}}^{(i)}\mathbf{B}_{\text{BB},u}^{(i)}|^2}{P\left|\mathbf{H}_{u,i}^{(i)}\mathbf{B}_{\text{RF}}^{(i)}\sum_{k\neq u}^{N_s}\mathbf{B}_{\text{BB},k}^{(i)}\right|^2 + P\left\|\sum_{l\neq i}^{N_{\text{BS}}}\mathbf{H}_{u,i}^{(l)}\mathbf{B}_{\text{RF}}^{(l)}\mathbf{B}_{\text{BB}}^{(l)}\right\|_{\text{F}}^2 + \sigma_n^2}, \tag{3.4}$$

where $\mathbf{B}_{\text{BB},k}^{(i)}$ denotes the k-th column of the matrix $\mathbf{B}_{\text{BB}}^{(i)}$.

3.3 MIMO Precoding Techniques

In this section, an overview of the MIMO precoding techniques available in the literature is provided, and the formulation of those techniques used throughout this Thesis is presented. For the sake of simplicity, both the number of antennas at the UEs, N, and the number of RF chains at the receiver, N_{r}^{RF}, are assumed to be 1 hereinafter.

3.3.1 Fully digital precoding

Fully digital precoding is the simplest and optimum approach when the number of available RF chains at the transmitter, N_{t}^{RF}, is equal to the number of antennas, M. In this case, data processing is applied to only the BB signal, without further modifications after the conversion to RF. Mathematically, this is equivalent to $\mathbf{B}_{\text{RF}} = \mathbf{I}_M$, and thus, Eq. (3.2) becomes:

$$\mathbf{x} = \mathbf{B}_{\text{BB}}\mathbf{s}. \tag{3.5}$$

The matrix $\mathbf{B}_{\text{BB}}$ can be designed to optimize a specific criterion [98]. For instance, in the case of Maximum Ratio Transmission (MRT) precoding, the computation of the precoding matrix is designed to maximize the received signal at the receivers. Denoting by $\mathbf{H}^{(i)} \in \mathbb{C}^{N_s\times M}$ the channel matrix between the BS i and its N_s users being served, given by:

$$\mathbf{H}^{(i)} = \begin{bmatrix} \mathbf{h}_{1,i}^{(i)} & \mathbf{h}_{2,i}^{(i)} & ... & \mathbf{h}_{N_s,i}^{(i)} \end{bmatrix}^{\intercal}, \tag{3.6}$$

with $\mathbf{h}_{u,i}^{(i)} \in \mathbb{C}^{M\times 1}, u = 1, ..., N_s$, the expression of the MRT precoding matrix at BS i is:

$$\begin{aligned} \tilde{\mathbf{B}}_{\text{BB}}^{(i),\text{MRT}} &= \mathbf{H}^{(i)^\dagger}, \\ \alpha_{\text{MRT}} &= \frac{1}{\sqrt{\text{tr}\{\tilde{\mathbf{B}}_{\text{BB}}^{(i),\text{MRT}}(\tilde{\mathbf{B}}_{\text{BB}}^{(i),\text{MRT}})^\dagger\}}} \\ \mathbf{B}_{\text{BB}}^{(i),\text{MRT}} &= \alpha_{\text{MRT}}\tilde{\mathbf{B}}_{\text{BB}}^{(i),\text{MRT}}. \end{aligned} \tag{3.7}$$

In the case of Zero Forcing precoding [99], the optimization criterion used is the cancellation of the intra-cell interference. ZF performs better at interference limited scenarios but at the expense of a higher complexity at the receiver, which must have knowledge about the channel state of the rest of users served at the same time, in order to perform the inversion of the channel matrix. An extension of Zero Forcing (ZF) known as Regularized Zero Forcing (RZF) has proven to provide good results in multi-cell scenarios, since this technique also considers the impact of the background noise and the unknown user interference originated by the neighbor cells [100]. RZF precoding matrix computed by BS i is shown in Eq. (3.8):

$$\begin{aligned} \tilde{\mathbf{B}}_{\mathrm{BB}}^{(i),\mathrm{RZF}} &= \mathbf{H}^{(i)^\dagger}(\mathbf{H}^{(i)}\mathbf{H}^{(i)^\dagger} + \alpha\mathbf{I})^{-1}, \\ \alpha_{\mathrm{RZF}}^{(i)} &= \frac{1}{\sqrt{\mathrm{tr}\{\tilde{\mathbf{B}}_{\mathrm{BB}}^{(i),\mathrm{RZF}}(\tilde{\mathbf{B}}_{\mathrm{BB}}^{(i),\mathrm{RZF}})^\dagger\}}}, \\ \mathbf{B}_{\mathrm{BB}}^{(i),\mathrm{RZF}} &= \alpha_{\mathrm{RZF}}^{(i)}\tilde{\mathbf{B}}_{\mathrm{BB}}^{(i),\mathrm{RZF}}, \end{aligned} \tag{3.8}$$

where $\mathbf{I} \in \mathbb{C}^{N_s \times N_s}$ is the identity matrix and $\alpha = N_\mathrm{s}\sigma_n^2$ to maximize SINR [100].

3.3.2 RF beamforming

In RF beamforming, the data symbols are converted to high frequency and pre-processed in the analog domain by means of the phase shifters. Mathematically, this is equivalent to $\mathbf{B}_{\mathrm{BB}} = \mathbf{I}_{N_\mathrm{t}^{\mathrm{RF}}}$, and thus, Eq. (3.2) becomes:

$$\mathbf{x} = \mathbf{B}_{\mathrm{RF}}\mathbf{s}. \tag{3.9}$$

With the full-connected architecture described in Section 3.2, this type of precoding is able to modify the phase of the data symbols but not their amplitude, which implies that power allocation strategies cannot be used to maximize cell capacity. Besides, RF beamforming is usually subject to a hardware constraint that restricts to a finite set the possible phase values to be applied to the signals. This is caused by the need to control the phase shifters digitally, what forces the application of some kind of quantification to the phase values [101].

RF beamforming reduces the number of required RF chains at the BS, and consequently the cost and power consumption of the mixed analog/digital components [40] of the RF units, what makes this kind of precoding interesting for mmW, where cost and power consumption are design limitations. Since the number of conformable beams in RF beamforming is already limited by hardware to a finite set, the use of predefined codebooks becomes a good strategy to reduce the amount of feedback information required by the system.

Several precoding codebooks are available in the literature [102]. The most widely used are the Grassmannian codebook, the Random Vector Quantization codebook, the Discrete Fourier Transform (DFT) matrix based codebook, and the codebook obtained by generalized Lloyd algorithm. Due to its simplicity and effectiveness for Uniform Linear Arrays (ULAs) as shown in [103], DFT codebook is often preferred to more complex designs. The c-th codeword of a DFT-based codebook is:

$$\mathbf{w}_c^{\mathrm{DFT}} = \frac{1}{\sqrt{M}} \left[1, e^{\frac{j2\pi c}{C}}, \ldots, e^{\frac{j2\pi c}{C}(M-1)}\right]^{\intercal}, \tag{3.10}$$

where C is the number of codewords in the codebook. If $C = M$, it can be shown that the maximum diversity order is guaranteed. The beamforming vector for the u-th user served by BS i, denoted as $\mathbf{b}_{u,i}^{\mathrm{DFT}}$ is chosen as:

$$\mathbf{b}_{u,i}^{\mathrm{DFT}} = \mathbf{w}_{c^*}^{\mathrm{DFT}}, \tag{3.11}$$

$$c^* = \arg\max_{c} \left(\left| \mathbf{h}_{u,i}^{(i)\intercal} \mathbf{w}_c^{\mathrm{DFT}} \right|^2 \right). \tag{3.12}$$

Note that Eq. (3.11) maximizes the signal power at the receiver. The beamforming matrix $\mathbf{B}_{\mathrm{RF}}^{(\mathrm{i}),\mathrm{DFT}}$ is built then by concatenating the beamforming vector for every user, as follows:

$$\mathbf{B}_{\mathrm{RF}}^{(\mathrm{i}),\mathrm{DFT}} = \left[\begin{array}{cccc} \mathbf{b}_{1,i}^{\mathrm{DFT}} & \mathbf{b}_{2,i}^{\mathrm{DFT}} & \ldots & \mathbf{b}_{N_s,i}^{\mathrm{DFT}} \end{array} \right]. \tag{3.13}$$

3.3.3 Hybrid beamforming/precoding

Although the terms hybrid beamforming and hybrid precoding are often used interchangeably in the literature, in this Thesis they are applied with different meanings. On the one hand, Hybrid Beamforming (HBF) schemes are denoted as those applying only RF processing by means of the hybrid architecture depicted in Figure 3.1. The performance of HBF can be maximized by optimizing $\mathbf{B}_{\mathrm{RF}}$ and the user selection procedure.

On the other hand, schemes applying both BB and RF processing are denoted as Hybrid Precoding (HP) schemes. The best performance of HP can be obtained by the joint optimization of $\mathbf{B}_{\mathrm{RF}}$ and $\mathbf{B}_{\mathrm{BB}}$ matrices. However, the high computational complexity of this approach for MU systems and the practical limitations imposed by the hybrid architecture motivates a separate optimization of the analog and digital stages [47, 48].

3.4 System model and evaluated schemes

3.4.1 System model description

This chapter studies a mmW downlink system with N_{BS} BSs and N_{UE} UE devices. Each BS is equipped with M co-located antennas and $N_{\mathrm{t}}^{\mathrm{RF}}$ RF chains. In the BB architecture, it is assumed that $N_{\mathrm{t}}^{\mathrm{RF}}$ is equal to the number of antennas M. However, in the hybrid architecture, with the aim to analyze the impact of a limited availability of RF chains, $N_{\mathrm{t}}^{\mathrm{RF}}$ is assumed to be variable and modeled by the parameter P, being $1 \leq P \ll M$. For the sake of simplicity in the simulations, a simplified model for the receiver is considered. In particular, a single narrow receive beam is assumed at each UE (which would require an antenna array in practice), in order to simulate a beamforming gain at the receiver as in [104]. Furthermore, the pointing direction of the directive beam is selected by the user to maximize the Signal to Noise Ratio (SNR) at the receiver.

The downlink transmission resources are partitioned in the time-frequency plane. In the time domain, the resource space is divided into subframes of a certain time duration. In the frequency domain, resources are grouped in Frequency Blocks (FBs). The minimum time-frequency resource is known as Resource Block (RB), and it is composed of one FB during one subframe period. This terminology is the same as the one used by Third Generation Partnership Project (3GPP) and Mobile and wireless communications Enablers for Twenty-twenty (2020) Information Society (METIS) project [105] to carry out performance evaluations.

3.4.2 Evaluated precoding schemes

In order to exploit the BS multi-antenna architecture to either multiplex different data streams or to provide beamforming gains to the different users, some form of precoding or beamforming must be applied at the transmitter side. The schemes considered in this chapter include:

- Both SU and MU transmission. In SU transmission, only one user is served on each RB, while MU transmission allows for a set of up to as many users as RF chains at the BS to be served simultaneously on each RB, by being spatially multiplexed.
- Both HBF and DP schemes. For the HBF, a DFT-based beamforming is applied, while for DP, MRT technique is selected.

Note that equal power sharing among users is considered, meaning that the available power per RF branch must be scaled to fulfill a per-BS power

restriction. The particularities of the evaluated schemes are described in detail hereinafter.

Hybrid beamforming schemes

In this chapter, a simple and practical method for mmW beamforming is considered. Motivated by the fact that the channel at mmW is characterized by limited scattering, in particular for the UEs in Line of Sight (LoS) conditions, it is assumed that:

(a) beamformers are designed only in the RF domain, using DFT-based codebook beamforming given by Eq. (3.10),

(b) user selection procedure is optimized to schedule up to P UEs in each subframe, each UE being served by a specific RF beamformer. It is worth noting that, in the case of $P = 1$, the scheme corresponds to the pure Analog Beamforming (ABF) baseline setup. In this setup, only one beam can be conformed at a given time and, thus, only one user is scheduled per subframe in the whole band.

For the SU HBF scheme, the P signals coming from the different RF branches are considered to be separated in the frequency domain, i.e., a different subband is utilized for each RF chain. In particular, the whole band is divided into P contiguous subbands, and each RF signal is mapped to one of these subbands. Note that SU HBF allows different UEs to be scheduled in different subbands of the same subframe, thus exploiting channel frequency diversity.

Conversely, in the MU HBF case, the whole bandwidth is available at each RF chain and multiple UEs are multiplexed in the spatial domain. The set of users to be multiplexed at each subframe is selected by means of an iterative scheduling algorithm, described at the end of Section 3.4.2.

Fully digital precoding schemes

In this chapter, the DP scheme selected is MRT linear precoder, which only requires the knowledge of the channel vector between each user and its serving BS (see Eq. (3.7)). The main reason for the selection of this linear precoder is that the performance of MRT in BSs with large antenna arrays becomes very close to that of other linear precoding schemes that require higher computational complexity, such as ZF or RZF [106].

The DP is implemented for both SU and MU transmission cases. In MU transmission, a set of as many users as RF chains can be served simultaneously at each subframe by multiplexing them in the spatial domain, following an

iterative scheduling algorithm. However, in SU transmission the multiplexing of several users in the spatial domain is not performed.

Furthermore, the effect of multiplexing different sets of users in different FBs of each subframe is investigated as well. To this end, two variants of DP have been implemented and simulated, denoted by DP Non Frequency Selective (NFS) and DP Frequency Selective (FS). In DP NFS, all FBs are allocated to a single set of UEs per subframe, while, in DP FS, the allocation is optimized per RB, thereby allowing different sets of UEs to be scheduled per subframe in different FBs.

A comparison of the main features of the evaluated schemes in this chapter is summarized in Table 3.1.

Table 3.1: Summary of the evaluated precoding algorithms in the chapter.

		N_t^{RF}	**Frequency multiplexing**	**Spatial multiplexing**
SU	**ABF**	1	No	No
	HBF	P	Yes	No
	DP NFS	M	No	No
	DP FS	M	Yes	No
MU	**HBF**	P	No	Yes
	DP NFS	M	No	Yes
	DP FS	M	Yes	Yes

User selection procedure

In the SU schemes, users are selected by simply following a Proportional Fair (PF) policy, since their multiplex in the frequency domain guarantees their orthogonality. However, in the MU schemes, a user selection procedure is required to optimize the set of users that are spatially multiplexed. In this chapter, user selection in the MU schemes is performed by means of an iterative scheduling algorithm, whose pseudocode is shown in Algorithm 1.

Let us denote as $\mathcal{U}$ the set of users being served by a BS, and as $\mathcal{R}$ the set of users to be allocated to $\mathcal{B}$ at a certain subframe, where $\mathcal{B}$ represents either a FB or the whole bandwidth, depending on whether the MU scheme optimizes the precoders per FB (as in DP FS) or wideband (as in HBF and DP NFS). Denote also as $\mathbf{b}_u^{\mathcal{B}} \in \mathbb{C}^{M\times 1}$ the optimum precoding vector for UE u, being computed with DFT and MRT in HBF and DP schemes, respectively. The goal of Algorithm 1 is to select, at each iteration, the user that maximizes a utility function U, defined as the weighted sum of the achievable throughputs of the

users in $\mathcal{R}$. The weights of the utility function, denoted as $\alpha_j, j = 1, ..., K$, are calculated to fulfill a PF scheduling policy. Note that, for the computation of the utility function, the SINR experienced by user $j \in \mathcal{R}$ in $\mathcal{B}$, $\text{SINR}_j^{\mathcal{B}}$, includes the intra-cell interference generated among the spatially multiplexed users in $\mathcal{R}$ once the precoding vectors $\mathbf{b}_{u\in\mathcal{R}}^{\mathcal{B}} \in \mathbb{C}^{M\times 1}$ have been applied. The algorithm stops when allocating any new user cannot increase the utility function any further.

Algorithm 1 Inputs: set of users served by the BS, $\mathcal{U}$; optimum precoding vector for each user $u \in \mathcal{U}$, $\mathbf{b}_u^{\mathcal{B}}$; scheduling policy weights of each user $u \in \mathcal{U}$, α_u; **Output:** set of allocated users, $\mathcal{R}$.

$\mathcal{Y} := \mathcal{U}$, $\mathcal{R} := \emptyset$, $U_o := 0$, $U := U_o$;
while $|\mathcal{Y}| > 0$ and $U \geq U_o$ **do**
  for $k \in \mathcal{Y}$ **do**
    $\mathcal{R}_k = \mathcal{R} \cup k$
    $U_k = \sum_{j\in\mathcal{R}_k} \alpha_j \log_2(1 + \text{SINR}_j^{\mathcal{B}}(\mathbf{b}_{l\in\mathcal{R}_k}^{\mathcal{B}}))$
  end
  $k^* \leftarrow \arg\max_k U_k$
  $U = U_{k^*}$
  if $U \geq U_o$ **then**
    $\mathcal{Y} \leftarrow \mathcal{Y} \setminus \{k^*\}$
    $\mathcal{R} \leftarrow \mathcal{R} \cup \{k^*\}$
    $U_o = U$
  end
end

3.4.3 Simulation setup

The simulations of this chapter were conducted by considering the 3-Dimensional (3D) mmW channel model proposed in [107], characterizing an urban micro-cellular scenario. This model is based on real measurements taken in New York City. It is consistent with the 3GPP ray-based modeling methodology, and includes the characterization of the channel in azimuth, elevation and polarization. This model takes into account channel variability in the frequency and time domains, considering also the actual correlation between antennas depending on the geometry of the antenna array deployment. The propagation condition has been taken from the urban micro (UMi) 3GPP channel model [108], which classifies users in LoS or Non Line of Sight (NLoS) condition by means of a probability distribution function of the distance between BS and UE. Simulations are performed in the lower edge of the mmW band,

using a carrier frequency of 28 GHz and a system bandwidth of 1 GHz. Unless otherwise stated, perfect channel knowledge is assumed at the transmitter and receiver side.

The simulation setup considers a wrap-around configuration of the seven-site layout depicted in Figure 3.2. The sites are deployed in an urban scenario with inter site distance of 200 m, which entails having approximately 70% of UEs in LoS condition. Each site includes three 120° sectors (cells), each one served by a BS equipped with a horizontal uniform linear array of 64 antenna elements. The antenna pattern of each element is parabolic as in [108], and then defined by a maximum gain (8 dBi), front-to-back ratio (20 dB), and half-power beamwidth (70°). Fifty UEs are randomly deployed per site, leading to an average of 16.7 UEs per BS. As already said, the modeling of beamforming at the UE side is simplified. Specifically, the UE is equipped with an array of antenna elements whose resulting pattern is parabolic with a maximum gain of 12 dBi, a front-to-back ratio of 20 dB, and a half-power beamwidth of 45° (the latter calculated according to [104]). In addition, it is considered that the UE beamformer is always pointing to the direction that maximizes the SNR at the receiver. For all the simulated schemes, a per-site power restriction of 40 dBm is assumed, with equal power allocated to each sector. In addition, equal power allocation among the active RF chains is considered at each BS for the hybrid implementations. A summary of these and other important simulation parameters is listed in Table 3.2.

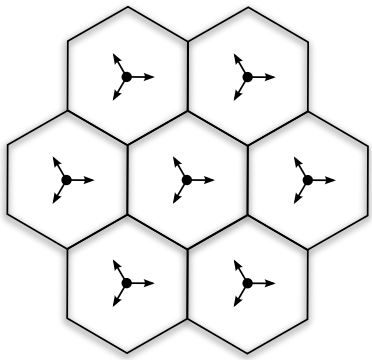

Figure 3.2: Seven-site layout considered for the simulations. Each site covers three 120° sectors, each one equipped with the antenna array boresight indicated by the arrows.

Table 3.2: Simulation parameters.

Simulation time per drop	1 s
Number of drops	10
Carrier frequency	28 GHz
Number of FBs	100
FB bandwidth	10 MHz
Subframe duration	1 ms
Scheduling policy	Proportional fair
Thermal noise power spectral density	−174 dBm/Hz
Site transmit power	40 dBm
BS antenna tilt	12°
BS height	10 m
BS antenna element gain	8 dBi
BS antenna element front-to-back ratio	20 dB
BS antenna element half-power beamwidth	70° (Both H and V planes)
UE noise figure	7 dB
UE speed	3 km/h
UE antenna pattern gain	12 dBi
UE antenna pattern front-to-back ratio	20 dB
UE antenna pattern half-power beamwidth	45° (Both H and V planes)
UE height	1.5 m
Min UE-BS distance	10 m

3.5 Performance with ideal assumptions

In this section, a performance comparison among DP and HBF schemes with both SU and MU transmission is carried out under ideal assumptions. More specifically, perfect and timely CSI available at the transmitters is assumed, ideal phase-shifters and combiners in the hybrid scheme and lack of any per-antenna power constraint in DP.

3.5.1 Single-user case

In this subsection, the performance of ABF ($P = 1$), HBF with $P = 4$ RF chains and DP schemes is compared. Recall that in the SU schemes under study, only one user per RB is allowed to be scheduled by each BS. Note also that the same user is allocated to the whole band in the ABF and DP NFS schemes, whereas several users per subframe are multiplexed in frequency in HBF (up to the number of RF chains P) and DP FS (up to the number of FBs) schemes.

Fig. 3.3 compares the Cumulative Distribution Function (CDF) of the user throughput for the different algorithms evaluated. It is shown that DP schemes achieve a better performance in terms of throughput for all users. This is due to the fact that digital precoders are specifically computed per FB and, thus, they can adapt better to the channel frequency response variation than the wideband beamforming vectors used in analog and hybrid schemes. This effect, however, becomes less significant in the higher throughput region, which corresponds to those users in LoS conditions with a flatter channel frequency response. Indeed, as better shown in Fig. 3.4, if the channel is nearly flat in the frequency domain, forcing the same precoding decision in the whole band is a suitable approach. On the other hand, in the presence of high frequency selectivity (NLoS users), there is a severe degradation in the user throughput provided by HBF, as extracted from Fig. 3.5. Furthermore, especially in the NLoS case, a little gain is observed in the user throughput when comparing either HBF with ABF or DP FS with DP NFS. This gain comes from the multiplexing in HBF and DP FS of several users per subframe in the frequency domain, which is here taking advantage from multi-user diversity.

Additional performance results about the SU schemes are included in Table 3.3. In particular, the values of average and 5th percentile user throughput and average cell throughput, and their corresponding gains with respect to ABF, considered as a baseline in this chapter are collected in this table. It can be observed that DP algorithms exhibit an overall performance superior to that of HBF, thanks to the better adaptation of these precoders to the channel variability, as mentioned before. Furthermore, regarding the comparison between

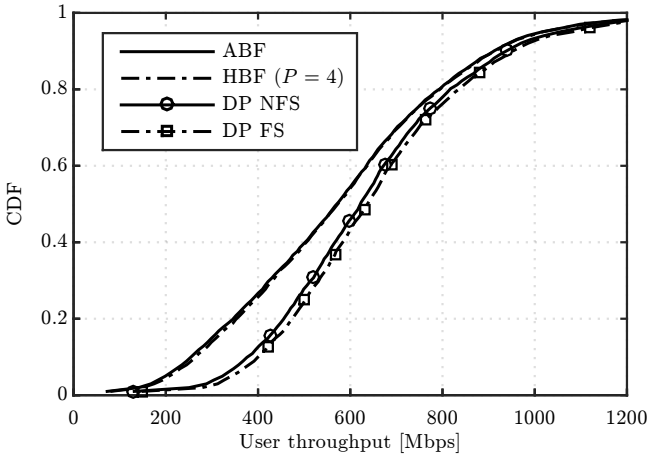

Figure 3.3: CDF of user throughput in the SU case.

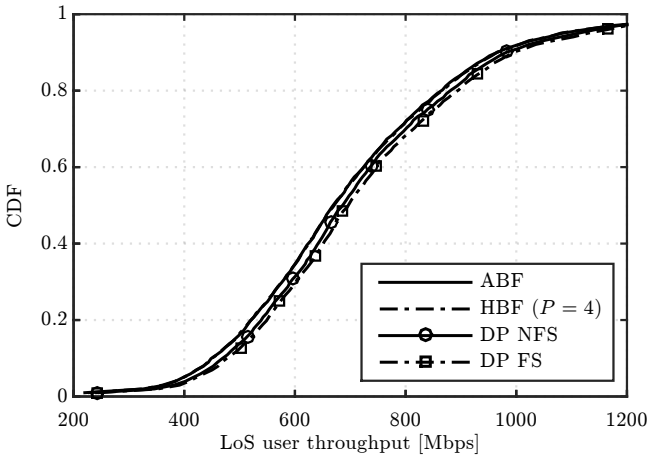

Figure 3.4: CDF of user throughput for LoS users in the SU case.

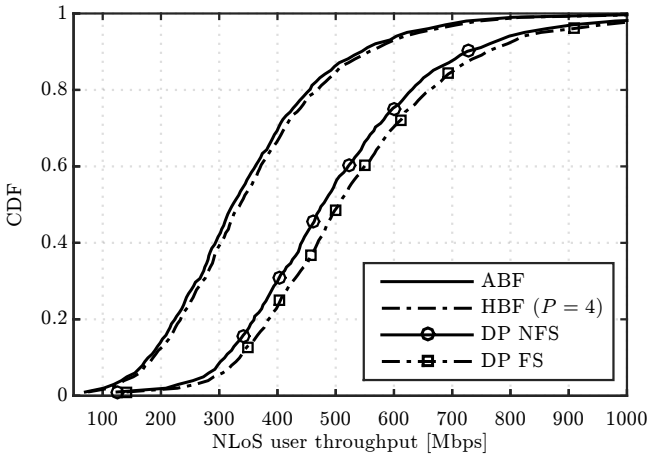

Figure 3.5: CDF of user throughput for NLoS users in the SU case.

Table 3.3: Summary of SU performance results with ideal assumptions.

	Average UE throughput		**5%-ile UE throughput**		**Average cell throughput**	
	[Gbps]	**Gain [%]**	**[Gbps]**	**Gain [%]**	**[Gbps]**	**Gain [%]**
SU ABF	0.59	-	0.20	-	9.80	-
SU HBF ($P = 4$)	0.60	1.7	0.21	5	9.83	0.3
SU DP NFS	0.66	11.9	0.32	62	10.80	10.2
SU DP FS	0.67	13.6	0.34	72	11.10	13.3

DP FS and DP NFS, the former shows higher gains for all the performance indicators, thanks to its more optimized user scheduling per FB. Nevertheless, the frequency multiplexing of users introduced by HBF is shown to achieve only modest gains with respect to ABF. As expected, the most significant performance improvement with respect to ABF appears in the 5th percentile of the user throughput, with only a 5% gain achieved by HBF compared to the 72% gain reached by DP FS. These results indicate that the application of HBF SU schemes does not provide significant benefits to the networks, being the gap in performance between them and that of the DP SU schemes remarkable. This motivates the study of MU schemes considering the spatial multiplexing of users.

3.5.2 Multi-user case

In this subsection, the performance of DP schemes and HBF with different number of RF chains is compared for the MU transmission case. Besides, the results relative to ABF are also included to allow for a comparison of the MU schemes to the baseline. In MU transmission, the maximum number of spatially multiplexed users per BS is limited by the number of available RF chains $N_{\mathrm{t}}^{\mathrm{RF}}$, which in the HBF scheme is given by the variable P and in the DP schemes is equal to the number of antennas M. Regarding the frequency multiplexing, HBF and DP NFS schemes keep the same set of scheduled UEs along the whole band, whereas DP FS can schedule a different set of users per FB.

The average number of different UEs simultaneously allocated per subframe is reported in Table 3.4. It can be observed how the hybrid scheme makes the most of the number of parallel RF chains until reaching a certain number of chains, from which no more users are multiplexed. In particular, for the simulation setup in this work, even with 16 RF chains, the hybrid scheme only multiplexes 11.9 users on average. Regarding the DP schemes, they show a higher average number of multiplexed users per subframe than the hybrid ones. It is worth noting also that the maximum number of UEs per BS is 16.7 and the DP FS scheme can meaningfully reach this number by performing a more elaborated per-FB allocation.

Table 3.4: Average number of scheduled users per subframe in the MU case.

ABF	**HBF**			**DP NFS**	**DP FS**
	$\boldsymbol{P=4}$	$\boldsymbol{P=8}$	$\boldsymbol{P=16}$		
1	3.9	7.9	11.9	14.1	16.7

Figure 3.6 shows the CDF of the user throughput for the algorithms under study. It is observed that, in the upper part of the CDF curves, the performance of HBF approaches the one of DP when the number of RF chains increases, but a significant gap in performance appears in the lower part, even when the number of RF chains is increased from four to sixteen. For the sake of completeness, the system performance having users in different conditions can be observed in Figures 3.7 and 3.8, which show the CDF curves of user throughput for only those users in LoS and NLoS, respectively. It can be seen that increasing the number of RF chains P in the hybrid scheme has a different impact depending on whether the user is in LoS or NLoS. Note that no benefit for NLoS users is obtained when increasing P beyond eight, since the greater the number of simultaneously scheduled users, the higher the inter-beam interference generated into the system. On the other hand, for the users in LoS, less affected by the interference, increasing P improves the user throughput, which

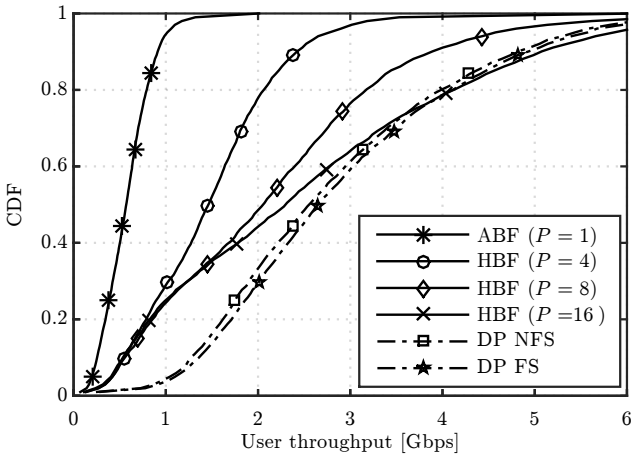

Figure 3.6: CDF of user throughput for the HBF and DP evaluated schemes in the MU case.

reaches similar values to the ones obtained by the DP schemes with sufficiently large P. Concerning the two considered DP variants, both schemes perform very similarly in the three cases (all the UEs, only UEs in LoS and only UEs in NLoS), but the DP FS attains slightly superior performance when compared to DP NFS, due to its higher flexibility in scheduling different sets of UEs in different RBs.

Finally, average user throughput, 5th percentile of the user throughput and average cell throughput values are compared in Table 3.5 for all the simulated algorithms. Table 3.5 also shows the gains with respect to a scheme without spatial multiplexing (i.e., ABF with $P = 1$), considered here as the baseline. This comparison shows the significant benefit of spatially multiplexing multiple users in each subframe. Focusing, for example, on the case of the HBF with four RF chains, it is observed that the gain in the average user throughput is about 150% when compared to the baseline scheme with only one RF chain. Results also highlight the main limitation of the HBF schemes, which, while able to approach the performance of the DP in terms of average user and cell throughput, cannot provide large gains for the 5th percentile user throughput, even when the number of RF chains P increases.

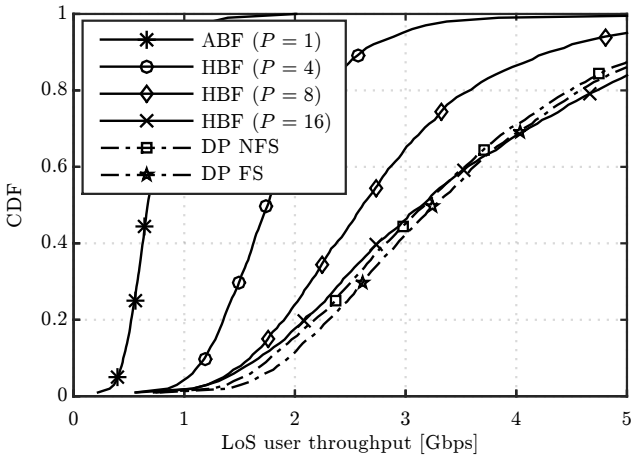

Figure 3.7: CDF of user throughput for the HBF and DP evaluated schemes considering only LoS users in the MU case.

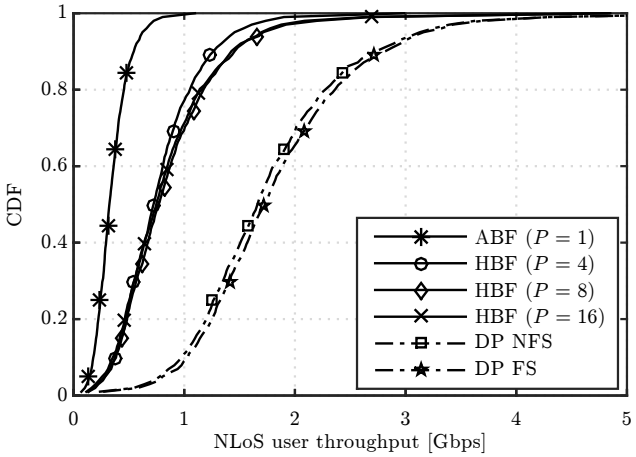

Figure 3.8: CDF of user throughput for the HBF and DP evaluated schemes considering only NLoS users in the MU case.

Table 3.5: Summary of MU performance results with ideal assumptions.

		Average UE throughput		5%-ile UE throughput		Average cell throughput	
		[Gbps]	Gain [%]	[Gbps]	Gain [%]	[Gbps]	Gain [%]
ABF	$\boldsymbol{P = 1}$	0.59	-	0.20	-	9.8	-
HBF	$\boldsymbol{P = 4}$	1.52	157	0.42	112	25.0	155
	$\boldsymbol{P = 8}$	2.22	276	0.42	111	36.4	272
	$\boldsymbol{P = 16}$	2.62	344	0.41	104	43.1	340
DP NFS		2.86	384	1.04	424	47.4	384
DP FS		2.96	401	1.10	453	49.0	400

3.6 Performance with non-ideal assumptions

In this section, results including more realistic assumptions like practical limitations in real systems or the presence of impairments in the hardware components are presented for the MU transmission schemes. More specifically, the following realistic assumptions are analyzed:

- Outdated CSI at the transmitters.
- PAPC in the digital precoding design.
- Inaccuracy errors caused by real phase shifters.
- Losses introduced by real combiners.

3.6.1 Effect of outdated Channel State Information

A very usual ideal assumption for simulation is the perfect knowledge of the instantaneous (per-subframe) channel at every BS, which allows the BS precoder to be adapted to the actual channel. However, practical systems must often deal with the problem of having imperfect CSI. In Frequency Division Duplexing (FDD) systems, the downlink channel is estimated at the UE and fed back to the BS. These estimation and feedback stages can, in practice, impair the CSI with quantization noise, due to the usually limited resources on the feedback channel. In addition, the presence of noise in the channel during the transmission of training sequences for CSI estimation contributes to an imperfect channel estimation. The latter effect is also present in the channel estimation stage of Time Division Duplexing (TDD) systems. Another important practical limitation in both FDD and TDD systems is the unavoidable

delay between the instant the channel is estimated and the instant the channel is used in designing the precoder for data transmission, which, in turn, can further degrade the system performance.

In this subsection, the focus is to evaluate the impact of having outdated CSI on the performance of HBF with $P = 4$, DP NFS and DP FS. To this end, it is here assumed that each BS receives an update of the channel coefficients only every certain period T, higher than the subframe duration $T_s = 1$ ms. It is worth noting that the T values considered cause changes only in the small scale fading components of the channel, i.e., the large scale fading components like path loss, shadowing and path angles of arrival/departure remain constant during T. For a better illustration of the small scale channel variation during the period T, the results will be presented as a function of the product $f_D \Delta T$, where $f_D = vf/c$ is the maximum Doppler shift at carrier frequency f with user speed equal to v, and $\Delta T = T - T_s$ is the CSI delay with respect to the subframe duration.

Figure 3.9 shows the CDF of user throughput for the HBF and DP FS schemes, considering different values of the channel update period, in particular $T = 1,\ 50,\ 150$ and 500 ms, which lead to $f_D \Delta T = 0,\ 3.8,\ 11.6$ and 38.8, respectively. Note that $f_D \Delta T = 0$ corresponds to the ideal case, where the channel is supposed to be updated every subframe. It can be first observed that the HBF scheme is more robust to outdated CSI, as it presents a nearly negligible performance degradation with $f_D \Delta T$. Such degradation of HBF is also much lower than for the DP FS approach, which results in a reduced performance gap between HBF and DP as T increases. The lower robustness to outdated CSI of DP is well justified by the fact that this scheme has a strong dependence on the small scale channel fading, whereas the HBF mainly relies on the large scale components, since it typically tends to point the beamformer towards the angle of departure of the strongest path.

In fact, while in a practical mmW system it is expected that the channel is tracked every few milliseconds or few tens of milliseconds, the higher values of T considered here, e.g., $T = 150,500$ ms, are useful to understand the robustness of the different schemes when there is basically no knowledge of the small scale fading, and, thus, beamformers are designed mainly based on the large scale fading components of the channel. In such a scenario, HBF, by simply selecting the beam that points toward the direction that maximizes the SINR at the receiver, turns out to be much more robust than DP.

For completeness, the average cell throughput for different values of the channel update period including also the DP NFS scheme is depicted in Figure 3.10. The latter results also confirm the robustness of HBF to the effect of outdated CSI, which presents a maximum penalty in cell throughput of 9.8% for $f_D \Delta T = 38.8$. On the other hand, the cell throughput values of DP FS and

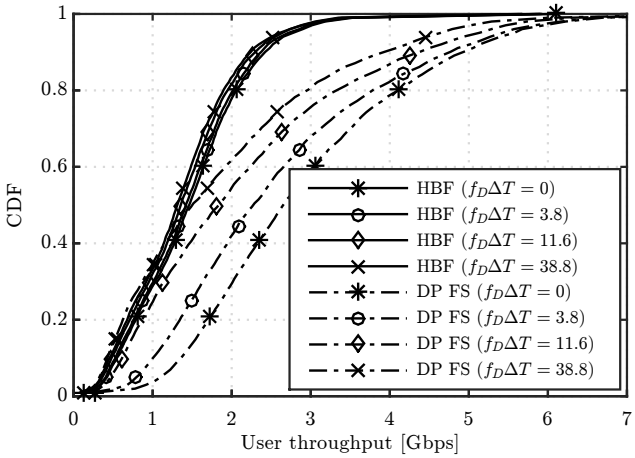

Figure 3.9: CDF of user throughput for the HBF with $P = 4$ and DP FS schemes considering different values of $f_D\Delta T$.

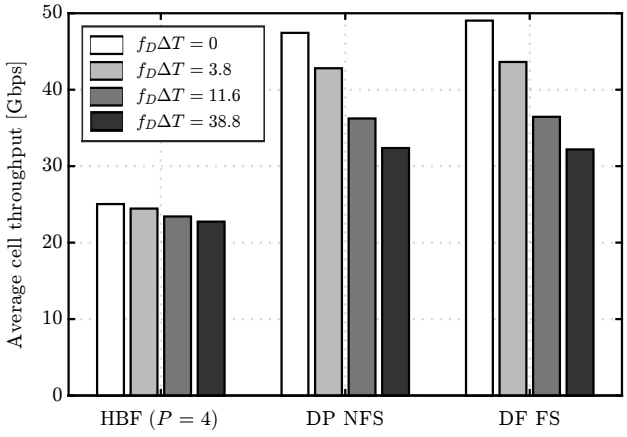

Figure 3.10: Average cell throughput for the HBF with $P = 4$ and DP evaluated schemes considering different values of $f_D\Delta T$.

DP NFS are reduced up to 32% and 34%, respectively. Regarding the comparison between DP NFS and DP FS, both show very similar performance, meaning that the additional complexity of DP FS to adapt the precoder per RB does not pay off with an outdated CSI.

3.6.2 Effect of per antenna power constraints

In practical multi-antenna systems, each element of the antenna array may be powered by its own amplifier and, thus, is limited by the linearity of that amplifier. For that reason, precoding schemes should apply a more restrictive assumption than the sum power constraint, that is, a per-antenna power constraint. In order to study the effect of limiting the maximum available power per antenna, in this section, a second DP alternative that takes into account this practical limitation is considered: the Equal Gain Transmission (EGT) scheme with per-antenna power constraints [56]. Note that PAPC is implicitly satisfied by the HBF scheme considered in this chapter, and, thus, the selection of EGT for DP allows a fair comparison from a power allocation perspective.

EGT ensures the allocation of the same amount of power per element of the antenna array. Moreover, its implementation is simple and has shown a bounded performance degradation in comparison to the MRT precoder when the number of antenna elements in the array is sufficiently high [109]. If the channel vector between UE u and its serving BS i in FB b is expressed as:

$$\mathbf{h}_{u,i}^{b} = \left[|h_1|e^{j\theta_1}, |h_2|e^{j\theta_2}, \ldots, |h_{N_t}|e^{j\theta_M}\right]^{\intercal}, \tag{3.14}$$

then, the corresponding EGT precoding vector for UE u in FB b, $\mathbf{b}_{u,i}^{b,\mathrm{EGT}}$ is:

$$\mathbf{b}_{u,i}^{b,\mathrm{EGT}} = \frac{1}{\sqrt{M}}\left[e^{-j\theta_1}, e^{-j\theta_2}, \ldots, e^{-j\theta_M}\right]^{\intercal}. \tag{3.15}$$

Figure 3.11 shows the CDF of user throughput for the two DP alternatives, MRT and EGT, both of them configured according to the two scheduling variants under study (DP NFS and DP FS). The performance results of HBF with $P = 4$ and $P = 16$ RF chains with ideal assumptions are also included in the figure for the sake of comparison. In general, the EGT precoder worsens the throughput performance of both DP variants, although not very significantly. A meaningful result is that MRT DP NFS achieves very similar performance to EGT DP FS. Therefore, the performance loss due to the PAPC constraint can be, in this case, compensated by a more elaborated scheduler (per FB instead of per subframe). Moreover, the power per antenna element limitation brings the performance of digital precoders a bit closer to the one of HBF with $P = 16$ RF chains, i.e., with the same multiplexing capacity, although there is still a substantial performance gap for NLoS UEs (lower part of the CDF curve).

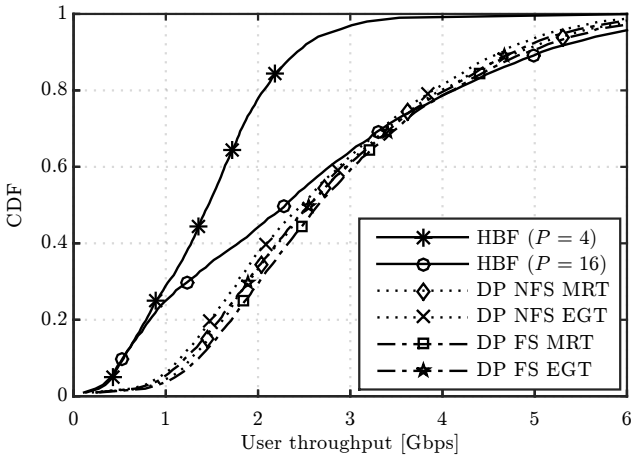

Figure 3.11: CDF of user throughput for the HBF, MRT and EGT evaluated schemes.

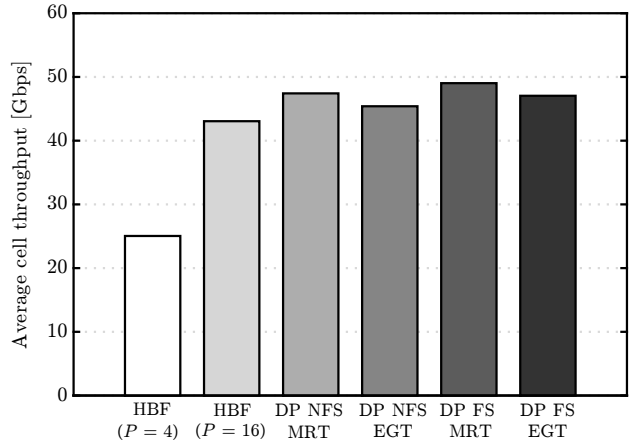

Figure 3.12: Average cell throughput values for the HBF, MRT and EGT evaluated schemes.

Finally, the average cell throughput values for the HBF, MRT and EGT evaluated schemes are included in Figure 3.12. From this figure, it can be confirmed that the EGT precoder causes approximately a 4% performance loss over both DP variants, a percentage much lower than the one caused by outdated CSI over DP.

3.6.3 Effect of phase-shifter errors

As shown in Figure 3.1, in the full connected HBF architecture, phase shifts are applied to each antenna element of the array in order to steer the beam towards a certain direction. In real implementations, the conformed beams are altered due to the phase errors introduced by the non-ideal phase shifters. In order to study the impact of this effect, the phase shifter error of the i-th phase shifter, denoted by δ_i, can be modeled as a uniformly-distributed random variable in the interval $[-\delta_{max}, \delta_{max}]$ [110]:

$$\delta_i \in [-\delta_{max}, \delta_{max}], 0 \leq \delta_{max} \leq 180^\circ, \tag{3.16}$$

where δ_{max} is a parameter depending on the phase shifter implementation [51, 52] and the δ_i variables are assumed independent among different phase shifters. Therefore, if θ_i is the ideal phase shift to be applied by phase shifter i, the actual phase shift applied including the phase shifter error is given by $\theta'_i = \theta_i + \delta_i$.

In this subsection, phase shifter errors constant over the bandwidth of interest but variable with time are studied. Note that phase shifter errors that are constant with time are mainly caused by manufacturing imperfections, and, thus, they could be estimated and compensated in the beamforming stage. Contrarily, phase shifter errors variable with time cause a random and unpredictable error that cannot be estimated and compensated. As a consequence, different beams for the channel estimation and transmission phases are conformed due to the inclusion of changing phase-shifter errors over time, what affects the performance of FDD systems. Indeed, the presence of the phase-shifter errors that vary over time causes that the beam selected from the codebook during the scheduling phase may be a suboptimum beam for the transmission phase. Note that this is a worst-case scenario for the evaluation of the impact of phase-shifter errors.

Table 3.6 collects several performance results for an HBF scheme with $P = 4$ affected by phase shifter errors, for three different values of the δ_{max} parameter in degrees: $\delta_{max} = 2^\circ, 6^\circ$ and 10°. Note that, according to previous works [51, 52], the value of $\delta_{max} = 10^\circ$ is very unlikely in practice, and, thus, it is here included for a worst-case evaluation. In particular, average and 5th percentile user throughput values have been obtained considering only the UEs in LoS, only the UEs in NLoS, or both types combined. Average cell throughput

Table 3.6: Performance results of the HBF scheme with $P = 4$ including phase shifter errors.

		$\delta_{max} = 2°$		$\delta_{max} = 6°$		$\delta_{max} = 10°$	
		[Gbps]	Loss [%]	[Gbps]	Loss [%]	[Gbps]	Loss [%]
Average UE throughput	**LoS**	1.871	0.12	1.847	1.41	1.807	3.55
	NLoS	0.794	−0.03	0.785	1.10	0.770	2.94
	All UEs	1.518	0.12	1.500	1.34	1.467	3.51
5%-ile UE throughput	**LoS**	1.029	0.34	1.021	1.15	1.004	2.77
	NLoS	0.311	−0.12	0.309	0.43	0.304	2.11
	All UEs	0.419	0.51	0.415	1.44	0.410	2.62
Average cell throughput		25.01	0.12	24.7	1.37	24.2	3.46

values are also included. In all cases, the performance loss with respect to the ideal case is also shown. The results reveal that the impact of phase shifter errors is very minor, and it only causes a maximum reduction of 3.5% in user throughput, particularly for LoS users with a pessimistic value of $\delta_{max} = 10°$. Indeed, LoS UEs are more affected by this impairment because they strongly depend on the accuracy of the direct beam. In addition, since the equivalent receive beams of LoS UEs are narrower (in meters) than those of NLoS UEs, generally located farther away from the BS, an error in the pointing direction is more critical when serving LoS UEs.

3.6.4 Effect of combiner losses

In the HBF architecture, the output signals of the different RF chains are mixed together by means of a combiner and fed to the antenna array. Non-ideal combiners are known to introduce a power loss in their outputs [111], which increases with the number of branches that the device has to combine. Let us denote with L_{lin} the power loss in linear units of a basic combiner with two input branches. Then, the output power of the combiner is given by the sum of the two input powers divided by L_{lin}, as shown in Figure 3.13.

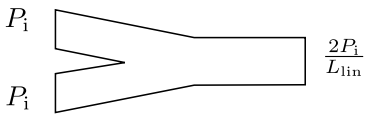

Figure 3.13: Example of a 2-inputs combiner with input power P_{i}

Considering that a combiner for a generic number P of RF chains is implemented by means of a cascade of $\log_2 P$ two-branch combiners, the total loss is given by:

$$L_{\text{lin}}^{(tot)} = L_{\text{lin}}^{\log_2 P}, \tag{3.17}$$

and expressed in logarithmic units:

$$L^{(tot)} = \log_2 P \cdot L \quad [\text{dB}], \tag{3.18}$$

where $L = 10 \log_{10}(L_{\text{lin}})$.

Note that, differently from the results with ideal hardware shown in Figure 3.3, where user throughput increases with the number of available RF chains in the hybrid architecture, the performance trend is different when considering the combiner power losses. Indeed, there exists an optimum number of RF chains depending on the scenario, caused by these two opposing effects of increasing the number of the RF chains: on the one hand, the number of users that can be served by the BS is higher thus improving the spatial multiplexing gain; on the other hand, a larger power loss is introduced by the combiners thus decreasing the SINR measured at the UEs.

Regarding the selection of L values, note that the case without any compensation of losses corresponds to $L = 3$ dB [53], where half of the input power is lost. However, in those cases where compensation of the losses is possible by adding power amplifiers after the combiner stages, realistic values for combiner losses range from 0 to 3 dB. In this sense, $L = 1$ dB is selected as a meaningful intermediate evaluation point. It is worth noting that compensation of losses involves an additional cost due to including extra per-antenna power amplifiers.

Figure 3.14 shows the CDF of user throughput for HBF with different number of RF chains, $P = 4,\ 8$ and 16, and two values of the two-branch combiner loss parameter, $L = 1,\ 3$ dB. Results show that, for $L = 1$ dB, the best results are obtained with $P = 16$ RF chains. However, when $L = 3$ dB is considered, the scheme with $P = 8$ RF chains achieves the best performance. Therefore, the optimum number of RF chains depends strongly on the combiner losses.

The results in Figure 3.14 are complemented by Table 3.7, which collects the average UE throughput, 5th percentile UE throughput and average cell throughput for the same schemes. More specifically, the table contains the average values of each performance indicator in Gbps and also the performance loss with respect to having ideal combiners ($L = 0$ dB). It is again observed that, for $L = 1$ dB, $P = 16$ RF chains is the best option, despite the fact that the higher the number of RF chains, the higher the total losses due to realistic combiners (for instance, the loss in average UE throughput is around 5% for

$P = 4$ but around 9% for $P = 16$). However, for the $P = 16$ case, the gain in average cell throughput is reduced from 10% with $L = 1$ dB to more than 45% with $L = 3$ dB. Furthermore, in the latter case, the degradation for the users in the cell edge is of around a factor of 4, which reinforces the conclusion that no more than eight parallel RF chains are recommended in the HBF scheme when $L = 3$ dB. All the results show the large impact that the combiner losses have on the performance of the algorithms, especially when the number of RF chains gets higher.

Finally, it is worth noting that the optimum number of RF chains is different for the users in LoS and NLoS conditions. In fact, for $L = 1$ dB, better results are obtained for both types of users when increasing the number of RF chains, as the user multiplexing offered by the massive MIMO setup compensates for the degradation due to combining losses. On the other hand, for $L = 3$ dB, LoS users achieve the best performance with eight RF chains, while NLoS users get higher throughputs when using only four RF chains. In the end, the percentage of LoS/NLoS users in the system together with the combiner losses will determine the optimum number of active RF chains for HBF.

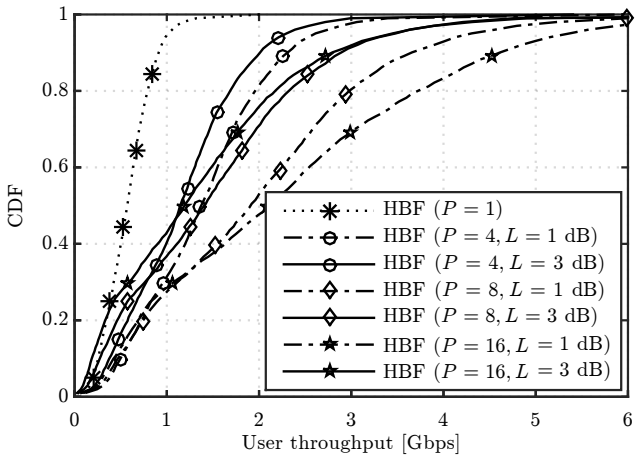

Figure 3.14: CDF of user throughput for the HBF scheme with different values of P and L.

Table 3.7: Average UE throughput of the HBF scheme with combiner losses for different numbers of RF chains.

	$P = 4$				$P = 8$				$P = 16$			
	$L = 1$ dB		$L = 3$ dB		$L = 1$ dB		$L = 3$ dB		$L = 1$ dB		$L = 3$ dB	
Average UE throughput												
	[Gbps]	Loss [%]	[Gbps]	Loss [%]	[Gbps]	Loss [%]	[Gbps]	Loss [%]	[Gbps]	Loss [%]	[Gbps]	Loss [%]
LoS	1.77	5.25	1.52	18.99	2.69	6.15	2.08	27.43	3.18	8.45	1.94	44.12
NLoS	0.74	7.25	0.59	25.72	0.77	12.51	0.51	42.69	0.73	16.54	0.38	56.41
All	1.44	5.52	1.21	20.10	2.07	6.89	1.57	29.08	2.38	9.23	1.44	45.11
5%-ile UE throughput												
	[Gbps]	Loss [%]	[Gbps]	Loss [%]	[Gbps]	Loss [%]	[Gbps]	Loss [%]	[Gbps]	Loss [%]	[Gbps]	Loss [%]
LoS	0.96	6.76	0.78	24.29	1.26	7.21	0.86	36.40	1.26	8.39	0.68	50.53
NLoS	0.28	9.15	0.20	34.51	0.24	22.09	0.13	59.50	0.21	27.52	0.09	69.97
All	0.38	9.37	0.28	33.38	0.34	18.66	0.18	57.51	0.30	25.85	0.12	70.53
Average cell throughput												
	23.63	5.64	19.98	20.20	33.90	6.95	25.58	29.79	38.97	9.50	23.19	46.14

3.7 Conclusions

This chapter has presented a thorough performance evaluation of digital precoding and hybrid beamforming schemes in a massive MIMO multi-cell deployment operating in the mmW frequency band. In the first part of the chapter, a description of the full-connected hybrid beamforming architecture has been provided, and a brief overview of the best-known analog and digital precoding techniques has been reviewed.

Then, a comparison among HBF and DP schemes has been carried out under ideal assumptions, namely, perfect and timely CSI at the transmitters, ideal phase-shifters and combiners in the hybrid architecture and lack of PAPC in digital precoding. SU and MU schemes have been compared against ABF without spatial multiplexing of users, considered here as the baseline scheme. It is observed that, by spatially multiplexing several users at a time, the throughput is substantially increased in all cases. Simulation results further show that HBF schemes can reach the performance of fully digital precoders when working under LoS conditions and with a sufficient number of parallel RF chains. On the other hand, HBF schemes have shown to be more sensitive to interference and, thus, more degraded in NLoS conditions, in which increasing the number of RF chains cannot provide any advantage.

After the initial performance comparison, the effect of several realistic impairments has been included in the simulation setup. To this aim, the effect of having only outdated CSI at the BS has been firstly analyzed. In addition, PAPC have been set in the two considered DP variants to also see the effect of this realistic constraint. Lastly, the errors introduced by both the phase shifters and combiners in the hybrid architecture have been modeled.

From the results with outdated channel information, it can be concluded that DP schemes are more sensitive to imperfections on the CSI knowledge at the BS, presenting large losses (up to 34%) when the CSI update period increases. On the other hand, HBF schemes have shown to be robust against the channel information inaccuracy, presenting a negligible reduction of performance when the channel reporting period increases.

The results with PAPC have exhibited a performance reduction in DP schemes based on MRT of about 4%, which leads to a small reduction of the performance gap between digital and hybrid implementations. In practice, the performance loss due to the PAPC could be compensated, for instance, by means of a more elaborated scheduler with a more frequent update of precoders.

Regarding the effect of phase-shifter errors, simulation results have shown that this impairment has little impact on the HBF performance, even when the magnitude of the introduced phase error is significantly higher than current state-of-the-art values known from manufacturing. Nevertheless, LoS UEs

suffer a stronger degradation due to this impairment when compared to the NLoS UEs, due to their narrower received beams. Conversely, combiner losses have indeed a significant impact on the system performance, mainly when the number of RF chains in the hybrid scheme is high. In fact, the magnitude of the power loss introduced by the combiner determines in the end the optimum number of RF chains to be selected for hybrid beamforming. Overall, it is more suitable to employ a low number of RF chains when the losses introduced by the combiner are large.

On the basis of these conclusions, next steps point to the study of Ultra Dense Networks (UDNs) in which the probability of users of being in LoS propagation conditions approaches the 100%, to make the most of the HBF schemes performances. Furthermore, the evaluation of more sophisticated precoding schemes that incorporate an optimized BB precoding stage will be also in the focus of next chapter.

Chapter 4

Distributed hybrid precoding for indoor deployments using millimeter wave band

4.1 Introduction

Distributed Antenna Systems (DAS) are network architectures in which the antenna elements of a Base Station (BS) are geographically distributed throughout the coverage area. This alternative of network densification allows for a reduction of the distance between transmitters and receivers at the same time as it enables a simpler coordination among the different Remote Antenna Units (RAUs), thanks to the high bandwidth and low latency dedicated connection between antennas and BSs. Several works in the literature have assessed the performance of DAS deployments working at currently used cellular frequencies, as reviewed in Section 1.2.2. Nevertheless, the closer proximity of the users to the antennas in DAS increases the probability of Line of Sight (LoS) transmission, what makes this kind of deployments particularly interesting for their use at millimeter wave (mmW) frequencies. Indeed, as it was shown in the previous chapter, high performance is achieved for those users in LoS propagation conditions when using Hybrid Beamforming (HBF) schemes in mmW.

The study conducted in the previous chapter encompassed the assessment of HBF in an outdoor urban micro-scenario. As pointed out by the conclusions

of that study, there is still a gap in performance between HBF and Digital Precoding (DP) schemes, even for those users in LoS propagation conditions. The main reasons are the limited availability of Radio Frequency (RF) chains in the hybrid architecture, but also the lack of per Frequency Block (FB) Baseband (BB) precoding design in the HBF schemes, to better adapt to the channel frequency variations. Motivated by this, the performance of Hybrid Precoding (HP) schemes including both BB and RF precoding are assessed in this chapter, considering an indoor scenario where almost 100% of the users are in LoS propagation conditions.

To this aim, three different deployment strategies are analyzed, including a conventional picocell deployment with co-located antenna arrays, a regular femtocell deployment and a DAS deployment. Moreover, a Distributed Hybrid Precoding (DHP) algorithm suitable for distributed antennas and with RAU selection capabilities is proposed for its application in indoor DAS. Its performance is evaluated and compared to the performance of other deployment strategies applying HP schemes, under ideal conditions. Further simulations are conducted including non-ideal assumptions, in order to better understand the impact on the performance of DHP in DAS of two important practical limitations of the hybrid architectures, the use of outdated Channel State Information (CSI) at the transmitter, and the power losses introduced by non-ideal RF combiners. The rest of this chapter is organized as follows:

- Section 4.2 describes the system model assumed throughout the chapter.
- Section 4.3 details the Distributed Hybrid Precoding (DHP) algorithm proposed for DAS deployments.
- Section 4.4 presents the simulation setup, including the definition of the different indoor deployment strategies compared along the chapter. In addition, the implementation particularities of the multi-antenna schemes assessed in the chapter are introduced.
- Section 4.5 includes the performance evaluation of DHP and HP under ideal simulation assumptions for all the indoor deployment strategies.
- Section 4.6 is devoted to the performance evaluation of of DHP and HP introducing non-ideal assumptions in the simulations, such as outdated CSI at the transmitter and power losses introduced by real RF combiners.
- Section 4.7 draws the main findings of this study.

4.2 System model

In this chapter, a downlink Orthogonal Frequency Division Multiplexing (OFDM) system working in Frequency Division Duplexing (FDD) mode at 73 GHz is considered. The scenario consists of an indoor rectangular room of 120 m $\times$ 50 m, where N_{BS} equipped with $N_{\mathrm{t}}^{\mathrm{RF}}$ RF chains and M antennas are regularly deployed. Regarding the User Equipment (UE) devices, N_{UE} single-antenna users are considered to be randomly deployed over the rectangular room, and cell selection is performed according to the maximum received power by the user.

It is also assumed that each BS implements the full-connected hybrid architecture for mmW described in Section 3.2. Note that the extension of this hybrid architecture to passive DAS is straightforward, by simply considering the antenna elements distributed over the coverage area of each cell via any transmission line such as wire or optical fiber. In any case, the power losses introduced by the distribution lines are considered to be negligible for the short deployment distances under consideration.

The channel model used is based on the 3-Dimensional (3D) mmW indoor channel model proposed by Sun *et al.* in [112]. This model has been derived at 73 GHz, using data extracted from a propagation measurement campaign performed in a typical office scenario, and filling the gaps in the measurements by means of a ray tracing tool. The model follows a Third Generation Partnership Project (3GPP)-style and characterizes the channel in azimuth, elevation and polarization terms. Concerning large scale fading, shadowing is added on top of the pathloss term [113], with standard deviations of 1 dB and 9 dB for LoS and Non Line of Sight (NLoS) conditions, respectively. Antenna pattern is considered to be omnidirectional.

The downlink transmission resources are partitioned in the time-frequency plane, as in Chapter 3. In the time domain, the resource space is divided into subframes of a certain time duration. In the frequency domain, resources are grouped in FB. The minimum time-frequency resource is known as Resource Block (RB), and it comprises one frequency block during one subframe period.

4.3 Distributed Hybrid Precoding for DAS

In this section, the proposed Distributed Hybrid Precoding (DHP) for DAS using mmW is presented. The particularity of DHP is its suitability for BSs implementing hybrid architectures with distributed antennas. As introduced in Section 3.3.3, most of the hybrid precoding schemes approach the design of the RF and BB precoding matrices independently, due to the high complexity

derived from a joint optimization. In this line, DHP is used by combining a precoding stage in BB and a beamforming stage in RF designed in a separated fashion. For the BB precoding, linear Regularized Zero Forcing (RZF) is applied, while in RF a codebook-based beamforming for distributed antennas, named Distributed Analog Beamforming (DAB), is used. The details of the DAB codebook generation are provided hereinafter.

Distributed Analog Beamforming (DAB)

Despite the good compromise between performance and complexity given by Discrete Fourier Transform (DFT)-based beamforming in conventional systems, its application to DAS results in an inevitable performance degradation [32]. The reasons are the distributed and not equally spaced antenna elements in DAS, which leads to non-orthogonal conformed beams at the RAUs and low beamforming gains. In addition, the fact that DFT beamforming vectors equally distribute the power among all the elements of the antenna array makes this beamforming technique unable to perform antenna selection schemes in DAS.

For that reason, a simple approach to generate a codebook suitable for RF beamforming in DAS and with RAU selection capabilities, called DAB, is proposed in this section. This approach consists of the following steps:

(i) To select a codebook for each RAU. Note that, in this chapter, the DFT-based codebook beamforming described in Section 3.3.2 has been selected for this step, but any other codebook could be chosen.

(ii) To update the selected codebook by including a null codeword that allows the deactivation of the RAU transmission.

(iii) To generate the DAB codebook by putting together all the possible combinations of codewords at the RAUs.

(iv) To remove the combination of codewords that deactivate all the RAUs at the same time, and to normalize the columns of the resulting codebook.

Let us assume that the M antennas of each BS are distributed among R RAUs, being $M_R = \frac{M}{R}$ the number of equally spaced antennas per RAU. Then, in step (i) the DFT sub-codebook $\mathbf{C}_{\text{DFT}} \in \mathbb{C}^{M_R \times M_R}$ for every RAU is created by using Eq. (3.10), and setting $C = M_R$, in order to guarantee the non-overlap

of the beams conformed at each RAU:

$$\mathbf{C}_{\mathrm{DFT}} = \frac{1}{\sqrt{M_R}} \begin{bmatrix} 1 & 1 & ... & 1 \\ 1 & e^{-j2\pi 1 \frac{1}{M_R}} & ... & e^{-j2\pi 1 \frac{M_R-1}{M_R}} \\ ... & & & \\ 1 & e^{-j2\pi (M_R-1) \frac{1}{M_R}} & ... & e^{-j2\pi (M_R-1) \frac{M_R-1}{M_R}} \end{bmatrix}. \quad (4.1)$$

In step (ii), a null codeword is aggregated to the codebook, which allows the BS to deactivate the use of the antennas at RAU r when required:

$$\mathbf{C}_{\mathrm{DAB}}^{(r)} = \left[\begin{array}{c|c} {\mathbf{C}_{\mathrm{DFT}}}^{(M_R \times M_R)} & \begin{matrix} 0 \\ \vdots \\ 0 \end{matrix} \end{array} \right] = \begin{bmatrix} \mathbf{c}_1 & \mathbf{c}_2 & ... & \mathbf{c}_{M_R+1} \end{bmatrix}, \quad (4.2)$$

where $\mathbf{c}_i \in \mathbb{C}^{M_R \times 1}$ represents each column or codeword in $\mathbf{C}_{\mathrm{DAB}}^{(r)}$.

In step (iii), a codebook containing the codewords of M elements for all the antennas in the BS is generated. This step is performed by creating all the possible combinations of R codewords $\mathbf{c}_i$ out of $\mathbf{C}_{\mathrm{DAB}}^{(r)}$. Note that there exist a total of $(M_R+1)^R$ possible combinations to create the new codewords $\mathbf{m}_i \in \mathbb{C}^{M \times 1}$:

$$\begin{aligned} \hat{\mathbf{C}}_{\mathrm{DAB}} &= \begin{bmatrix} \mathbf{c}_1 & \mathbf{c}_1 & ... & \mathbf{c}_1 & \mathbf{c}_1 & ... & ... & \mathbf{c}_{M_R+1} \\ \mathbf{c}_1 & \mathbf{c}_1 & ... & \mathbf{c}_1 & \mathbf{c}_1 & ... & ... & \mathbf{c}_{M_R+1} \\ & & \vdots & & & \vdots & \vdots & \\ \mathbf{c}_1 & \mathbf{c}_1 & ... & \mathbf{c}_1 & \mathbf{c}_2 & ... & ... & \mathbf{c}_{M_R+1} \\ \mathbf{c}_1 & \mathbf{c}_2 & ... & \mathbf{c}_{M_R+1} & \mathbf{c}_1 & ... & ... & \mathbf{c}_{M_R+1} \end{bmatrix} = \\ &= \begin{bmatrix} \mathbf{m}_1 & \mathbf{m}_2 & ... & \mathbf{m}_{(M_R+1)^R} \end{bmatrix}. \end{aligned} \quad (4.3)$$

Finally, in step (iv), the last codeword $\mathbf{m}_{(M_R+1)^R}$ is removed, since it would result in the deactivation of all the RAUs at the same time. Therefore, $\mathbf{C}_{\mathrm{DAB}} \in \mathbb{C}^{M \times (M_R+1)^R - 1}$ is given by:

$$\mathbf{C}_{\mathrm{DAB}} = \begin{bmatrix} \alpha_1 \mathbf{m}_1 & \alpha_2 \mathbf{m}_2 & ... & \alpha_{(M_R+1)^R-1} \mathbf{m}_{(M_R+1)^R-1} \end{bmatrix}, \quad (4.4)$$

where $\alpha_i = 1/|\mathbf{m}_i|$, $i = 1, ..., (M_R+1)^R - 1$, is applied to normalize the columns of $\hat{\mathbf{C}}_{\mathrm{DAB}}$.

The main advantages of DAB codebook are the inclusion of RAU selection, which permits that each user is served by its optimum set of RAUs, and the deletion of overlapped beams at each sub-array. An example of DAB codebook

creation is shown in Table 4.1 for a system with BSs equipped with 4 antennas distributed in two RAUs.

Table 4.1: Example of DAB creation for a DAS system with BSs equipped with four antennas distributed in two RAUs.

i. Selection of a DFT codebook suitable for each RAU.

$$\mathbf{C}_{\mathrm{DFT}}^{(r)} = \begin{bmatrix} 1 & -1 \\ 1 & 1 \end{bmatrix}$$

ii. Addition of the null codeword:

$$\mathbf{C}_{\mathrm{DAB}}^{(r)} = \begin{bmatrix} 1 & -1 & 0 \\ 1 & 1 & 0 \end{bmatrix}$$

iii. Generation of codewords combination:

$$\hat{\mathbf{C}}_{\mathrm{DAB}} = \begin{bmatrix} 1 & 1 & 1 & -1 & -1 & -1 & 0 & 0 & 0 \\ 1 & 1 & 1 & 1 & 1 & 1 & 0 & 0 & 0 \\ 1 & -1 & 0 & 1 & -1 & 0 & 1 & -1 & 0 \\ 1 & 1 & 0 & 1 & 1 & 0 & 1 & 1 & 0 \end{bmatrix}$$

iv. Deletion of null codeword and normalization of every codeword:

$$\mathbf{C}_{\mathrm{DAB}} = \begin{bmatrix} 1/2 & 1/2 & 1/\sqrt{2} & -1/2 & -1/2 & -1/\sqrt{2} & 0 & 0 \\ 1/2 & 1/2 & 1/\sqrt{2} & 1/2 & 1/2 & 1/\sqrt{2} & 0 & 0 \\ 1/2 & -1/2 & 0 & 1/2 & -1/2 & 0 & 1/\sqrt{2} & -1/\sqrt{2} \\ 1/2 & 1/2 & 0 & 1/2 & 1/2 & 0 & 1/\sqrt{2} & 1/\sqrt{2} \end{bmatrix}$$

4.4 Simulation setup and evaluated precoding schemes

In this section, a description of the indoor deployment strategies evaluated throughout the chapter as well as the digital and hybrid precoding schemes used for that aim is provided. In addition, all the configuration parameters used for the simulations are detailed.

4.4.1 Deployment strategies

The performance of digital and hybrid precoding schemes is analyzed for three typical Small Cell (SC) indoor deployment strategies [23], depicted in Figure 4.1 and characterized as follows:

CON The first strategy, labeled as CON, consists of a conventional deployment of two picocells, each one equipped with a co-located Uniform Linear Array (ULA) of 24 elements.

Fx The second strategy is the use of regular femtocell deployments, where x indicates the total number of SCs deployed in the scenario. This deployment strategy corresponds to scenarios F4 and F8 in the figure. For the sake of a fair comparison among scenarios, the same total number of antenna elements is configured at each of them, so femtocells in F4 and F8 are equipped with 12-element ULA and 6-element ULA, respectively.

DASx The last strategy is the use of DAS, considering a deployment of two picocells, each one equipped with 24 antenna elements. Note that in DAS scenarios antennas are not co-located but distributed among x RAUs. In DAS4, each SC has 2 RAU equipped with a 12-element ULA, while in DAS8 each SC has 4 RAU equipped with 6-element ULA. Although no coordination among BSs is considered, joint transmission from all the RAUs belonging to a BS is assumed in these deployments.

For the sake of a fair comparison among the defined scenarios, a site comprises at each deployment the set of cells located in a half of the scenario, considering a vertical dividing line located at the center of it. Therefore, for CON, DAS4 and DAS8 scenarios, a site corresponds to a cell, whereas for F4 and F8 deployments a site is composed by two and four femtocells, respectively. Note that, by using this definition, the power and number of antenna elements per site is exactly the same for all deployments. Note also that the antenna locations in DASx and Fx are coincident for the same value of x. A summary of the configuration details for each scenario is collected in Table 4.2. It is also important to remark that, with the implemented channel model, all deployments lead to a 99% of the users being in LoS propagation, reason why contrarily to Chapter 3, simulation results in this chapter do not differentiate among users in LoS or NLoS conditions.

4.4.2 Evaluated precoding schemes

The selected precoding schemes considered to accomplish the performance evaluation of the aforementioned scenarios include:

- Only Multi-User (MU) transmission. The work in this chapter focuses on precoding schemes that allow multiplexing users in the spatial domain. The set of users to be simultaneously served by a BS are allocated to the whole available bandwidth, i.e., schemes exploiting frequency diversity are out of the scope of this chapter.

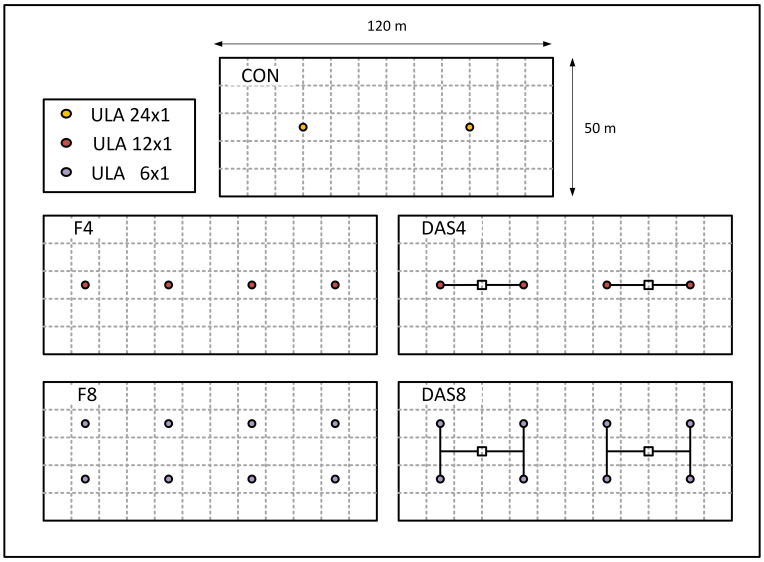

Figure 4.1: Scenarios defined for the comparison of different indoor deployment strategies, including a conventional deployment with two picocells (CON), two femtocell deployments with 4 and 8 cells (F4 and F8) and DAS with 4 and 8 RAUs (DAS4 and DAS8).

Table 4.2: Configuration details of the simulated scenarios, where M is the number of antennas per SC, R is the number of RAUs per BS, and M_R is the number of antennas per RAU.

	Number of SCs	$\boldsymbol{R}$	$\boldsymbol{P_t}$ **[dBm]**	$\boldsymbol{M}$	$\boldsymbol{M_R}$
CON	2	-	30	24	-
F4	4	-	27	12	-
F8	8	-	24	6	-
DAS4	2	2	30	24	12
DAS8	2	4	30	24	6

- Schemes for both digital and hybrid architectures. The performance of hybrid schemes is assessed and compared to the performance of fully digital implementations, which are considered as an upper-bound of performance.

- Hybrid precoding schemes for both co-located and distributed antenna arrays. HP is performed in CON and Fx scenarios, while the Distributed Hybrid Precoding (DHP) scheme proposed in this chapter, DHP, is applied to DAS scenarios, where its performance is compared to the one of conventional HP schemes.

Hybrid precoding schemes

In this chapter, the HP scheme is performed by applying RZF precoding in the digital stage and a DFT-based codebook in the analog one. Furthermore, DHP for DAS deployments is performed by applying RZF and DAB in the digital and analog stages, respectively. Note that all these techniques, together with their benefits, have been explained in Sections 3.3 and 4.3.

User selection in DHP and HP schemes is designed to maximize the orthogonality of the conformed beams in the RF stage. To this aim, the iterative user scheduling Algorithm 1 described in Chapter 3 is applied as well in this chapter, with the following particularities:

- variable $\mathcal{B}$ refers in this case to the whole bandwidth, since user scheduling in DHP and HP is performed only wideband;

- the optimum beamforming vector for each user u, $\mathbf{b}_u^{\mathcal{B}} \in \mathbb{C}^{M\times 1}$, is chosen from DFT and DAB codebooks in HP and DHP schemes, respectively. Note that digital precoders do not affect the user scheduling decisions made in the hybrid schemes;

- scheduling weights of each user $u \in \mathcal{U}$, α_u, are computed to fulfill a Round Robin (RR) policy.

Digital precoding schemes

Fully DP schemes are implemented and evaluated in this chapter for the three deployment strategies in order to provide an upper bound of system performance. RZF has been chosen as digital precoder for a fair comparison with the HP schemes, which also use RZF in their BB stage. User selection is performed according to a RR scheduling policy, multiplexing as many users as BS antennas per subframe.

Finally, Table 4.3 shows a comparison of the evaluated precoding schemes in this chapter. It is important to highlight that hybrid schemes are analyzed considering a reduced number P of RF chains per BS. Besides, note that this number will also depend on the number of cells deployed at each scenario, since the total number of RF chains is kept fixed for all of them.

Table 4.3: Summary of the evaluated precoding algorithms in the chapter.

		Precoding	$\boldsymbol{N}_{\mathrm{t}}^{\mathrm{RF}}$
MU	**HP**	RZF+DFT	$P < M$
	DHP	RZF+DAB	$P < M$
	DP	RZF	M

4.4.3 Setup configuration

A total frequency bandwidth of 20 MHz is considered for the simulations, divided in N_{FB} FBs, each of bandwidth $\Delta f = 200$ kHz. User selection and RF precoding are performed wideband, while BB precoding is computed per FB. The expected throughput achieved by the u-th user served by BS i is computed by using the following expression:

$$\mathrm{Th}_{u,i} = \sum_{f=1}^{N_{\mathrm{FB}}} \Delta f \log_2(1 + \mathrm{SINR}_{u,i}^{f}), \tag{4.5}$$

where $\mathrm{SINR}_{u,i}^{f}$ particularizes the Signal to Interference plus Noise Ratio (SINR) for the FB f. Other important parameters used for the simulations are collected in Table 4.4.

4.5 Performance comparison of ideal indoor deployment strategies

In this subsection, a performance comparison of the different indoor deployment strategies is conducted for both fully digital and hybrid precoding under ideal assumptions. Although fully digital precoding schemes are not suitable for mmW systems with large antenna arrays, their simulation can provide us with an upper bound of performance for the evaluation of the hybrid implemented schemes. For that reason, simulation results with DP precoding are

Table 4.4: Simulation Parameters.

Simulation time per drop	1 s
Number of drops	10
Subframe duration, T_{s}	1 ms
Carrier frequency f	73 GHz
Number of FBs, $N_{\mathbf{FB}}$	100
FB bandwidth, Δf	200 kHz
Scheduling policy	Round Robin
Thermal noise PSD	-174 dBm/Hz
BS height	6 m
BS antenna element pattern	omnidirectional
Number of deployed UEs	100
UE antenna element pattern	omnidirectional
UE noise figure	7 dB
UE speed	3 km/h
UE height	1.5 m

presented in the first place, and the performance of HP and DHP in the different deployments is analyzed afterwards. Finally, a brief comparison between RZF and DHP is performed focusing on one specific scenario.

4.5.1 Results using fully digital precoding

Recall that for the simulation of DP precoding in the different deployments, each BS is considered to be equipped with as many RF chains as antennas, which results in a total of 48 RF chains in the network. The average number of multiplexed users per site is collected in Table 4.5 for all the simulated scenarios, where it is shown that RZF makes the most of the available RF chains and multiplexes as much users per site as possible. Only a small loss in the number of multiplexed users is seen for F8, given by a small imbalance among the amount of users assigned to each femtocell, that will disappear with the average of more simulation drops.

Table 4.5: Average number of multiplexed users per site with DP (RZF) for every simulated scenario.

	CON	**DAS4**	**F4**	**DAS8**	**F8**
DP	24.00	24.00	24.00*	24.00	23.95*

* In this case, a site is assumed to be the group of cells located in half the scenario.

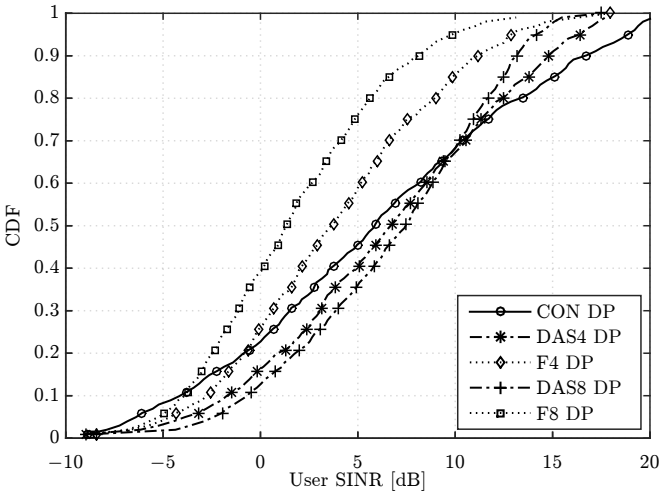

Figure 4.2: User SINR CDF comparison using DP for all the simulated scenarios.

Figure 4.2 shows the Cumulative Distribution Function (CDF) of the user SINR when DP is applied. As expected, SINR values are in general smaller for those deployments with lower degree of coordination, such as F4 and F8. Note that in F8 only up to 6 users can be multiplexed simultaneously avoiding inter-user interference, while in CON or DAS deployments, up to 24 users are multiplexed with no intra-cell interference. On the other hand, the difference between CON and DAS is related to the antenna elements location. While in DAS deployments the antennas are distributed over the space, bringing a larger benefit to those users located on the cell-edges, in CON deployment all the antenna elements are co-located at the cell center, providing higher beamforming gains that benefit those users located near the BS. These results point to a very interesting conclusion, meaning that DAS deployments imply a significant gain in terms of average user throughput and cell-edge user throughput, at the cost of reducing the system peak throughput. This conclusion is in good consonance with the results discussed in [114].

Regarding the user spectral efficiency, the same behavior as for the SINR is observed in Figure 4.3, where it is shown that increasing the number of coordinated antennas enhances the user spectral efficiency, while distributing the antennas over the space improves the user fairness. The CDF of the system throughput is depicted in Figure 4.4. This figure highlights the fact that cell throughput distribution is much more similar among the different options of DAS and CON deployments than their user throughput distributions. This

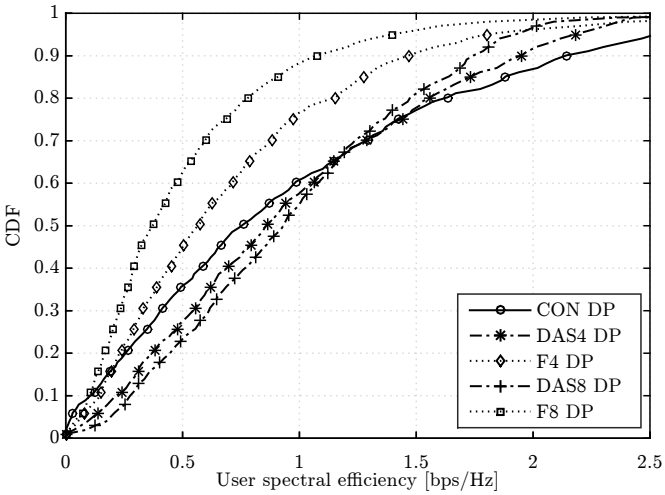

Figure 4.3: User spectral efficiency CDF comparison using RZF precoding for all the simulated scenarios.

is basically caused by the following effect: the more the antenna elements are distributed, provided that the transmission is coordinated among them, the better for the fairness in the system. However, this fairness gain comes at the expense of a throughput reduction of those users in best radio conditions, what leads to small differences in terms of system throughput values of the different deployments. Still, there is a big gap in performance between the femtocell deployments and the other options of deployment, in which more antenna elements either co-located or distributed are coordinated for transmission, such as CON or DAS.

Finally, Table 4.6 collects the comparison of some network performance indicators, including also the gains achieved by the different deployments with respect to the conventional deployment. Approximately same average values of user throughput and site throughput are achieved by CON and DAS, while the best 5% percentile user throughput is reached by DAS8. It is worth noting the huge improvement in terms of cell-edge user throughput achieved by DAS deployments, which can outperform the conventional deployment by a factor of 6.

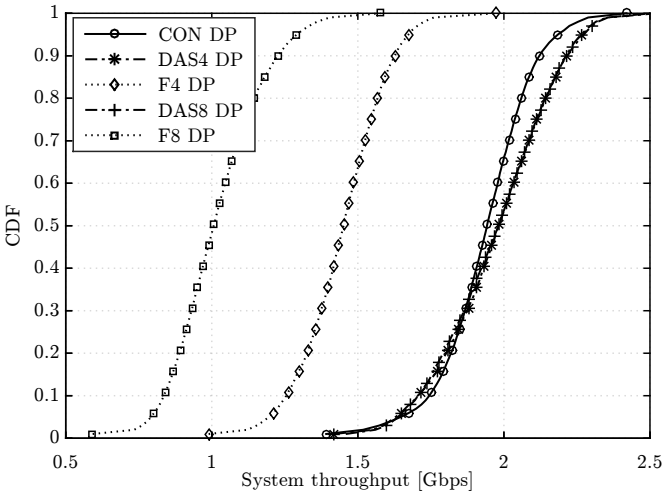

Figure 4.4: System throughput CDF comparison using RZF precoding for all the simulated scenarios.

Table 4.6: Comparison of average performance indicators with DP.

		DP				
		CON	**DAS4**	**F4**	**DAS8**	**F8**
Average UE throughput	**[Mbps]**	19.39	19.75	14.49	19.74	10.22
	Gain [%]	-	1.86	-25.29	1.78	-47.28
5%-ile UE throughput	**[Mbps]**	0.58	2.70	1.66	4.10	1.39
	Gain [%]	-	366.76	186.56	609.09	140.89
Average site throughput	**[Gbps]**	0.97	0.99	0.72*	0.99	0.51*
	Gain [%]	-	1.86	-25.29	1.78	-47.28

* In this case, a site is assumed to be the group of cells located in half the scenario.

4.5.2 Results using hybrid precoding

Simulation results considering hybrid precoding are hereafter presented. For all the scenarios, HP is applied by performing RZF at baseband and DFT-based precoding at RF. Besides, for DAS deployments also DHP described in Section 4.3 is used to better exploit the distributed nature of the system, which consists in the application of RZF and DAB at BB and RF stages, respectively. In all the scenarios, the number of RF chains is limited to 8 per site. The choice of this number of RF chains is motivated by current limitations of BSs.

Table 4.7: Average number of multiplexed users per site with HP and DHP for every simulated scenario.

CON	DAS4		F4	DAS8		F8
HP	HP	DHP	HP	HP	DHP	HP
7.69	7.86	7.93	7.85*	6.72	7.72	7.39*

* In this case, a site is assumed to be the group of cells located in half the scenario.

Table 4.7 shows the average number of simultaneous multiplexed users per site for all the considered scenarios when using hybrid precoding. Taking into account that the maximum number of multiplexed users is limited by the available RF chains, it can be observed that almost all the algorithms harness the multiplexing gain. Only DAS8 with HP shows a lower number of multiplexed users in comparison to the others.

Regarding the user SINR, Figure 4.5 shows the CDF for the different scenarios and hybrid precoding techniques. DAS deployments present the highest SINR values when using the DHP scheme proposed in this chapter, while the application of HP in DAS entails a strong degradation of the SINR meaning that conventional HP techniques cannot be applied as such to distributed systems. This behavior can be explained by the overlap of the beams created by HP when it is applied to distributed antennas, as well as the lack of RAU selection of the algorithm.

User spectral efficiency is depicted in Figure 4.6, where two different areas can be distinguished. For the lower part of the CDF, femtocell deployments show the best performance, followed by DAS systems using DHP. However, for the upper part of the CDF, femtocell deployments provide the poorest performance among all the algorithms. Indeed, limiting the number of RF chains greatly affects conventional systems, and it is here that there is a need to distribute the transmitters in some way, increasing the deployment density. Compared to a more dense femtocell solution, DAS deployments offer practically the same performance as dense femtocells for users in worse radio conditions, while ostensibly improving the quality of the users in good radio conditions.

In terms of system performance, curves in Figure 4.7 show that the application of DHP in DAS brings a large increase of the system throughput with respect to the use of HP. Moreover, the use of DAS is shown to be by far the best indoor deployment and, in general, the distribution of the antennas over the scenario is beneficial. Having a look at the network performance indicators collected in Table 4.8, enormous gains in 5th percentile of user throughput for DAS and femtocell deployments can be observed with respect to the conventional scenario.

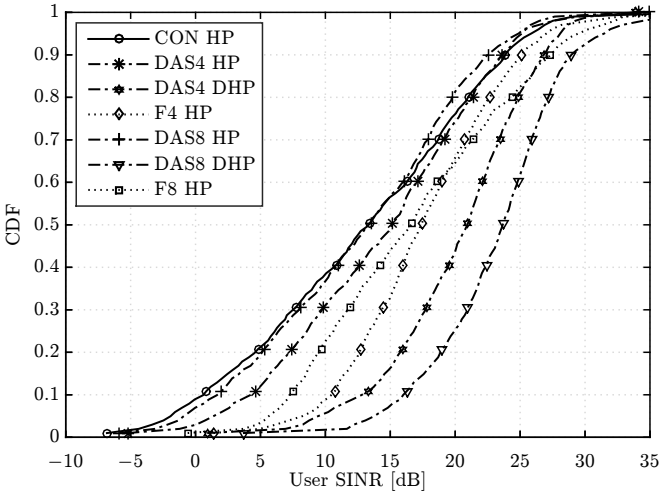

Figure 4.5: User SINR CDF comparison using hybrid precoding for all the considered deployments.

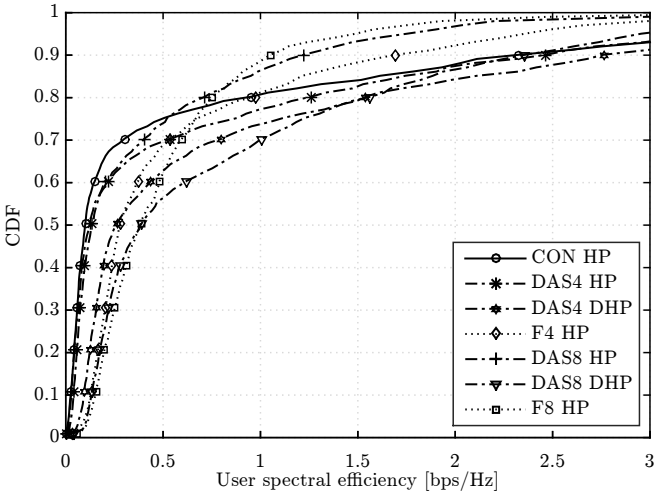

Figure 4.6: User spectral efficiency CDF comparison using hybrid precoding for all the considered deployments.

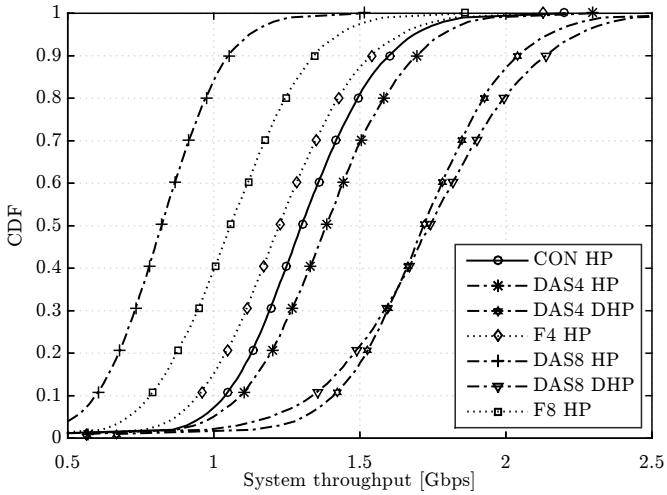

Figure 4.7: System throughput CDF comparison using hybrid precoding for all the considered deployments.

Table 4.8: Comparison of average performance indicator values for indoor deployments using hybrid precoding.

		CON	**DAS4**		**F4**	**DAS8**		**F8**
		HP	**HP**	**DHP**	**HP**	**HP**	**DHP**	**HP**
Avg. UE through.	**[Mbps]**	13.15	13.93	17.27	12.40	8.27	17.42	10.66
	Gain[%]	-	5.9	31.4	-5.7	-37.1	32.4	-18.9
5%-ile UE through.	**[Mbps]**	0.35	0.64	1.53	2.14	0.40	2.29	2.59
	Gain[%]	-	80.6	332.8	504.7	13.3	547.4	629.3
Avg. site through.	**[Gbps]**	0.66	0.70	0.86	0.62*	0.41	0.87	0.53*
	Gain[%]	-	5.9	31.4	-5.7	-37.1	32.4	-18.9

* In this case, a site is assumed to be the group of cells located in half the scenario.

Finally, a brief comparison between the performance of DAS8 deployment using DP and DHP is presented in Table 4.9. Note that the use of hybrid architectures implies a reduction in the number of RF chains with respect to digital architectures. In particular for this simulation study, the number of RF chains has been reduced from a total of 48 to 16. Due to this, the average number of spatially multiplexed users per cell in DAS8 turns from 24 in the DP scheme to 7.72 with DHP, what leads to a loss in average user and cell throughputs around the 12% with respect to the digital precoding. It is

also interesting to observe that the use of hybrid architectures penalizes more aggressively the throughput values of cell-edge users.

Table 4.9: Comparison of average values.

		DAS8	
		DP	**DHP**
Average UE throughput	**[Mbps]**	19.74	17.42
	Gain [%]	-	-11.77
5%-ile UE throughput	**[Mbps]**	4.10	2.29
	Gain [%]	-	-44.01
Average cell throughput	**[Gbps]**	0.99	0.87
	Gain [%]	-	-11.77

4.6 Performance comparison of non-ideal indoor deployment strategies

The results presented in the previous section assumed ideal conditions for all the components in the system. However, the presence of practical limitations or hardware impairments in real systems may deteriorate significantly the network performance. For that reason, a performance evaluation is presented in this section including two non-ideal phenomenons with high impact in hybrid architectures, such as the use of outdated CSI at the transmitter and the power losses introduced by real combiners.

4.6.1 Outdated Channel State Information

The unavoidable delay between the instants in which channel is estimated and used for the design of the precoders has been described and analyzed for HBF schemes in a urban-micro scenario in Section 3.6.1. Results showed that the beamforming and multiplexing gains obtained by using multi-user HBF schemes are quite robust to inaccuracies of the CSI at the transmitter, contrasting to the high sensitivity of DP schemes in that scenario.

In this section, the same analysis is replicated now for the HP and DHP schemes in the indoor deployments described in Section 4.4, in order to study the impact of having outdated CSI on schemes applying both BB and RF precoding. To this aim, hybrid schemes have been simulated considering that each SC receives an update of the channel coefficients only every T ms, being T greater than the subframe duration T_s. For a better illustration of the small scale channel variation during the period T, results are again presented as a

function of the product $f_D\Delta T$, where $f_D = vf/c$ is the maximum Doppler shift at carrier frequency f with user speed equal to v, and $\Delta T = T - T_s$ is the CSI delay with respect to the subframe duration.

In particular, Figure 4.8 represents the CDF of the user spectral efficiency when $T = 10$ ms ($f_D\Delta T = 1.8$) in comparison with the ideal case of timely CSI ($T = T_s = 1$, $f_D\Delta T = 0$). It is easily observed that the outdated CSI reduces the user spectral efficiency in all cases, but the degradation is particularly significant for those users with better channel conditions, i.e., the users with higher spectral efficiencies.

Average UE throughput values are depicted in Figure 4.9 for $T = 1, 5, 10$ and 20 ms ($f_D\Delta T = 0, 0.8, 1.8$ and 3.8, respectively). Note that, despite showing the DAS deployments a better performance when perfect CSI is available at the transmitter, they are more sensitive to outdated CSI than femtocell deployments. This can be explained by the size of the channel vector used in the scheduling decisions, which is of 24 elements in CON, DAS4 and DAS8 deployments (the number of all the antennas belonging to the same cell) and only of 12 and 6 elements in F4 and F8, respectively. Indeed, the most robust deployment to outdated CSI is shown to be F8, which overcomes the performance of the other deployments for $T \geq 5$ ms.

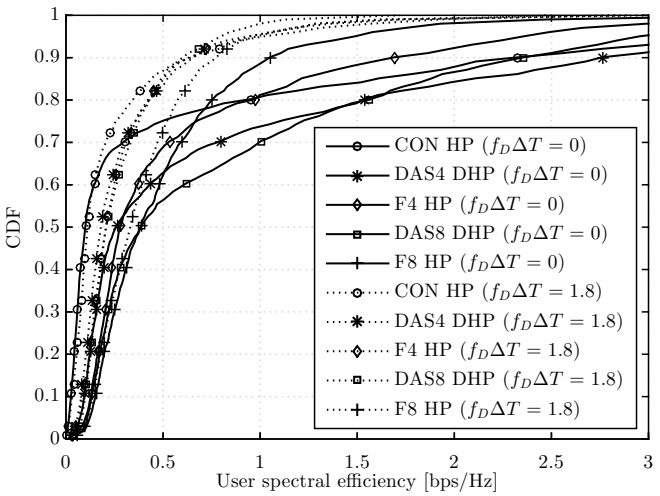

Figure 4.8: CDFs of the user spectral efficiency with outdated CSI.

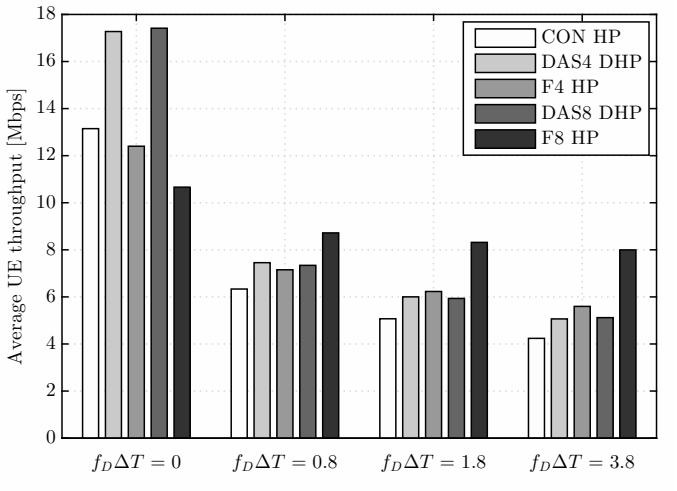

Figure 4.9: Average UE throughput with outdated CSI.

It is also interesting to remark how the inclusion of a BB precoding stage turns HP and DHP much more sensitive to outdated CSI than the HBF schemes evaluated in Chapter 3, where only user scheduling optimization was performed in BB. This can be explained by the higher dependence of the RZF precoders computed per FB in the BB stage on the small scale channel variations. Indeed, the improvement in network performance achieved by the better adaptability to the channel variations of the BB precoding under ideal conditions is rapidly lost when precoders are computed based on outdated CSI.

4.6.2 Combiner losses

Combiners are used in the full-connected hybrid architecture for the mix of the signals of the different RF chains before feeding the antenna array. As described in Section 3.6.4, the use of non-ideal combiners introduce significant power losses in their outputs, which escalate with the number of branches to be combined.

In this subsection, the impact of the combiner losses on the system performance of the hybrid schemes is analyzed for the three different deployment strategies considered in this chapter. Recall that L denotes the power loss in logarithmic units of a basic combiner with two input branches, and that a combiner for a generic number P of RF chains is implemented by means of a cascade of $\log_2 P$ two-branch combiners, leading to a total loss of $\log_2 P \cdot L$ dB.

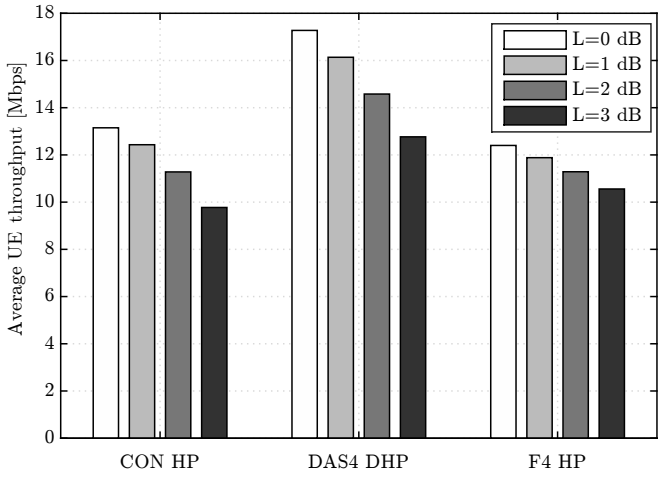

Figure 4.10: Average UE throughput achieved by hybrid schemes when considering combiner losses.

Simulations have been conducted for combiner losses of $L = 1, 2$ and 3 dB, and results are compared to the case of ideal combiners ($L = 0$ dB). Note that the number of required combiners differs from one scenario to the other, since the number of RF chains per SC in each case is different. For instance, in DAS4 scenario each SC has 8 RF chains, hence signals pass through 3 combiners before reaching the antenna array, while in F4 scenario there are 4 RF chains per SC and only 2 combiners are required to distribute signals.

Figure 4.10 shows the average user rate achieved by CON, DAS4 and F4 as a function of the parameter L. Despite being DAS the deployment option most affected by combiner losses, it remains the solution providing the highest average user rates even for the largest value of L.

The CDF of the system throughput is represented in Figure 4.11 for L equal to 0 and 3 dB. Here, the effectiveness of DAS deployments using DHP is shown, being DAS4 DHP with large combiner losses still comparable to the other two deployment strategies with ideal conditions.

Table 4.10: Comparison of average performance indicator values when considering combiner losses.

		$L = 0$ dB			$L = 1$ dB			$L = 2$ dB			$L = 3$ dB		
		CON HP	**DAS4 DHP**	**F4 HP**	**CON HP**	**DAS4 DHP**	**F4 HP**	**CON HP**	**DAS4 DHP**	**F4 HP**	**CON HP**	**DAS4 DHP**	**F4 HP**
Avg. UE through.	**[Mbps]**	13.15	17.27	12.40	12.43	16.14	11.88	11.28	14.58	11.29	9.77	12.77	10.56
	Gain [%]	-	-	-	-5.45	-6.59	-4.18	-14.21	-15.60	-8.99	-25.67	-26.10	-14.87
5%-ile UE through.	**[Mbps]**	0.35	1.53	2.14	0.35	1.63	2.02	0.33	1.49	1.91	0.22	1.29	1.73
	Gain [%]	-	-	-	-2.14	6.04	-5.83	-5.68	-3.00	-10.76	-38.35	-16.07	-19.34
Avg. site through.	**[Gbps]**	0.66	0.86	0.62*	0.62	0.81	0.59*	0.56	0.73	0.56*	0.49	0.64	0.53*
	Gain [%]	-	-	-	-5.45	-6.59	-4.18	-14.21	-15.60	-8.99	-25.67	-26.10	-14.87

* In this case, a site is assumed to be the group of cells located in half the scenario.

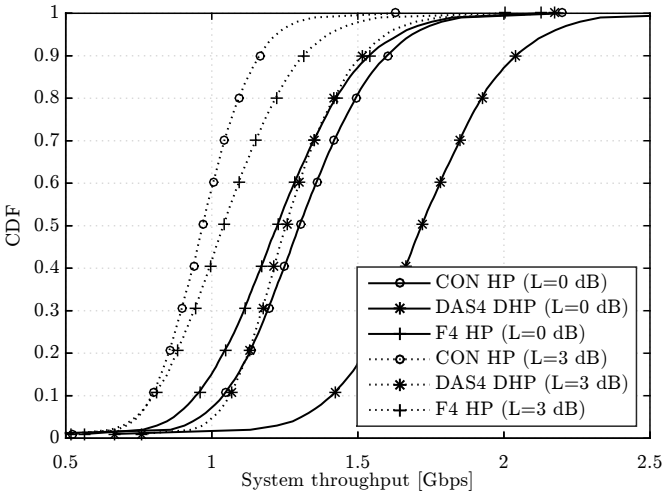

Figure 4.11: System throughput CDF of the hybrid schemes when considering combiner losses.

4.7 Conclusion

In this chapter, a performance evaluation of hybrid precoding schemes in indoor DAS deployments has been presented. To this end, a Distributed Hybrid Precoding (DHP) algorithm suitable for distributed antennas and with RAU selection capabilities has been firstly proposed for its application in a full-connected hybrid architecture for mmW communications. Furthermore, the performance of DHP in DAS has been compared to other two typical indoor deployment strategies, including a conventional deployment with two picocells and large co-located antenna arrays, and a regular femtocell deployment.

System level simulations have been firstly presented for MU Multiple Input Multiple Output (MIMO) digital and hybrid precoding schemes under ideal conditions for the three indoor deployment strategies. Simulation results show that femtocell deployments provide slightly higher throughputs for cell-edge users. Nevertheless, DAS deployments achieve the best overall performance when using the proposed DHP technique, showing more than 30% increase in both average user and cell throughput in comparison to the conventional deployment with co-located antennas. Regarding the comparison between hybrid and fully digital schemes, it is shown that, by reducing the number of RF chains

to one third, the system throughput achieved by DHP in DAS only decreases about 12%, affecting mostly to the cell-edge users.

Additional results have been obtained for the three indoor deployment strategies considering two important practical limitations of the hybrid architectures. In particular, the impact of outdated CSI at the transmitter and power losses introduced by real combiners on the performance of the hybrid schemes has been analyzed. Results state that DAS are more sensitive to inaccuracies in the CSI than femtocell deployments, what makes the latter the more suitable option when the CSI update period is greater than 5 ms. On the other hand, results point out that DAS deployments are less affected by the losses introduced by the combiners, and keep the best performance in comparison to the rest of strategies even for large combiner loss values.

The above conclusions suggest DAS as the overall optimum strategy deployment for indoor scenarios working in mmW. Besides, the performance of DHP has shown to become closer to that of DP thanks to the combined precoding in BB and RF domains, being only limited by the reduced availability of RF chains at the transmitters. Further improvement of DAS performance could be obtained by the application of Inter-Cell Interference Coordination (ICIC) mechanisms.

Chapter 5

eICIC technique for ultra dense small cell indoor deployments

5.1 Introduction

Ultra Dense Networks (UDNs) bring an important challenge in terms of Inter-Cell Interference Coordination (ICIC), due to the increase of the number of deployed base stations per area. The higher level of densification in this type of networks causes a reduction of the distance between the users and their serving base stations as well as to the rest of cells in the network, increasing the inter-cell interference in both uplink and downlink. The nature of the mechanisms required to combat the growing interference depends on the particular scenario to be addressed, as it has been carefully reviewed in Section 1.2.4. On the one hand, Heterogeneous Networks (HetNets) need ICIC schemes to handle the inter-tier interference, which affects more severely the small cell users under the coverage of a macrocell. On the other hand, in indoor Small Cell (SC) deployments, considered to be isolated from the macrocell interference thanks to the penetration losses introduced by the walls of the buildings, the ICIC techniques must focus on the management of the intra-tier interference that takes place among nodes with similar levels of power.

The application of ICIC algorithms in such isolated indoor deployments has received less attention by the research community. This is mainly due to the fact that, contrarily to the huge gains achieved in HetNets by means of resource

partitioning techniques, their application in indoor SC deployments usually results in an improvement of the cell-edge users rates at the expense of reducing the cell spectral efficiency. This behavior can be explained by noticing that the improvement in Signal to Interference plus Noise Ratio (SINR) experienced by the users thanks to a lower resource reuse factor does not compensate the reduction in the amount of resources available for transmission. Knowing this, it is expected that the application of algorithms relying on resource partitioning, such as those techniques based in Fractional Frequency Reuse (FFR) schemes, may be interesting only for scenarios with strong interference conditions, as it is the case of UDN. Furthermore, it is important to highlight that, due to the large amount of nodes deployed in the UDN deployments, ICIC solutions for this type of scenarios should be simple and scalable, which practically prevents the use of centralized solutions.

In this chapter, a time and frequency ICIC scheme for ultra dense SC indoor deployments is presented, called Dynamic Time and Frequency Reuse (DTFR) scheme. The goal of DTFR is to coordinate over time the transmission of the SCs in the network in such a way that interference generated at the neighbor cells is reduced while the reuse factor of the resources is kept close to one. With this aim, SCs apply a user scheduling algorithm that, taking into account information about the resources being used at the neighbors, maximizes the system throughput while ensuring fairness among users. The presented solution is easy to implement and requires the exchange of few information among the nodes, being suitable for UDNs with limited backhaul capabilities.

The rest of the chapter is organized as follows:

- Section 5.2 describes the system model considered for the design of the proposed ICIC technique.
- Section 5.3 presents a detailed description of the DTFR algorithm.
- Section 5.4 defines the simulation setup used to assess the performance of DTFR and describes the baseline techniques implemented for its comparison. Also in this section, simulation results relative to DTFR performance are presented for different UDN deployments.
- Section 5.5 outlines the main conclusions of this chapter.

5.2 System model

A downlink Orthogonal Frequency Division Multiplexing (OFDM) system with N_{SC} SCs and K User Equipments (UEs) is considered, working in Frequency Division Duplexing (FDD) mode. SCs are regularly deployed over the scenario and are configured in open access mode, so any user is granted access to any SC. UEs are randomly deployed in the scenario and follow a pedestrian mobility model. Cell selection is done according to the maximum received power by the user. Moreover, SCs are connected to the core network using broadband transmission links. In case of cooperation among them, SCs are grouped in clusters, and a logical interface is available to support the exchange of control messages among the SCs belonging to the same cluster.

Transmission resources are assumed to be partitioned in a time-frequency grid. In the time domain, a subframe is defined as the smallest unit of time in which scheduling decisions are made at the SCs. In the frequency domain, the total available bandwidth W_{t} is divided in Frequency Blocks (FBs). The minimum time-frequency resource is known as Resource Block (RB), and consists of one FB during one subframe period. The scheduler can allocate a user per RB, and only single-user and single-stream transmissions are considered in this work. Regarding the power allocation, total available power per cell is equally distributed per RB, and the power corresponding to muted RB is saved.

Channel model is implemented following the Indoor Hotspot (InH) model proposed by the International Telecommunication Union Radiocommunication (ITU-R) in [108]. In this model, the channel coefficients are determined stochastically based on statistical distributions characterizing multipath propagation, which were extracted from channel measurements. Besides, this model includes distance dependent path losses and shadowing. The channel coefficients are considered to remain constant during a subframe period. Furthermore, perfect channel estimation is assumed at the transmitter and receiver sides.

Let us consider γ_u^f as the estimated SINR experienced by user u when is allocated to a certain FB f of bandwidth W, considering the interference generated by all the rest of SCs in the scenario. Then, the throughput achieved by user u in that FB is computed as:

$$\mathrm{Th}_u^f = W \log_2(1 + \gamma_u^f), \tag{5.1}$$

and the total throughput experienced by the user u is given by $\mathrm{Th}_u = \sum_{f \in \mathcal{F}_u} \mathrm{Th}_u^f$, where $\mathcal{F}_u$ denotes the set of FBs allocated to user u.

5.3 Dynamic Time and Frequency Reuse (DTFR) coordinated scheduling for UDNs

In this section, the proposed DTFR coordinated scheduling technique for ultra dense SC deployments is presented. DTFR is divided into two phases: the resource reuse pattern configuration, and the user scheduling. In the first phase, SCs within the same cluster exchange control messages to decide which resources are used with maximum priority by each cell, following a FFR-based pattern. Moreover, each cell configures a time pattern in which it will mute periodically its transmission over the resources used with maximum priority by the neighbors within its cluster. In the second phase, user scheduling is performed by optimizing in each cluster the resource allocation decisions that maximize certain fairness-based utility function. The details of the two stages of the DTFR algorithm are presented in the following subsections.

5.3.1 DTFR pattern configuration phase

Let us assume that the N_{SC} cells are grouped in clusters of size C_{s}, by means of any centralized or decentralized clustering algorithm. In this phase, a time and frequency reuse pattern is configured in each cluster independently. With this aim, total frequency bandwidth W_{t} available in the system is divided into $C_{\mathrm{s}}+1$ different sub-bands: an Ordinary Sub-band (OSb), a Preferential Sub-band (PSb), and $C_{\mathrm{s}}-1$ Non-Preferential Sub-bands (NPSbs). These sub-bands are characterized by different features, which are detailed hereunder.

On the one hand, the OSb is common to every cell in the network and is configured in a centralized fashion by selecting its bandwidth, given by W_{o}. Resources within OSb are always available to be used simultaneously by every cell, resulting in a set of resources with frequency reuse factor of one. Since interference power in OSb is thus expected to be high, users with better channel conditions are supposed to be allocated to this sub-band.

On the other hand, PSb and NPSbs are configured per cluster in a distributed fashion, by exchanging messages among neighbor cells. These sub-bands have a frequency reuse factor lower than 1 that depends on the cluster size applied. The bandwidths of the PSb and each NPSb are equal, and denoted by W_{r}:

$$W_{\mathrm{r}} = (W_{\mathrm{t}} - W_{\mathrm{o}})/C_{\mathrm{s}}. \tag{5.2}$$

The main difference between PSb and NPSbs is that the PSb at each cell is used for transmission uninterruptedly while, conversely, the NPSbs of a cell are muted cyclically over time, reducing the interference generated to the neighbors and allowing for certain energy saving.

To better explain the muting pattern, Figure 5.1 represents an example of the sub-bands configuration for a cluster of 4 SCs. This figure shows the patterns configured for three consecutive subframes, labeled as T1, T2 and T3. The OSb remains constant over time and coincides for all the cells in the cluster. The PSbs are also fixed over time, but they are not coincident among cells. Note that the muted NPSbs change over time and are distributed in a way that at each subframe exactly one cell is muted on the PSbs of every neighbor. For example, in subframe T1, SC4, SC1, SC2 and SC3 are muted on the PSbs of SC1, SC2, SC3 and SC4, respectively.

The process in which cells within a cluster select their PSb is performed sequentially. Each cell interrogates its neighbors about which set of resources with bandwidth W_{r} they are using as PSbs. After receiving the answers from them, the cell selects as PSb the first available sub-band outside of the OSb and not already used as preferential in any of the neighbors. Once the PSbs are configured for all the cells in the cluster, the time muting pattern is self-configured at each of them. To coordinate over time and distribute the muting patterns, each cell starts muting the first sub-band after its own PSb in the first subframe, and mutes cyclically the consecutive NPSb in the following subframes. Going back to the example in Figure 5.1, it can be observed that for SC1 the first sub-band after the OSb is chosen as preferential, and therefore, the following sub-band is the first to be muted.

Note that since one non-preferential sub-band is muted in each subframe, the total available bandwidth per cell is $W_{\mathrm{t}} - W_{\mathrm{r}}$. As fixed power per RB is assumed, the transmission over smaller bandwidths results in certain energy savings when compared to reuse 1 schemes. In particular, the percentage of power saved can be expressed as:

$$\eta_{\mathrm{DFTR}} = \frac{W_{\mathrm{t}} - W_{\mathrm{r}}}{W_{\mathrm{t}}} \times 100. \tag{5.3}$$

5.3.2 User scheduling optimization phase

In this phase, user scheduling is performed considering the DTFR pattern configured in the previous phase. As defined before, OSb is always available for transmission at every cell, so users allocated to this sub-band suffer interference from every cell in the scenario. However, at each subframe the NPSbs available for transmission and the PSb of any cell have their corresponding RBs muted in one of the neighbors within the cluster. In other words, each cell has a specific sub-band per subframe in which it can avoid the interference from a particular neighbor in the cluster.

Based on this idea, the goal of the user scheduling optimization phase is, considering a fairness criterion, to allocate each users in those sub-bands in

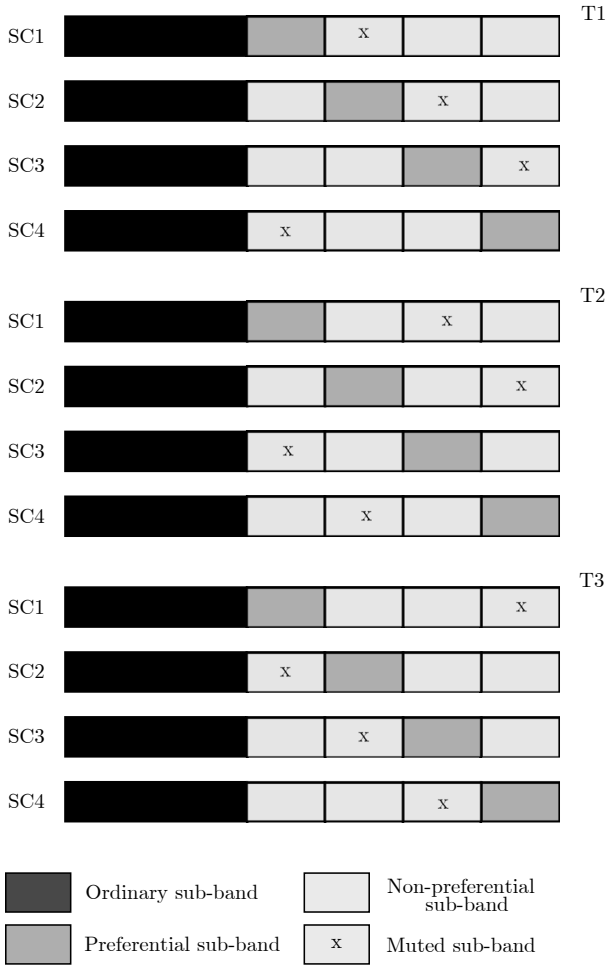

Figure 5.1: Example of DTFR per-cluster sub-band configuration, for a cluster composed of 4 small cells.

which the throughput per cluster is maximized. To this aim, the most interfering neighbor for each user is firstly determined, and using this information, the resource allocation is consequently optimized.

Identification of the most interfering neighbor for each user

Let us assume that user u is served by cell s and $\mathcal{G}_s$ denotes the set of cells within the cluster including cell s. Assume also that $\hat{\gamma}_u$ denotes the wideband SINR experienced by user u, which is estimated on the basis of the long term channel components. Then, the most interfering neighbor for user u is given by:

$$\hat{c}_u = \underset{c \in \mathcal{G}_s, c \neq s}{\arg\max}\ \hat{\gamma}_{u,c}, \tag{5.4}$$

where $\hat{\gamma}_{u,c}$ represents the estimated wideband SINR experienced by user u when cell c is muted.

Moreover, considering that $\mathcal{U}_s$ is the set of users served by the same serving cell s, the users in $\mathcal{U}_s$ sharing the same most interfering cell are denoted as $\mathcal{I}_{s,c} = \{u \in \mathcal{U}_s | \hat{c}_u = c\}$.

Resource allocation optimization

The throughput achieved by user u is estimated as the sum of the throughput achieved in the different sub-bands:

$$\mathrm{Th}_u(\alpha_u, \beta_u) = \alpha_u W_\mathrm{r} \log_2(1 + \hat{\gamma}_{u,\hat{c}_u}) + \beta_u W_\mathrm{o} \log_2(1 + \hat{\gamma}_u), \tag{5.5}$$

where α_u represents the percentage of W_r allocated to user u at the PSb or NPSbs, and β_u the percentage of W_o allocated to user u at the OSb. Note that the first term in Eq. (5.5) reflects the throughput achieved by the users allocated to those sub-bands in which their most interfering neighbors are muted.

Defining $\boldsymbol{\alpha} = [\alpha_1 ... \alpha_K]$ and $\boldsymbol{\beta} = [\beta_1 ... \beta_K]$, from Eq. (5.5) the utility function is defined as:

$$\xi(\boldsymbol{\alpha}, \boldsymbol{\beta}) = \sum_{u=1}^{K} \log\left(\mathrm{Th}_u(\alpha_u, \beta_u)\right), \tag{5.6}$$

and the resource allocation optimization is expressed as:

$$\begin{aligned} \max_{\boldsymbol{\alpha},\boldsymbol{\beta}} \quad & \xi(\boldsymbol{\alpha},\boldsymbol{\beta}) \\ \text{s.t.} \quad & \textstyle\sum_{u\in\mathcal{I}_{s,c}} \alpha_u = 1, \quad \forall s, \forall c \\ & \textstyle\sum_{u\in\mathcal{U}_s} \beta_u = 1, \quad \forall s \\ & \alpha_u \geq 0, \beta_u \geq 0, \quad \forall u, \end{aligned} \tag{5.7}$$

where this optimization maximizes the system throughput at the same time as it guarantees fairness among users.

Note that the restrictions aim to guarantee that the resource allocation does not exceed the available bandwidth. Each PSb or NPSb is shared among the users with the same most interfering neighbor. The ordinary sub-band is shared among all the users belonging to a cell. The results of this optimization, $\boldsymbol{\alpha}$ and $\boldsymbol{\beta}$, are used in the user scheduling decisions as weights for a Weighted Round Robin (WRR) policy. These weights can be optimized periodically to achieve a dynamical adaption of the scheduling algorithm to the changing users positions.

5.4 Results and discussion

In this section, the performance of the proposed DTFR scheme is analyzed and compared to other two schemes: a conventional user scheduling algorithm without ICIC, hereinafter referred as no-ICIC; and an algorithm based on the FFR scheme. Firstly, the simulation setup and the configuration parameters set for each algorithm are provided in Subsection 5.4.1. Secondly, simulation results are discussed for several scenarios and under different assumptions in subsections 5.4.2 and 5.4.3.

5.4.1 Simulation setup and algorithms configuration

The analyzed scenario consists of a rectangular floor spanning 120 m × 50 m. The number of cells deployed, N_{SC}, is varied between 4 and 24, and their exact locations for each case are collected in Table 5.1. Users are randomly distributed over the area, with different density values, and their positions are considered static during the simulation time. The maximum density of users considered is 2 users per 100 m^2, what results in a total number of 120 users in the scenario. Besides, both users and base stations are considered to be single antenna, unless otherwise specified. The total transmission power in

the system is maintained constant and equal to 27 dBm, independently of the number of SCs deployed. Simulations were conducted using a carrier frequency of 3.4 GHz and a system bandwidth of 20 MHz, and other important simulation parameters are listed in Table 5.2.

Table 5.1: Small cells location of all simulated deployments.

	X [m]	**Y [m]**
4 SCs	15,45,75,105	25
8 SCs	15,45,75,105	15,35
12 SCs	10,30,50,70,90,110	15,35
24 SCs	10,30,50,70,90,110	6.25,18.75,31.25,43.75

Table 5.2: Simulation parameters.

Number of simulated drops	50
Simulation time per drop	1 s
RB bandwidth	200 kHz
Number of RBs	100
Subframe duration	1 ms
Total system power, $P_{\mathbf{T}}$	27 dBm
Thermal noise PSD	-174 dBm/Hz
UE noise figure	5 dB
UE speed	3 km/h
BS height	6 m
UE height	1.5 m
Traffic model	Full buffer

In the no-ICIC case, all the RBs are available for transmission at every cell in the network, i.e., the OSb is the whole bandwidth. Users are allocated to any RB by following a Round Robin (RR) scheduling policy. Since all RB are used for transmission in the no-ICIC algorithm, all the power available in the system is consumed.

For the configuration of the FFR scheme, sub-bands are defined following the same structure as in DTFR. In this way, the OSb is common to all the cells in the network and it is always available for transmission. However, NPSbs in FFR are always muted, which means that users allocated to the PSb are free of interference from all the neighbors within the cluster of its serving cell. At each subframe, users are allocated either to the PSb or to the OSb, but never to both sub-bands simultaneously. In order to decide which sub-band they are

allocated to, users are regularly classified in critical or non-critical, after estimating whether they achieve higher throughput in the PSb or the OSb, given the current classification of the rest of users. The classification instants are randomly chosen for each user, in such a way that the periods between consecutive classifications follow a uniform distribution, thus avoiding the simultaneous classification of all the users and ensuring classification convergence. The scheduler allocates critical users to the PSb and non-critical users to the OSb, using a RR policy for both of them. An example of the FFR sub-bands configuration is shown in Figure 5.2, for the case of a cluster with 4 SCs. Note that the bandwidth muted per cell in FFR is higher than in DTFR, and the percentage of energy saved is given by:

$$\eta_{\mathrm{FFR}} = \frac{W_{\mathrm{t}} - (C_{\mathrm{s}} - 1)W_{\mathrm{r}}}{W_{\mathrm{t}}} \times 100. \tag{5.8}$$

A comparison of the parameters used to configure each algorithm is summarized in Table 5.3. Note that the selected values for W_{o} and C_{s} determine the performance of DTFR. These values were derived from a set of simulations considering different pair of values for W_{o} and C_{s}, choosing the pair of them maximizing the utility function in Eq. 5.6. The performance of these three algorithms is evaluated and compared in the next subsections under different assumptions. In the first place, the effect of increasing the number of users in the scenario is studied in Section 5.4.2. Secondly, the performance of DTFR, FFR and no-ICIC user scheduling algorithms is evaluated for different SC densities in Section 5.4.3.

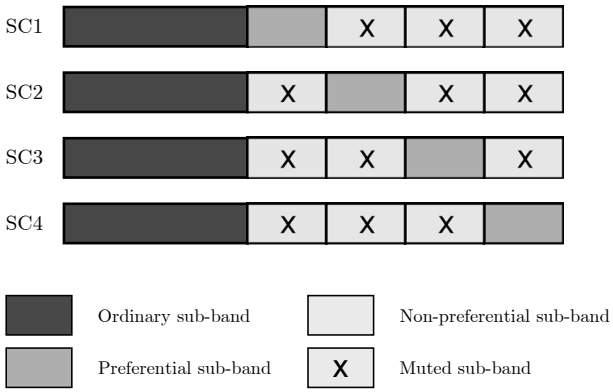

Figure 5.2: Example of FFR per-cluster sub-band configuration, for a cluster composed by 4 small cells.

Table 5.3: Comparison of the sub-band configuration parameters for the three compared algorithms.

	Number of OSb	**Number of PSb**	**Number of NPSb**	W_{o}
no-ICIC	1	0	0	W_{t}
FFR	1	1	0	$0.2W_{\mathrm{t}}$
DTFR	1	1	$C_s - 1$	$0.2W_{\mathrm{t}}$

5.4.2 Performance with increasing number of users

In this subsection, a scenario composed of 8 SCs is evaluated for several user densities, considering deployments ranging from 20 to 120 users randomly distributed. Simulations of DTFR and FFR schemes are conducted considering static clusters of cells that are formed by grouping the cells according to a proximity criterion and using a cluster size of $C_s = 4$ cells. Cooperation among cells is not considered in the no-ICIC scheme.

Figure 5.3 shows the user SINR Cumulative Distribution Function (CDF) achieved by the three compared algorithms in a scenario with 40, 80 and 120 users. User SINR values are obtained as an average in both time and frequency domains. It is observed that, for a specific algorithm, the number of deployed users does not affect significantly the SINR experienced by them. Regarding the comparison among algorithms, the large gap in the user SINR values can be explained by the frequency reuse factor applied by each technique. In the case of no-ICIC, frequency reuse factor of 1 is applied for the whole bandwidth. However, the reduction of the frequency reuse factor of DTFR increases the SINR experienced by the users allocated to PSb and NPSbs, which avoid the interference of their most interfering neighbor within the cluster. The best SINR values are achieved by the FFR algorithm in the PSb, since users allocated to this sub-band avoid the interference not only from one but from all the neighbors cells within the cluster of its serving cell. Recall that users in FFR algorithm are classified to critical or non-critical and thus, they can be allocated either to the OSb or PSb in a certain subframe, but never to both simultaneously. This explains the two distinct parts in the SINR curves for FFR algorithm, where the higher SINR values correspond to users classified to critical during most of the simulation time.

The CDF of the user throughput is compared in Figure 5.4 for the three simulated algorithms. As expected, increasing the number of users reduces the achievable throughput per user, since more users need to share the available resources. For all the simulated user densities, FFR is the scheme providing higher throughput values in the lower part of the CDF, followed by DTFR.

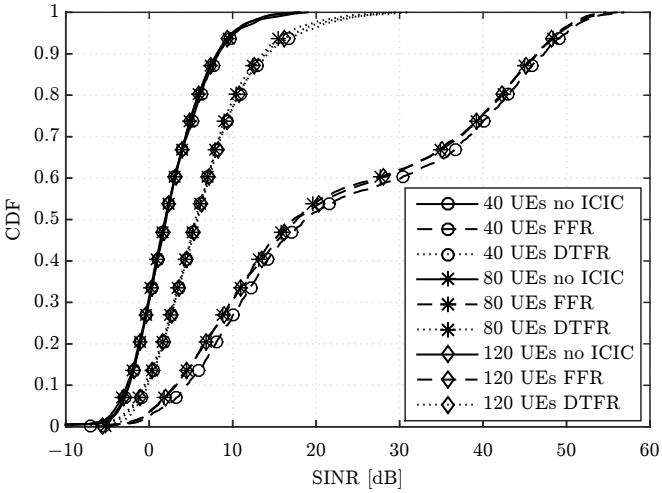

Figure 5.3: CDF of the user SINR for the three compared algorithms.

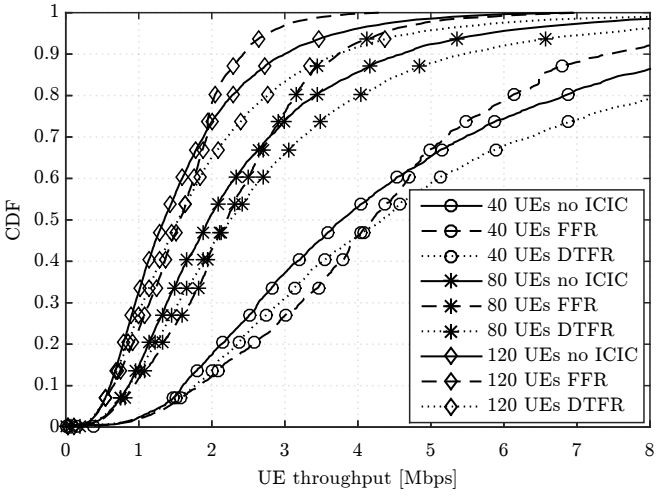

Figure 5.4: CDF of the user throughput for the three compared algorithms.

This is because the cell-edge users allocated to the PSbs in FFR avoid the interference of every neighbor cell in the cluster of the user serving cell, while in DTFR interference is avoided from only one of the neighbor cells at a time. Anyway, the performance gap between FFR and DTFR in the lower part of the CDF becomes smaller as long as the number of deployed users increases. Besides, in the higher part of the CDF DTFR outperforms FFR significantly. Note that DTFR improves the throughput for all users in comparison to no-ICIC algorithm.

Average UE throughput, 5th percentile UE throughput and utility function measures are collected in Table 5.4 for all the simulated algorithms. Numeric values show that FFR presents a bad performance in terms of average UE throughput for all the analyzed user densities. With regards to 5th percentile UE throughput, it is observed that FFR presents the highest gains with respect to no-ICIC for the cases with lower user densities.

Table 5.4: Comparison of average UE throughput, 5%-ile UE throughput and utility function for a scenario with 8 SCs and several UE densities.

		Average UE throughput		**5%-ile UE throughput**		**Utility function**	
		[Mbps]	**Gain [%]**	**[Mbps]**	**Gain [%]**	**ξ**	**Gain [%]**
20 UEs	**no ICIC**	9.60	-	2.09	-	1984.87	-
	FFR	8.45	-11.95	2.42	16.17	1951.19	-1.70
	DTFR	10.25	6.71	2.24	7.34	2062.18	3.89
40 UEs	**no ICIC**	4.88	-	1.33	-	2700.86	-
	FFR	4.58	-6.16	1.43	7.21	2752.89	1.93
	DTFR	5.64	15.49	1.35	1.44	2827.05	4.67
60 UEs	**no ICIC**	3.33	-	0.92	-	2904.95	-
	FFR	3.15	-5.44	0.98	6.51	3031.80	4.37
	DTFR	3.90	17.19	0.90	-1.99	3284.66	13.07
80 UEs	**no ICIC**	2.45	-	0.68	-	2731.86	-
	FFR	2.34	-4.85	0.73	6.16	2866.12	4.91
	DTFR	2.91	18.46	0.68	-1.10	3222.36	17.95
100 UEs	**no ICIC**	1.97	-	0.56	-	2362.70	-
	FFR	1.87	-5.34	0.56	-0.91	2465.07	4.33
	DTFR	2.36	19.51	0.56	0.85	2901.80	22.82
120 UEs	**no ICIC**	1.64	-	0.49	-	1810.89	-
	FFR	1.58	-3.98	0.50	1.30	2002.77	10.60
	DTFR	1.99	21.40	0.49	-1.05	2597.27	43.43

However, for higher densities of users, the three algorithms achieve very similar performance for cell-edge users. Another interesting conclusion drawn from these results is that the gains in average UE throughput and utility function achieved by DTFR increase with the number of users deployed in the scenario.

Regarding the cell throughput, Figure 5.5 shows a comparison of its CDF for the three algorithms. DTFR is revealed as the algorithm providing the best performance, with higher cell throughput values in nearly all cases, regardless of the user density in the deployment. This good performance is due to the compromise of DTFR between the amount of active and muted bandwidth, and the ability of the algorithm to schedule the users to sub-bands in which their most interfering sources are muted. Thanks to the coordination between cells, a higher reuse factor is allowed at the resources within PSb and NPSbs when compared to FFR. The cell spectral efficiency values achieved by each algorithm are presented in Table 5.5 for the different evaluated user densities. Again, the highest average cell spectral efficiencies are reached by DTFR, and moreover, the gain with respect to the other two algorithms increases with the number of deployed users.

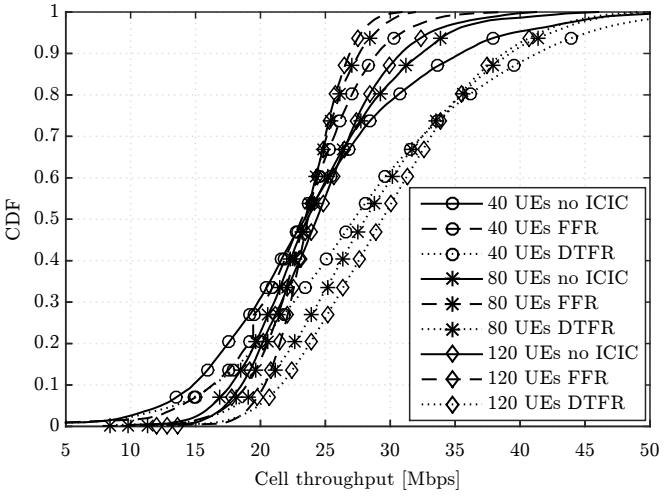

Figure 5.5: Cell throughput for the three compared algorithms.

All the results presented so far correspond to single antenna base stations and UEs. Motivated by some works indicating that increasing the number of antennas at both transmitters and receivers might reduce the performance gain achieved by the application of ICIC schemes [87], results comparing the per-

Table 5.5: Comparison of cell spectral efficiencies for a scenario with 8 SCs and different number of UEs.

		Cell spectral efficiency [b/s/Hz]	**Gain [%]**
20 UEs	**no ICIC**	1.20	-
	FFR	1.06	-11.93
	DTFR	1.28	6.66
40 UEs	**no ICIC**	1.22	-
	FFR	1.15	-6.14
	DTFR	1.41	15.39
60 UEs	**no ICIC**	1.25	-
	FFR	1.18	-5.37
	DTFR	1.46	17.20
80 UEs	**no ICIC**	1.23	-
	FFR	1.17	-4.80
	DTFR	1.45	18.39
100 UEs	**no ICIC**	1.23	-
	FFR	1.17	-5.23
	DTFR	1.47	19.58
120 UEs	**no ICIC**	1.23	-
	FFR	1.18	-3.89
	DTFR	1.49	21.35

formance of the three algorithms with the availability of multiple antennas are shown below. In particular, a Multiple Input Multiple Output (MIMO) system with 2 antennas at both base stations and users is considered. Furthermore, in order to exploit the multi-antenna architecture, codebook-based beamforming is applied at transmission [115] and a Minimum Mean Square Error (MMSE) receiver is implemented at the UE [116]. Simulations were performed considering a scenario with 8 SCs and 120 UEs.

Figure 5.6 shows the CDF of the cell throughput achieved by the three algorithms with Single Input Single Output (SISO) and MIMO configurations. As expected, higher cell throughput values are achieved when increasing the number of antennas. The greatest improvement is achieved by no-ICIC algorithm, which makes the most of the full reuse of resources thanks to both the increase of the received signal due to the applied beamforming and the reduction of the interference achieved by the MMSE receiver. However, overall the best cell throughput values are reached by DTFR.

Average UE throughput, 5th percentile UE throughput and utility function values for SISO and MIMO configurations are compared in Table 5.6. It is shown that MIMO preprocessing significantly increases the utility function values achieved by the no-ICIC algorithm, thus decreasing the gains achieved by both ICIC schemes with respect to no-ICIC. Indeed, average UE throughput gain achieved by DTFR is strongly reduced as well, turning from a 20% in SISO systems to only about 5% in MIMO systems. Furthermore, 5th percentile UE

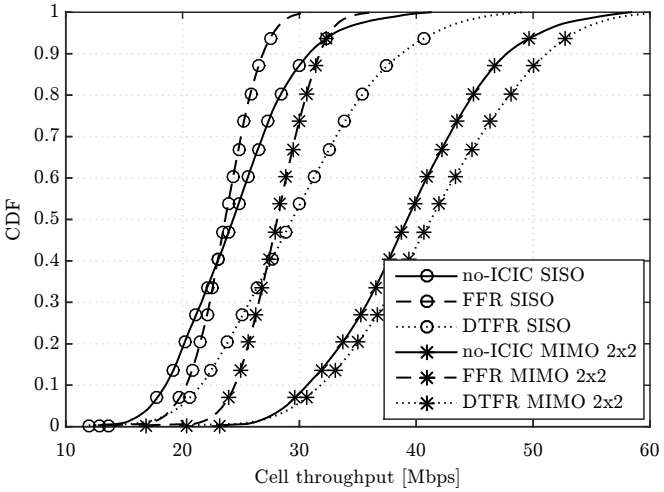

Figure 5.6: CDF of the cell throughput for the three compared algorithms with SISO and MIMO configurations.

Table 5.6: Comparison of UE average statistics for a scenario with 8 SCs for SISO and MIMO 2x2 configurations.

		Average UE throughput		**5%-ile UE throughput**		**Utility function**	
		[Mbps]	**Gain [%]**	**[Mbps]**	**Gain [%]**	**ξ**	**Gain [%]**
SISO	**no ICIC**	1.64	-	0.49	-	1810.89	-
	FFR	1.58	-3.98	0.50	1.30	2002.77	10.60
	DTFR	1.99	21.40	0.49	-1.05	2597.27	43.43
MIMO 2x2	**no ICIC**	2.63	-	0.82	-	4791.95	-
	FFR	1.88	-28.75	0.79	-2.72	3284.93	-31.45
	DTFR	2.77	5.21	0.75	-8.25	4802.40	0.22

throughput is shown to be higher in no-ICIC algorithm when multiple antennas are used. The reason is the greater bandwidth available in the no-ICIC scheme, which allows to allocate more resources to all the users in comparison to DTFR or FFR, taking advantage of the beamforming gains at transmission and reception that reduce the interference and permit a higher reuse of the resources. Note that, even so, the application of DTFR results in better system spectral efficiencies, as shown in Figure 5.7, maintaining the lower power consumption inherent to this scheme.

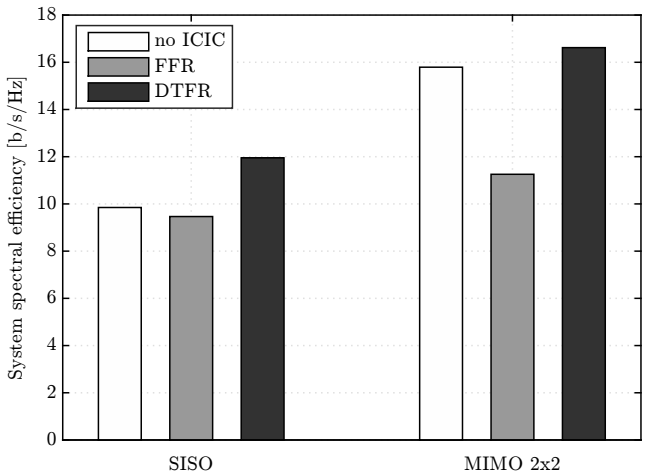

Figure 5.7: Average system spectral efficiency values for the three compared algorithms with SISO and MIMO configurations.

5.4.3 Performance with increasing number of cells

In this subsection, with the aim to study the effect of densification in DTFR, FFR, and no-ICIC algorithms, simulations are conducted considering increasing SC densities. In particular, the performance of deployments with 4, 8, 12 and 24 SCs is analyzed, considering the locations given by Table 5.1. In order to guarantee a fair comparison among the simulated scenarios, the total available power in the scenario remains constant and equal to $P_{\mathrm{T}} = 27$ dBm, independently of the number of deployed SCs. This implies that the available power per SC varies with the SC density, as reflected in Table 5.7. All the results presented in this subsection were obtained through simulations considering 60 UEs randomly distributed over the scenario. For DTFR and FFR

schemes, static clusters of SCs are formed by grouping the cells according to a proximity criterion, and using a cluster size of $C_s = 4$ cells.

Figure 5.8 shows a comparison of the user SINR CDFs for the deployments with 4, 12 and 24 SCs. As expected, an increase of the number of deployed SCs results in lower values of SINR for the three compared algorithms. The main reasons are the reduction of the Signal to Noise Ratio (SNR) caused by the lower level of power per SC available as long as the number of cells increases, and the increase of the Interference to Noise Ratio (INR) caused by a higher spatial reuse of the resources. Note that the higher SINR values of FFR with 4 SCs can be justified considering that interference is completely removed for the users allocated to the PSb of each cell, since no interference sources exist out of the cluster.

Table 5.7: Available power per SC depending on the SC density in the scenario.

	4 SCs	**8 SCs**	**12 SCs**	**24 SCs**
P_{SC} [dBm]	20.98	17.97	16.21	13.20

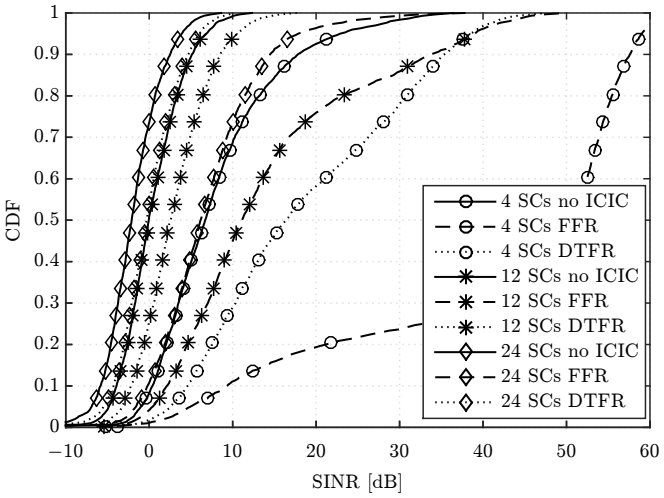

Figure 5.8: CDF of the user SINR for the three compared algorithms.

In terms of user throughput, numeric values in Table 5.8 show the clear benefit of densification. In particular, moving from 4 to 24 SCs while keeping the total power constant to 27 dBm provides an increase in the average throughput

of more than 30%. Values of utility function and 5th percentile UE throughput are shown to be improved by denser deployments as well. It is worth to highlight here the effect of increasing the number of SCs per area while maintaining the total power constant. As shown in the study presented in Chapter 2, having a constant power density results in more noise-limited networks as long as the number of cells per area increases, and thus, the application of cooperation techniques based on resource partitioning does not provide gains in the network performance. This effect can be observed in the utility function gains achieved by DTFR with respect to no-ICIC, which are reduced from about a 30% to only a 1% when the number of SCs in the scenario is increased from 4 to 24 SCs.

Table 5.8: Comparison of average UE statistics for a scenario with 60 UEs and increasing number of SCs.

		Average UE throughput		**5%-ile UE throughput**		**Utility function**	
		[Mbps]	**Gain [%]**	**[Mbps]**	**Gain [%]**	ξ	**Gain [%]**
4 SCs	**no ICIC**	2.82	-	0.82	-	2515.41	-
	FFR	2.10	-25.26	1.04	27.2	1984.87	-21.09
	DTFR	3.66	30.12	0.94	15.4	3223.60	28.15
8 SCs	**no ICIC**	3.33	-	0.92	-	2904.95	-
	FFR	3.15	-5.44	0.98	6.5	3031.80	4.37
	DTFR	3.90	17.19	0.90	-2.0	3284.66	13.07
12 SCs	**no ICIC**	3.62	-	0.94	-	3136.00	-
	FFR	3.71	2.64	1.07	13.5	3381.31	7.82
	DTFR	3.99	10.40	0.96	2.2	3361.71	7.20
24 SCs	**no ICIC**	4.71	-	1.00	-	3735.73	-
	FFR	4.73	0.33	1.14	13.9	3886.74	4.04
	DTFR	4.84	2.79	1.00	0.2	3769.83	0.91

The throughput per cell decreases with higher SCs densities, caused by the reduction of the SINR values experienced by the users when the spatial resource reuse is increased by densification. This effect can be observed in Table 5.9, where the cell and system spectral efficiencies of the three algorithms are collected for all the simulated SC densities. Note that while the cell spectral efficiency is reduced when increasing the number of cells, the system spectral efficiencies improve with densification.

Regarding the comparison of the algorithms evolution with densification, it is also shown that increasing the number of cells diminishes the performance

Table 5.9: Comparison of system and cell spectral efficiencies for a scenario with 60 UEs.

		Cell spec. efficiency [b/s/Hz]	System spec. effic. [b/s/Hz]	Gain wrt. no-ICIC [%]	Gain wrt. FFR [%]
4 SCs	**no ICIC**	2.11	8.44	-	-
	FFR	1.58	6.32	-25.18	-
	DTFR	2.75	10.99	30.18	73.99
8 SCs	**no ICIC**	1.25	9.98	-	-
	FFR	1.18	9.44	-5.37	-
	DTFR	1.46	11.69	17.20	23.85
12 SCs	**no ICIC**	0.91	10.87	-	-
	FFR	0.93	11.14	2.50	-
	DTFR	1.00	11.99	10.37	7.68
24 SCs	**no ICIC**	0.59	14.14	-	-
	FFR	0.59	14.18	0.28	-
	DTFR	0.61	14.53	2.78	2.50

gain achieved by DTFR not only with respect to no-ICIC but also to FFR. This can be explained by noticing the following two effects:

- First, the fact that as long as the distance among SCs is reduced, the probability of having the most interfering source of each user out of the cluster of its serving cell increases. When this happens, DTFR is not able to allocate the user to the sub-band in which its most interfering source is muted, and thus, the gain of DTFR is reduced.
- Second, there may exist more than one significant interference source for each user, situation that cannot be handled by DTFR. This effect is less harmful in FFR as long as the significant interfering sources belong to the cluster.

For the first limitation, slightly increasing the cluster size can improve the performance of DTFR, while too large cluster sizes will provoke a waste of resources. Simulation results with cluster sizes of 4, 6 and 8 SCs are collected in Table 5.10. Note that the performance of FFR is always deteriorated with larger cluster sizes, due to the lower resource reuse factor as long as the cluster size increases. Contrarily, the performance of DTFR is slightly improved when considering a cluster size of 6 SCs.

For the second limitation, DTFR could be enhanced to allow for a coordination pattern that enables the mute of two or more interfering neighbors at a time. The resource allocation optimized in Eq. (5.7) should be reformulated

Table 5.10: Comparison of system and cell spectral efficiencies for different values of cluster size.

		Cell spec. efficiency [b/s/Hz]	System spec. effic. [b/s/Hz]	Gain wrt. no-ICIC [%]	Gain wrt. FFR [%]
no ICIC		0.59	14.14	-	-
$C_s = 4$	**FFR**	0.59	14.18	0.28	-
	DTFR	0.61	14.53	2.78	2.50
$C_s = 6$	**FFR**	0.53	12.77	-9.67	-
	DTFR	0.61	14.57	3.03	14.06
$C_s = 8$	**FFR**	0.50	12.01	-15.03	-
	DTFR	0.61	14.53	2.81	20.99

to consider the actual bandwidth for each set of users sharing the same combination of most interfering cells. An example of this extension of DTFR in the sub-bands configuration is shown in Figure 5.9.

Finally, it is important to highlight that in spite of the smaller gains of FFR and DTFR with respect to no-ICIC application in denser networks, the schemes with fractional reuse of the resources present a very important benefit in power saving. Table 5.11 shows the total power consumed in the network by the different algorithms as a function of the SC density considered. Note that not only the power consumption does not increase with densification but it is reduced thanks to the mute of some SCs when they do not have any active user. Energy savings are computed with respect to the total amount of power available at the system, that corresponds to 27 dBm. For instance, the application of DTFR in the scenario with 24 SCs achieves a power reduction of 30%. Therefore, the energy saved could be used to improve the performance of both ICIC schemes in denser networks by means of more sophisticated power profiles.

Table 5.11: Comparison of the power consumed by the three algorithms.

	Power consumption [dBm]			Energy saving [%]		
	no-ICIC	**FFR**	**DTFR**	**no-ICIC**	**FFR**	**DTFR**
4 SCs	27.00	23.02	26.03	0.0	60.0	20.0
8 SCs	27.00	23.00	26.03	0.0	60.2	20.0
12 SCs	27.00	22.83	26.03	0.0	61.7	20.0
24 SCs	26.42	21.95	25.45	12.5	68.7	30.0

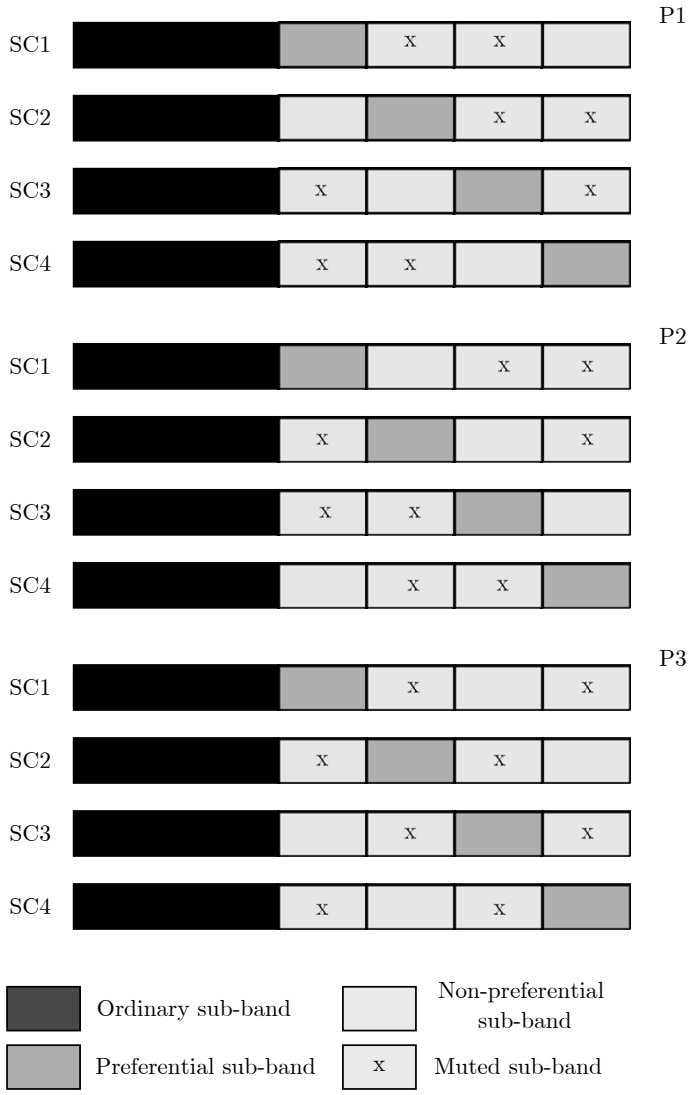

Figure 5.9: Example of sub-band configuration in an enhanced version of DTFR with 2 muted neighbors at a time, for a cluster composed by 4 small cells.

5.5 Conclusions

In this chapter, an ICIC technique suitable for ultra dense indoor deployments has been proposed. This technique, called Dynamic Time and Frequency Reuse (DTFR), coordinates the resource allocation among cells in both time and frequency domains, in such a way that users are allocated to those resources in which their most interfering sources are not transmitting.

The performance of DTFR has been evaluated in different scenarios, and compared to other two scheduling algorithms: a conventional user scheduling algorithm with no ICIC mechanism and an algorithm based on the FFR scheme. Simulation results have been firstly presented for an indoor scenario with 8 SCs and an increasing number of users. Results have shown that the proposed DTFR scheme achieves large performance gains compared to the other two algorithms for all the user densities analyzed. Indeed, performance gains increase with the number of deployed users in the scenario. For a user density of 2 users/100 m^2, cell spectral efficiencies are increased in more than 20% with respect to both FFR and no-ICIC algorithms, while reaching a energy saving of the 20%. Also in the case of MIMO configuration, DTFR increases the cell spectral efficiency in more than 5% but still saving a 20% of power with respect to no-ICIC.

Secondly, the effect of densification on the performance of DTFR has been also analyzed. Results have been presented for an increasing number of cells in the scenario, keeping the total available power constant. For the three algorithms, it has been shown that increasing the density of cells improves the system spectral efficiency and the fairness among users. Also in denser deployments, DTFR achieves the best system performance in comparison to the other two algorithms and reduces the power consumption of the network. However, the performance gains achieved by the application of ICIC in denser networks have shown to be significantly reduced when the availability of power in the system is limited.

Finally, two different lines have been presented to increase the gains of DTFR in UDN, consisting in the consideration of larger cluster sizes for the cooperation among cells, and the enhance of the time and frequency pattern configuration to include sub-bands free of the interference from more than one neighbor at a time.

Chapter 6

Conclusions and future work

6.1 Concluding remarks

This dissertation has investigated the Ultra Dense Networks (UDNs) deployment as a solution for beyond 2020 technologies. To this aim, the focus has been firstly pointed out to analyze whether it exists a fundamental limit of densification in cellular networks or, contrarily, the further deployment of access points brings indefinitely an improvement in network performance. Moreover, UDN have been studied in conjunction with the other two key enablers considered for the broadband and massive connectivity required in future Fifth Generation (5G) networks, which are the use of massive number of antennas and larger amounts of spectrum. In this line, the performance of hybrid beamforming and precoding Multiple Input Multiple Output (MIMO) schemes have been assessed in both indoor and outdoor scenarios with multiple cells and users, working in the millimeter wave (mmW) frequency band. Finally, this Thesis has addressed one of the main limitations of the UDN, which is the increase of inter-cell interference in the network. In order to tackle this problem, an enhanced Inter-Cell Interference Coordination (eICIC) scheduling algorithm based on resource partitioning techniques has been proposed and its performance has been evaluated and compared to other scheduling algorithms under several degrees of network densification.

The analysis of the limits of densification has brought new useful insights about UDN performance. The most important one is the fact that there exist certain limits of densification over which further increasing the number of de-

ployed Base Stations (BSs) in the network does not provide an improvement in network performance. Besides, it has been shown that this limit depends on both the density of users and the available power in the system. Another important conclusion of this study is the suitability of cooperation among BSs as a function of the available level of power in the system. Results indicate that with low levels of available power, increasing the density of BSs leads to noise-limited scenarios, and in this case the best approach is to limit the cooperation among cells. Contrarily, when high levels of power are available, it is shown that cooperation is beneficial and the optimum cluster size of cooperative cells is larger for scenarios with higher densities of users.

Regarding the performance study of UDN working in mmW bands, important conclusions have been drawn about the beamforming and precoding schemes behavior in hybrid architectures. On the one hand, hybrid beamforming schemes have been analyzed in an urban-dense outdoor scenario with users in different propagation conditions. Results have pointed out that hybrid beamforming schemes with a sufficient number of Radio Frequency (RF) chains can provide performances close to that of the fully digital schemes for those users in Line of Sight (LoS) propagation conditions. However, the performance of the network is significantly worsen for those users in Non Line of Sight (NLoS) propagation conditions, for which increasing the number of RF chains does not bring any benefit. This conclusion highlights the necessity of increasing the density of BSs in those networks working in mmW bands, in order to increase the LoS probability of the users and improve the network performance for all of them.

On the other hand, the performance of hybrid precoding schemes has been analyzed in an indoor scenario, considering three different deployment strategies: a conventional deployment of two Small Cells (SCs) with co-located antenna arrays, the use of regular femtocells deployment and the use of Distributed Antenna Systems (DAS). For the DAS scenario, a distributed hybrid precoding scheme has been proposed to better exploit the antennas disposition and to allow for the selection of the optimum Remote Antenna Units (RAUs) for the transmission to each user. From this study, it has been concluded that the use of DAS is the most suitable strategy for indoor environments, since it provides an excellent trade-off between the other two strategies. In particular, the distribution of the antennas over the scenario allows delivering almost the same throughput to cell-edge users as the femtocell deployments. Moreover, the joint transmission from several RAUs enables coordinating the intra-cell interference as in conventional deployments with co-located antennas, providing high peak throughputs that significantly increase the system spectral efficiency.

Furthermore, the presence of practical limitations and hardware impairments in the use of hybrid architectures has been also evaluated for both indoor and outdoor scenarios. It has been shown that hybrid schemes are very robust to the errors introduced by non-ideal phase shifters. Besides, the use of outdated Channel State Information (CSI) has been revealed as critical for those schemes applying baseband precoding, while the hybrid schemes using only RF beamforming are quite robust to this practical limitation. The last effect considered in this study is the impact of the combiner losses introduced by real combiners. Results have shown that this impairment has a significant impact on the system performance for architectures with high number of RF chains. Indeed, the magnitude of the power loss introduced by the combiner determines in the end the optimum number of RF chains to be used, preferring a lower number of RF chains when the losses introduced by the combiners are large.

Lastly, the use of eICIC algorithms based on resource partitioning techniques has been analyzed in the context of UDNs. The proposed algorithm, called Dynamic Time and Frequency Reuse (DTFR), applies a fractional reuse of the resources in both time and frequency domains. Its performance has been evaluated and compared to a conventional Fractional Frequency Reuse (FFR) scheme and to a user scheduling algorithm with no Inter-Cell Interference Coordination (ICIC). Results have highlighted that DTFR provides higher system spectral efficiencies with respect to the two other schemes, while reducing the power consumption of the network. Moreover, two important conclusions have been extracted from this study. The former is that, given a particular scenario, the introduction of more antennas and the use of MIMO techniques reduce the gain achieved by resource partitioning schemes with respect to no ICIC application when the total system power remains constant. The latter conclusion derived from the simulations, and in consonance with the theoretical study of the UDNs, states that adding more BSs to the network while keeping the total system power constant leads to noise-limited scenarios in which the application of ICIC schemes is not beneficial.

Overall, UDNs have shown an enormous potential for their use in future mobile communications systems, due to several reasons. The first of them is the increase in capacity achieved by densification without the need to augment the power consumption of the network, which implies important benefits from an economic point of view. Besides, UDNs have been pointed out as a very interesting deployment strategy for the use of massive MIMO in mmW frequencies, making the most of the large bandwidth available at this band and boosting the achievable data rates. Finally, interference has been proved as an avoidable limitation of UDNs thanks to the application of the proper ICICs mechanisms. Therefore, the only question that remains to be seen is how mo-

bile operators will face the high economical costs derived from densification, and whether these costs will be passed onto the consumers.

6.2 Future research lines

Several research topics requiring further study have been identified in this Thesis. Some of these research directions are the following:

- The analysis of the densification limits presented in this Thesis has been conducted by using a 1-dimensional network model. As a future research line, it is worth to replicate the study by extending the model to a 2-dimensional or even 3-dimensional network deployment.

- In the context of UDNs working in mmW frequencies, users have been considered static during simulations. Further research is needed to include more advanced user mobility models and realistic deployment scenarios, in which there are not regular patterns in the interference and power distributions. More specifically, beam-tracking mechanisms must be introduced and further investigated in order to update the beamforming decisions as the users move along distances longer than the decorrelation distance of the large-scale channel parameters.

- Further investigation is also required on different DAS deployments in mmW bands. In particular, this dissertation has focused on passive DAS, which has been selected due to its good performance in small to medium size scenarios. For that reason, the power losses introduced by the cables connecting the distributed antennas to the BSs have been neglected. However, there is a need to investigate the impact on the system performance of the power losses introduced by non-ideal cables in large scenarios, where losses may be not negligible.

  Moreover, another related line of research is the study of active DAS deployments, in which not only the antennas but also the radio units are distributed over the space. With this disposition, RF chains are not co-located and the full-connected hybrid architecture cannot be employed. Further work is required to analyze the performance of active DAS deployments using other types of hybrid architectures.

- Regarding the application of ICIC schemes in UDNs, the performance of the proposed algorithm DTFR has been assessed by applying a static clustering algorithm among the regularly distributed femtocells. New

dynamic clustering algorithms need to be defined with self-organizing capabilities for their application in scenarios where femtocells are randomly deployed.

Besides, the performance evaluation of DTFR has shown that, depending on the BS density of the network, a user can be experiencing strong interference from more than one neighbor cell within the cluster. In order to solve this problem, further research is required to extend the proposed algorithm in such a way that the interference of more than one neighbor cell within a cluster can be avoided simultaneously.

References

[1] V. Jungnickel, K. Manolakis, W. Zirwas, B. Panzner, V. Braun, M. Lossow, M. Sternad, R. Apelfrojd, and T. Svensson, "The role of small cells, coordinated multipoint, and massive MIMO in 5G," *IEEE Communications Magazine*, vol. 52, no. 5, pp. 44–51, May 2014.

[2] J. F. Monserrat, H. Droste, O. Bulakci, J. Eichinger, O. Queseth, M. Stamatelatos, H. Tullberg, V. Venkatkumar, G. Zimmermann, U. Dotsch, and A. Osseiran, "Rethinking the mobile and wireless network architecture: The METIS research into 5G," in *European Conference on Networks and Communications (EuCNC), 2014*, June 2014, pp. 1–5.

[3] M. Maternia, S. E. E. Ayoubi, M. Fallgren, P. Spapis, Y. Qi, D. Martín-Sacristán, O. Carrasco, M. Fresia, M. Payaró, M. Schubert, J. S. Bedo, and V. Kulkarni, "5G PPP use cases and performance evaluation models," 5G PPP, Tech. Rep., 2016.

[4] M. Agiwal, A. Roy, and N. Saxena, "Next Generation 5G Wireless Networks: A Comprehensive Survey," *IEEE Communications Surveys Tutorials*, vol. 18, no. 3, pp. 1617–1655, February 2016.

[5] F. Boccardi, R. W. Heath, A. Lozano, T. L. Marzetta, and P. Popovski, "Five disruptive technology directions for 5G," *IEEE Communications Magazine*, vol. 52, no. 2, pp. 74–80, February 2014.

[6] E. Larsson, O. Edfors, F. Tufvesson, and T. Marzetta, "Massive MIMO for next generation wireless systems," *IEEE Communications Magazine*, vol. 52, no. 2, pp. 186–195, February 2014.

[7] T. S. Rappaport, S. Sun, R. Mayzus, H. Zhao, Y. Azar, K. Wang, G. N. Wong, J. K. Schulz, M. Samimi, and F. Gutierrez, "Millimeter Wave Mobile Communications for 5G Cellular: It Will Work!" *IEEE Access*, vol. 1, pp. 335–349, May 2013.

[8] N. Bhushan, J. Li, D. Malladi, R. Gilmore, D. Brenner, A. Damnjanovic, R. T. Sukhavasi, C. Patel, and S. Geirhofer, "Network densification: the dominant theme for wireless evolution into 5G," *IEEE Communications Magazine*, vol. 52, no. 2, pp. 82–89, February 2014.

[9] A. Osseiran, F. Boccardi, V. Braun, K. Kusume, P. Marsch, M. Maternia, O. Queseth, M. Schellmann, H. Schotten, H. Taoka, H. Tullberg, M. A. Uusitalo, B. Timus, and M. Fallgren, "Scenarios for 5G mobile and wireless communications: the vision of the METIS project," *IEEE Communications Magazine*, vol. 52, no. 5, pp. 26–35, May 2014.

[10] M. Kamel, W. Hamouda, and A. Youssef, "Ultra-Dense Networks: A Survey," *IEEE Communications Surveys Tutorials*, vol. 18, no. 4, pp. 2522–2545, May 2016.

[11] B. Soret, K. I. Pedersen, N. T. K. Jørgensen, and V. Fernández-López, "Interference coordination for dense wireless networks," *IEEE Communications Magazine*, vol. 53, no. 1, pp. 102–109, January 2015.

[12] D. López-Pérez, M. Ding, H. Claussen, and A. H. Jafari, "Towards 1 Gbps/UE in Cellular Systems: Understanding Ultra-Dense Small Cell Deployments," *IEEE Communications Surveys Tutorials*, vol. 17, no. 4, pp. 2078–2101, June 2015.

[13] W. Nam, D. Bai, J. Lee, and I. Kang, "Advanced interference management for 5G cellular networks," *IEEE Communications Magazine*, vol. 52, no. 5, pp. 52–60, May 2014.

[14] J. G. Andrews, F. Baccelli, and R. K. Ganti, "A Tractable Approach to Coverage and Rate in Cellular Networks," *IEEE Transactions on Communications*, vol. 59, no. 11, pp. 3122–3134, November 2011.

[15] H. S. Dhillon, R. K. Ganti, F. Baccelli, and J. G. Andrews, "Modeling and Analysis of K-Tier Downlink Heterogeneous Cellular Networks," *IEEE Journal on Selected Areas in Communications*, vol. 30, no. 3, pp. 550–560, April 2012.

[16] X. Zhang and J. G. Andrews, "Downlink Cellular Network Analysis With Multi-Slope Path Loss Models," *IEEE Transactions on Communications*, vol. 63, no. 5, pp. 1881–1894, May 2015.

[17] J. G. Andrews and X. Zhang and G. D. Durgin and A. K. Gupta, "Are we approaching the fundamental limits of wireless network densification?" *IEEE Communications Magazine*, vol. 54, no. 10, pp. 184–190, October 2016.

[18] F. P. Kelly, A. K. Maulloo, and D. K. H. Tan, "Rate control for communication networks: shadow prices, proportional fairness and stability," *Journal of the Operational Research Society*, vol. 49, no. 3, pp. 237–252, April 1998.

[19] A. D. Wyner, "Shannon-theoretic approach to a Gaussian cellular multiple-access channel," *IEEE Transactions on Information Theory*, vol. 40, no. 6, pp. 1713–1727, November 1994.

[20] D. Gesbert, S. Hanly, H. Huang, S. S. Shitz, O. Simeone, and W. Yu, "Multi-Cell MIMO Cooperative Networks: A New Look at Interference," *IEEE Journal on Selected Areas in Communications*, vol. 28, no. 9, pp. 1380–1408, December 2010.

[21] J. Xu, J. Zhang, and J. G. Andrews, "On the Accuracy of the Wyner Model in Cellular Networks," *IEEE Transactions on Wireless Communications*, vol. 10, no. 9, pp. 3098–3109, September 2011.

[22] C. X. Wang, F. Haider, X. Gao, X. H. You, Y. Yang, D. Yuan, H. M. Aggoune, H. Haas, S. Fletcher, and E. Hepsaydir, "Cellular architecture and key technologies for 5G wireless communication networks," *IEEE Communications Magazine*, vol. 52, no. 2, pp. 122–130, February 2014.

[23] Nokia, "White Paper: Indoor Deployment Strategies," Tech. Rep., 2014.

[24] R. Heath, S. Peters, Y. Wang, and J. Zhang, "A current perspective on distributed antenna systems for the downlink of cellular systems," *IEEE Communications Magazine*, vol. 51, no. 4, pp. 161–167, April 2013.

[25] W. Choi and J. G. Andrews, "Downlink performance and capacity of distributed antenna systems in a multicell environment," *IEEE Transactions on Wireless Communications*, vol. 6, no. 1, pp. 69–73, January 2007.

[26] M. Tolstrup, *Indoor Radio Planning: A Practical Guide for GSM, DCS, UMTS, HSPA and LTE, 3rd Edition.* John Wiley and Sons, Inc., 2015.

[27] J. Yan, W. Wu, Y. Wang, G. Yang, and Y. Guo, "Transmit beamforming optimization for energy efficiency maximization in downlink distributed antenna systems," in *8th IEEE International Conference on Communication Software and Networks (ICCSN)*, June 2016, pp. 254–259.

[28] X. Li, X. Ge, X. Wang, J. Cheng, and V. C. M. Leung, "Energy Efficiency Optimization: Joint Antenna-Subcarrier-Power Allocation in OFDM-DASs," *IEEE Transactions on Wireless Communications*, vol. 15, no. 11, pp. 7470–7483, November 2016.

[29] Y. Dong, J. Hossain, J. Cheng, and V. C. M. Leung, "Joint RRH selection and beamforming in distributed antenna systems with energy harvesting," in *International Conference on Computing, Networking and Communications (ICNC)*, January 2017, pp. 582–586.

[30] N. Petrović and D. Savković, "LTE performance in a hybrid indoor DAS (Active vs. Passive)," in *23rd Telecommunications Forum Telfor (TELFOR)*, November 2015, pp. 141–144.

[31] Q. Sun, S. Jin, J. Wang, Y. Zhang, X. Gao, and K. K. Wong, "Downlink massive distributed antenna systems scheduling," *IET Communications*, vol. 9, no. 7, pp. 1006–1016, April 2015.

[32] X. Chen, Z. Zhang, and H. H. Chen, "On distributed antenna systems with limited feedback precoding: Opportunities and challenges," *IEEE Wireless Communications*, vol. 17, no. 2, pp. 80–88, April 2010.

[33] S. Schwarz, R. Heath, and M. Rupp, "Single-user MIMO versus multi-user MIMO in distributed antenna systems with limited feedback," *EURASIP Journal on Advances in Signal Processing*, vol. 2013, no. 1, p. 54, March 2013.

[34] R. W. Heath, N. González-Prelcic, S. Rangan, W. Roh, and A. M. Sayeed, "An Overview of Signal Processing Techniques for Millimeter Wave MIMO Systems," *IEEE Journal of Selected Topics in Signal Processing*, vol. 10, no. 3, pp. 436–453, April 2016.

[35] S. Sun, T. S. Rappaport, R. W. Heath, A. Nix, and S. Rangan, "MIMO for millimeter-wave wireless communications: beamforming, spatial multiplexing, or both?" *IEEE Communications Magazine*, vol. 52, no. 12, pp. 110–121, December 2014.

[36] H. Weingarten, Y. Steinberg, and S. S. Shamai, "The Capacity Region of the Gaussian Multiple-Input Multiple-Output Broadcast Channel," *IEEE Transactions on Information Theory*, vol. 52, no. 9, pp. 3936–3964, September 2006.

[37] L. Lu, G. Y. Li, A. L. Swindlehurst, A. Ashikhmin, and R. Zhang, "An Overview of Massive MIMO: Benefits and Challenges," *IEEE Journal of Selected Topics in Signal Processing*, vol. 8, no. 5, pp. 742–758, October 2014.

[38] M. Akdeniz, Y. Liu, M. Samimi, S. Sun, S. Rangan, T. Rappaport, and E. Erkip, "Millimeter wave channel modeling and cellular capacity evaluation," *IEEE Journal on Selected Areas in Communications*, vol. 32, no. 6, pp. 1164–1179, June 2014.

[39] A. L. Swindlehurst, E. Ayanoglu, P. Heydari, and F. Capolino, "Millimeter-wave massive MIMO: the next wireless revolution?" *IEEE Communications Magazine*, vol. 52, no. 9, pp. 56–62, September 2014.

[40] R. Méndez-Rial, C. Rusu, N. González-Prelcic, A. Alkhateeb, and R. W. Heath, "Hybrid MIMO Architectures for Millimeter Wave Communications: Phase Shifters or Switches?" *IEEE Access*, vol. 4, pp. 247–267, January 2016.

[41] A. Osseiran, J. F. Monserrat, and P. Marsch, Eds., *5G Mobile and Wireless Communications Technology*. Cambridge University Press, 2016.

[42] A. Alkhateeb, J. Mo, N. González-Prelcic, and R. W. Heath, "MIMO Precoding and Combining Solutions for Millimeter-Wave Systems," *IEEE Communications Magazine*, vol. 52, no. 12, pp. 122–131, December 2014.

[43] W. Roh, J. Y. Seol, J. Park, B. Lee, J. Lee, Y. Kim, J. Cho, K. Cheun, and F. Aryanfar, "Millimeter-wave beamforming as an enabling technology for 5G cellular communications: theoretical feasibility and prototype results," *IEEE Communications Magazine*, vol. 52, no. 2, pp. 106–113, February 2014.

[44] S. Park, A. Alkhateeb, and R. Heath, "Dynamic subarrays for hybrid precoding in wideband mmWave MIMO systems," *IEEE Transactions on Wireless Communications*, vol. PP, no. 99, pp. 1–1, 2017.

[45] O. El Ayach, S. Rajagopal, S. Abu-Surra, Z. Pi, and R. Heath, "Spatially sparse precoding in millimeter wave MIMO systems," *IEEE Transactions on Wireless Communications*, vol. 13, no. 3, pp. 1499–1513, March 2014.

[46] A. Alkhateeb, O. El Ayach, G. Leus, and R. Heath, "Channel estimation and hybrid precoding for millimeter wave cellular systems," *IEEE Journal of Selected Topics in Signal Processing*, vol. 8, no. 5, pp. 831–846, October 2014.

[47] C. Rusu, R. Méndez-Rial, N. González-Prelcic, and R. W. Heath, "Low Complexity Hybrid Precoding Strategies for Millimeter Wave Communication Systems," *IEEE Transactions on Wireless Communications*, vol. 15, no. 12, pp. 8380–8393, December 2016.

[48] F. Sohrabi and W. Yu, "Hybrid Digital and Analog Beamforming Design for Large-Scale Antenna Arrays," *IEEE Journal of Selected Topics in Signal Processing*, vol. 10, pp. 501–513, April 2016.

[49] F. Vook, A. Ghosh, and T. Thomas, "MIMO and beamforming solutions for 5G technology," in *IEEE MTT-S International Microwave Symposium (IMS)*, June 2014, pp. 1–4.

[50] A. Alkhateeb, G. Leus, and R. Heath, "Limited feedback hybrid precoding for multi-user millimeter wave systems," *IEEE Transactions on Wireless Communications*, vol. 14, no. 11, pp. 6481–6494, November 2015.

[51] N. Somjit, G. Stemme, and J. Oberhammer, "Phase error and nonlinearity investigation of millimeter-wave MEMS 7-stage dielectric-block phase shifters," in *European Microwave Integrated Circuits Conference (EuMIC)*, September 2009, pp. 519–522.

[52] W. Li, Y. Chiang, J. Tsai, H. Yang, J. Cheng, and T. Huang, "60-GHz 5-bit Phase Shifter With Integrated VGA Phase-Error Compensation," *IEEE Transactions on Microwave Theory and Techniques*, vol. 61, no. 3, pp. 1224–1235, March 2013.

[53] A. García-Rodríguez, V. Venkateswaran, P. Rulikowski, and C. Masouros, "Hybrid Analog-Digital Precoding Revisited under Realistic RF Modeling," *IEEE Wireless Communications Letters*, vol. 5, no. 5, pp. 528–531, October 2016.

[54] E. Björnson, M. Matthaiou, and M. Debbah, "Massive MIMO Systems with Hardware-Constrained Base Stations," in *International Conference on Acoustics, Speech and Signal Processing*, May 2014, pp. 3142–3146.

[55] S. K. Mohammed and E. G. Larsson, "Per-antenna Constant Envelope Precoding for Large Multi-User MIMO Systems," *IEEE Transactions on Communications*, vol. 61, no. 3, pp. 1059–1071, March 2013.

[56] D. J. Love and R. W. Heath, "Equal Gain Transmission in Multiple-Input Multiple-Output Wireless Systems," *IEEE Transactions on Communications*, vol. 51, no. 7, pp. 1102–1110, July 2003.

[57] R. Ghaffar and R. Knopp, "Fractional frequency reuse and interference suppression for OFDMA networks," in *8th International Symposium on Modeling and Optimization in Mobile, Ad Hoc, and Wireless Networks*, May 2010, pp. 273–277.

[58] M. Sternad, T. Ottosson, A. Ahlen, and A. Svensson, "Attaining both coverage and high spectral efficiency with adaptive OFDM downlinks," in *IEEE 58th Vehicular Technology Conference (VTC Fall)*, vol. 4, October 2003, pp. 2486–2490.

[59] Ericsson, "Inter-cell interference handling for E-UTRA," 3GPP, Tech. Rep. R1-050764, 2005.

[60] B. Krasniqi, "Partial Frequency Reuse for Long Term Evolution," Ph.D. dissertation, Technischen Universität Wien, 2011.

[61] Huawei, "Further analysis of soft frequency reuse scheme," 3GPP, Tech. Rep. R1-050841, 2005.

[62] C. He, F. Liu, H. Yang, C. Clark, H. Sun, M. Wu, and J. Zhang, "Co-Channel Interference Mitigation in MIMO-OFDM System," in *International Conference on Wireless Communications, Networking and Mobile Computing*, September 2007, pp. 204–208.

[63] M. Assaad, "Optimal Fractional Frequency Reuse (FFR) in Multicellular OFDMA System," in *IEEE 68th Vehicular Technology Conference*, September 2008, pp. 1–5.

[64] L. Chen and D. Yuan, "Soft frequency reuse in large networks with irregular cell pattern: How much gain to expect?" in *IEEE 20th International Symposium on Personal, Indoor and Mobile Radio Communications*, September 2009, pp. 1467–1471.

[65] R. Y. Chang, Z. Tao, J. Zhang, and C. C. Kuo, "A Graph Approach to Dynamic Fractional Frequency Reuse (FFR) in Multi-Cell OFDMA Networks," in *IEEE International Conference on Communications*, June 2009, pp. 1–6.

[66] I. G. Fraimis, V. D. Papoutsis, and S. A. Kotsopoulos, "A Decentralized Subchannel Allocation Scheme with Inter-Cell Interference Coordination (ICIC) for Multi-Cell OFDMA Systems," in *IEEE Global Telecommunications Conference (GLOBECOM)*, December 2010, pp. 1–5.

[67] D. Kimura, Y. Harada, and H. Seki, "De-Centralized Dynamic ICIC Using X2 Interfaces for Downlink LTE Systems," in *IEEE 73rd Vehicular Technology Conference (VTC Spring)*, May 2011, pp. 1–5.

[68] L. Liu, D. Qu, and T. Jiang, "Dynamic Fractional Frequency Reuse Based on Interference Avoidance Request for Downlink OFDMA Cellular Networks," in *Proceedings of the 6th International Wireless Communications and Mobile Computing Conference*, 2010, pp. 381–386.

[69] H. B. Sidi, R. El-Azouzi, and M. Haddad, "A two-stage game theoretic approach for self-organizing networks," *EURASIP Journal on Wireless Communications and Networking*, vol. 2013, no. 1, p. 119, May 2013.

[70] TSG RAN, "Scenarios and requirements for small cell enhancements for E-UTRA and E-UTRAN (Release 12)," 3GPP, TR 36.932 V12.1.0, March 2013.

[71] D. T. Ngo and T. Le-Ngoc, *Architectures of Small Cell Networks and Interference Management*. Springer, 2014.

[72] D. López-Pérez, I. Guvenc, G. de la Roche, M. Kountouris, T. Q. S. Quek, and J. Zhang, "Enhanced intercell interference coordination challenges in heterogeneous networks," *IEEE Wireless Communications*, vol. 18, no. 3, June 2011.

[73] TSG RAN, "Evolved Universal Terrestrial Radio Access (E-UTRA) and Evolved Universal Terrestrial Radio Access Network (E-UTRAN); Overall description; Stage 2," 3GPP, TS 36.300 v10.12.0, 2014.

[74] B. Soret and K. I. Pedersen, "Centralized and Distributed Solutions for Fast Muting Adaptation in LTE-Advanced HetNets," *IEEE Transactions on Vehicular Technology*, vol. 64, January 2015.

[75] J. Oh and Y. Han, "Cell selection for range expansion with almost blank subframe in heterogeneous networks," in *IEEE 23rd International Symposium on Personal, Indoor and Mobile Radio Communications - (PIMRC)*, September 2012, pp. 653–657.

[76] S. N. S. Kshatriya, S. Kaimalettu, S. R. Yerrapareddy, K. Milleth, and N. Akhtar, "On interference management based on subframe blanking in Heterogeneous LTE networks," in *5th International Conference on Communication Systems and Networks (COMSNETS)*, January 2013, pp. 1–7.

[77] S. Uygungelen, G. Bauch, H. Taoka, and Z. Bharucha, "Protection of Cell-Edge Users in Wireless Systems by Using Almost Blank Subframes," in *9th International ITG Conference on Systems, Communication and Coding (SCC 2013)*, January 2013, pp. 1–6.

[78] M. Al-Rawi, J. Huschke, and M. Sedra, "Dynamic Protected-Subframe Density Configuration in LTE Heterogeneous Networks," in *21st International Conference on Computer Communications and Networks (ICCCN)*, July 2012, pp. 1–6.

[79] S. Sardellitti, A. Carfagna, and S. Barbarossa, "Optimal resource allocation in fetmocell networks based on Markov modeling of interferers' activity," *EURASIP Journal on Wireless Communications and Networking*, vol. 2012, no. 1, p. 371, 2012.

[80] A. Imran, M. Bennis, and L. Giupponi, "Use of learning, game theory and optimization as biomimetic approaches for Self-Organization in macro-femtocell coexistence," in *IEEE Wireless Communications and Networking Conference Workshops (WCNCW)*, April 2012, pp. 103–108.

[81] M. Bennis and D. Niyato, "A Q-learning based approach to interference avoidance in self-organized femtocell networks," in *IEEE Globecom Workshops*, December 2010, pp. 706–710.

[82] I. W. Mustika, K. Yamamoto, H. Murata, and S. Yoshida, "Potential Game Approach for Self-Organized Interference Management in Closed Access Femtocell Networks," in *IEEE 73rd Vehicular Technology Conference (VTC Spring)*, May 2011, pp. 1–5.

[83] J. Wang, L. Liu, K. Takeda, and H. Jiang, "Time Domain Inter-Cell Interference Coordination for Dense Small Cell Deployments," in *IEEE 80th Vehicular Technology Conference (VTC Fall)*, September 2014.

[84] S. A. R. Zaidi, D. C. McLernon, M. Ghogho, and M. A. Imran, "Cloud empowered Cognitive Inter-cell Interference Coordination for small cellular networks," in *IEEE International Conference on Communication Workshop (ICCW)*, June 2015.

[85] G. Huang and J. Li, "Interference Mitigation for Femtocell Networks via Adaptive Frequency Reuse," *IEEE Transactions on Vehicular Technology*, vol. 65, no. 4, pp. 2413–2423, April 2015.

[86] Y. Wu, H. Jiang, and D. Zhang, "A Novel Coordinated Spectrum Assignment Scheme for Densely Deployed Enterprise LTE Femtocells," in *IEEE 75th Vehicular Technology Conference (VTC Spring)*, May 2012, pp. 1–6.

[87] P. Luoto, J. Leinonen, P. Pirinen, V. V. Phan, and M. Latva-aho, "Bit-map based resource partitioning in LTE-A femto deployment," in *IEEE International Conference on Communications (ICC)*, June 2013, pp. 5005–5009.

[88] H. Burchardt, S. Sinanovic, Z. Bharucha, and H. Haas, "Distributed and Autonomous Resource and Power Allocation for Wireless Networks,"

IEEE Transactions on Communications, vol. 61, no. 7, pp. 2758–2771, July 2013.

[89] J. Cabrejas, D. García, I. Alepuz, C. Herranz, and S. Giménez, *3GPP LTE-Advanced: Hacia la 5G móvil*. Marcombo S.A., 2017, ch. Tecnologías SON.

[90] S. Park and S. Bahk, "Dynamic Inter-Cell Interference Avoidance in Self-Organizing Femtocell Networks," in *IEEE International Conference on Communications (ICC)*, June 2011, pp. 1–5.

[91] D. López-Pérez, A. Ladányi, A. Jüttner, and J. Zhang, "OFDMA femtocells: A self-organizing approach for frequency assignment," in *IEEE 20th International Symposium on Personal, Indoor and Mobile Radio Communications*, September 2009, pp. 2202–2207.

[92] F. Tariq, L. S. Dooley, and A. S. Poulton, "Virtual clustering for resource management in cognitive femtocell networks," in *3rd International Congress on Ultra Modern Telecommunications and Control Systems and Workshops (ICUMT)*, October 2011, pp. 1–7.

[93] K. L. Haldar, H. Li, and D. P. Agrawal, "A Cluster-Aware Soft Frequency Reuse scheme for inter-cell interference mitigation in LTE based femtocell networks," in *IEEE 14th International Symposium on "A World of Wireless, Mobile and Multimedia Networks" (WoWMoM)*, June 2013, pp. 1–6.

[94] J. Liu, J. Wu, J. Chen, P. Wang, and J. Zhang, "Radio Resource Allocation in Buildings with Dense Femtocell Deployment," in *21st International Conference on Computer Communications and Networks (ICCCN)*, July 2012, pp. 1–5.

[95] D. Calabuig, S. Giménez, and J. F. Monserrat, "Asymptotic Analysis of Ultra-Dense Networks based on a Spatially Periodic System Model," under review, submitted 2017.

[96] K. Kirsten and F. Williams, *A Window into Zeta and Modular Physics*. Cambridge, UK: Cambridge University Press, 2010.

[97] G. Nigam, P. Minero, and M. Haenggi, "Coordinated multipoint in heterogeneous networks: A stochastic geometry approach," in *IEEE Globecom Workshops*, December 2013, pp. 145–150.

[98] J. Zhou and J. Thompson, "Linear precoding for the downlink of multiple input single output coexisting wireless systems," *IET Communications*, vol. 2, no. 6, pp. 742–752, July 2008.

[99] A. Wiesel, Y. C. Eldar, and S. Shamai, "Zero-forcing precoding and generalized inverses," *IEEE Transactions on Signal Processing*, vol. 56, no. 9, pp. 4409–4418, September 2008.

[100] C. B. Peel, B. M. Hochwald, and A. L. Swindlehurst, "A vector-perturbation technique for near-capacity multiantenna multiuser communication-part I: channel inversion and regularization," *IEEE Transactions on Communications*, vol. 53, no. 1, pp. 195–202, January 2005.

[101] A. Alkhateeb and R. Heath, "Frequency selective hybrid precoding for limited feedback millimeter wave systems," *IEEE Transactions on Communications*, no. 5, pp. 1801–1818, May 2016.

[102] Y. T. Wu, Y. Y. Zhao, and F. Yu, "Comparison of codebooks for beamforming in limited feedback MIMO systems," in *IEEE International Conference on Computer Science and Automation Engineering (CSAE)*, vol. 2, May 2012, pp. 32–36.

[103] D. Yang, L. L. Yang, and L. Hanzo, "DFT-Based Beamforming Weight-Vector Codebook Design for Spatially Correlated Channels in the Unitary Precoding Aided Multiuser Downlink," in *IEEE International Conference on Communications (ICC)*, May 2010, pp. 1–5.

[104] Z. Pi and F. Khan, "A Millimeter-Wave Massive MIMO System for Next Generation Mobile Broadband," in *46th Asilomar Conference on Signals, Systems and Computers (ASILOMAR)*, November 2012, pp. 693–698.

[105] J. F. Monserrat, G. Mange, V. Braun, H. Tullberg, G. Zimmermann, and O. Bulakci, "METIS research advances towards the 5G mobile and wireless system definition," *EURASIP Journal on Wireless Communications and Networking*, vol. 2015, no. 53, March 2015.

[106] H. Yang and T. L. Marzetta, "Performance of Conjugate and Zero-Forcing Beamforming in Large-Scale Antenna Systems," *IEEE Journal on Selected Areas in Communications*, vol. 31, no. 2, pp. 172–179, February 2013.

[107] T. A. Thomas, H. C. Nguyen, G. R. MacCartney, and T. S. Rappaport, "3D mmWave channel model proposal," in *IEEE Vehicular Technology Conference (VTC Fall)*, September 2014, pp. 1–6.

[108] "ITU-R M.2135-1 Report: Guidelines for evaluation of radio interface technologies for IMT-Advanced," Tech. Rep., 2009.

[109] S. Zhang, R. Zhang, and T. Lim, "Massive MIMO with per-antenna power constraint," in *IEEE Global Conference on Signal and Information Processing (GlobalSIP)*, December 2014, pp. 642–646.

[110] O. Bakr and M. Johnson, "Impact of phase and amplitude errors on array performance," Electrical Engineering and Computer Sciences, University of California at Berkeley, Tech. Rep. UCB/EECS-2009-1, January 2009.

[111] D. M. Pozar, *Microwave Engineering [Chapter 7]*. John Wiley and Sons, Inc., 2012.

[112] S. Sun, T. S. Rappaport, T. A. Thomas, and A. Ghosh, "A preliminary 3D mm wave indoor office channel model," in *International Conference on Computing, Networking and Communications (ICNC)*, February 2015, pp. 26–31.

[113] J. Monserrat, R. Fraile, and L. Rubio, "Application of alternating projection method to ensure feasibility of shadowing cross-correlation models," *Electronics Letters*, vol. 43, no. 13, pp. 724–725, 2007.

[114] X. You, D. Wang, B. Sheng, X. Gao, X. Zhao, and M. Chen, "Cooperative distributed antenna systems for mobile communications [coordinated and distributed MIMO]," *IEEE Wireless Communications*, vol. 17, no. 3, pp. 35–43, 2010.

[115] J. Wang, M. Wu, and F. Zheng, "The Codebook Design for MIMO Precoding Systems in LTE and LTE-A," in *6th International Conference on Wireless Communications Networking and Mobile Computing (WiCOM)*, September 2010, pp. 1–4.

[116] H. Busche, A. Vanaev, and H. Rohling, "SVD-based MIMO Precoding and Equalization Schemes for Realistic Channel Knowledge: Design Criteria and Performance Evaluation," *Wireless Personal Communications*, vol. 48, no. 3, pp. 347–359, February 2009.